AD NUMBER

AD874154

LIMITATION CHANGES

TO:

Approved for public release; distribution is unlimited.

FROM:

Distribution authorized to U.S. Gov't. agencies and their contractors; Critical Technology; JUL 1970. Other requests shall be referred to U.S. Army Aviation Materiel Laboratories, Fort Eustist VA 23604. This document contains export-controlled technical data.

AUTHORITY

USMMARDL ltr, 18 Jul 1971

AD

USAAVLABS TECHNICAL REPORT 70-19

INVESTIGATION OF HIGH-PRESSURE HYDRAULIC VORTEX RATE SENSOR

By

Michael J. DeSantis
Edward L. Rakowsky

July 1970

U. S. ARMY AVIATION MATERIEL LABORATORIES
FORT EUSTIS, VIRGINIA

CONTRACT DAAJ02-69-C-0008
SINGER-GENERAL PRECISION, INC.
KEARFOTT DIVISION
LITTLE FALLS, NEW JERSEY

Disclaimers

The findings in this report are not to be construed as an official Department of the Army position unless so designated by other authorized documents.

When Government drawings, specifications, or other data are used for any purpose other than in connection with a definitely related Government procurement operation, the United States Government thereby incurs no responsibility nor any obligation whatsoever; and the fact that the Government may have formulated, furnished, or in any way supplied the said drawings, specifications, or other data is not to be regarded by implication or otherwise as in any manner licensing the holder or any other person or corporation, or conveying any rights or permission, to manufacture, use, or sell any patented invention that may in any way be related thereto.

Disposition Instructions

Destroy this report when no longer needed. Do not return it to the originator.

DEPARTMENT OF THE ARMY
HEADQUARTERS US ARMY AVIATION MATERIEL LABORATORIES
FORT EUSTIS, VIRGINIA 23604

This report has been reviewed by the U. S. Army Aviation Materiel Laboratories and is considered to be technically sound. The report is published for the exchange of information and the stimulation of ideas.

Task 1F162203A14186
Contract DAAJ02-69-C-0008
USAAVLABS Technical Report 70-19
July 1970

INVESTIGATION OF HIGH-PRESSURE HYDRAULIC VORTEX RATE SENSOR

Final Report

by

Michael J. DeSantis
Edward L. Rakowsky

Prepared by

Singer-General Precision, Inc.
Kearfott Division
Little Falls, New Jersey

for

U. S. ARMY AVIATION MATERIEL LABORATORIES
FORT EUSTIS, VIRGINIA

ABSTRACT

An experimental investigation was undertaken to establish the feasibility of a high-pressure (3000 psi) hydraulic vortex rate sensor for application in a helicopter hydraulic stability-augmentation system. The high-pressure rate sensor offers the capability of using directly the vehicle's on-board supply of hydraulic fluid which is used in the primary hydromechanical flight control system.

Breadboard models of a fixed-geometry vortex rate sensor and a variable-geometry vortex rate sensor were designed and fabricated. A trade-off study was conducted to determine the effect of flow rate and geometry on the output pressure signal of the device. Impact pressure signal probes located in the sink were used as the sensing elements. Based on this study, a model was fabricated such that the pancake chamber diameter could be varied between 3.0 and 6.5 inches. The geometrical (physical) variables in the variable-geometry vortex rate sensor are viscous coupling gap, pancake chamber gap height, pancake chamber diameter, and signal pick-off location within the sink outlet. The only physical dimension that could be varied is the pancake chamber gap height in the fixed-geometry vortex rate sensor.

In the variable-geometry vortex rate sensor, blocked-output signal pressures were obtained over a range of temperature and supply pressure from $-10^{\circ}F$ to $160^{\circ}F$ and from 100 psi to 3000 psi, respectively, using MIL-H-5606 oil as the working fluid. Experimental results show that signal output pressure varies a maximum of 15 percent for supply pressures between 100 psi and 3000 psi. Fluid temperatures seriously affect the output signal due to viscous degradation. Since viscosity decreases with increasing temperature, signal output increases as temperature increases. In addition, the output signal reaches a maximum at a pancake chamber gap height of 0.45 inch and then levels off. The output pressure signal increases rapidly for pancake chamber diameters between 3 and 5 inches and then levels off above 5 inches.

No useful output pressure signals as a function of flow through the signal pick-offs could be obtained with the variable-geometry vortex rate sensor. Further experimentation indicated that the signal pick-off geometry was responsible. This fact was corroborated by the output pressure signals obtained with the fixed-geometry vortex rate sensor. The maximum output pressure obtained was 0.008 psi/deg/sec at a flow rate of 140 cc/min at 3000-psi supply pressure and 0.5-gpm supply flow in a non-optimum geometrical configuration.

FOREWORD

This report has been prepared by the Fluidics Department of the Research Center, Kearfott Division, Singer-General Precision, Inc., Little Falls, New Jersey, under Contract DAAJ02-69-C-0008. The study has been conducted under the direction of the U.S. Army Aviation Materiel Laboratories, Fort Eustis, Virginia, with Mr. William D. Vann acting as Project Engineer.

The participation of Mr. Herbert Hoffmann and Mr. Frank Morici in performing the experimental phases is gratefully acknowledged.

BLANK PAGE

TABLE OF CONTENTS

LIST OF ILLUSTRATIONS

LIST OF SYMBOLS

C_p	pressure coefficient = $\Delta p / \frac{1}{2} \rho V_\infty^2$
h	pancake chamber gap height, inch
h'	viscous coupling gap, inch
N_R	Reynolds number
p	fluid static pressure, psi
P_s	fluid supply pressure, psi
Δp	differential pressure at pick-off, psi
Q	supply flow rate, gpm
R	inlet radius of pancake chamber, inch
r_E	exit radius, inch
r	radial cylindrical coordinate
S	differential output pressure per degree per sec (sensitivity), psi/deg/sec
T	fluid temperature, ^{o}F
t_d	transport time, sec
U	radial velocity, ft/sec
U_E	radial exit velocity, ft/sec
v_t	tangential velocity, component, ft/sec
V	resultant velocity at inlet, ft/sec
V_∞	resultant velocity through outlet, ft/sec
W	axial exit velocity, ft/sec
α	deflection angle, deg
θ	angle of pick-off hole in cylinder with respect to symmetry plane of cylinder, deg
μ	coefficient of viscosity, lb-sec/ft^2
ν	kinematic viscosity, ft^2/sec
ρ	fluid density, lb-sec^2/ft^4
ω	angular rate input to rate sensor, deg/sec

1. INTRODUCTION

The present study was undertaken to establish the feasibility of a high-pressure (3000 psi) hydraulic vortex rate sensor for application in a helicopter hydraulic stability-augmentation system. The feasibility of low-pressure fluid stabilization systems has been demonstrated. The primary component that requires development for implementation in a high-pressure system is the vortex rate sensor. The high-pressure hydraulic vortex rate sensor offers the advantage of having an on-board built-in supply of hydraulic fluid which is used in the primary hydromechanical flight control system of the vehicle. A small amount of hydraulic fluid under high pressure can be diverted from the main system to the vortex rate sensor, used to perform a sensing function, and returned to the main hydraulic system.

The fluid systems approach incorporating the high-pressure hydraulic vortex rate sensor offers improved reliability, maintainability, and reduced cost over conventional electromechanical systems. Hence, a program of research, supported by the U.S. Army Aviation Materiel Laboratories, was conducted at Singer-General Precision, Inc., to demonstrate through the design, fabrication and laboratory test evaluation of a breadboard model the ultimate feasibility and performance characteristics of a high-pressure hydraulic vortex rate sensor to meet specific system requirements.

The vortex rate sensor device under consideration consists basically of an ideal sink flow between two coaxial closely spaced discs with a single outlet at the center of the discs. Figure 1 is a schematic representation of the device. The vortex rate sensor is mounted on the vehicle, and any angular motion of the vehicle imparts an angular rotation to the device. The induced angular rotation of the vortex rate sensor about its axis of symmetry is transmitted to the fluid through viscous coupling between the working fluid and the wall surfaces of the sensor in contact with the fluid. Thus a vortex flow is created. The circumferential velocity of a fluid particle increases or "is amplified" as the particle approaches the outlet sink, since the velocity ideally is inversely proportional to the radial distance from the axis of the sink outlet. Viscous effects influence the behavior of this vortex flow and must be considered in the design of an angular rate sensor. A suitable signal pick-off device that senses this circumferential velocity, either in the form of a pressure differential or a flow differential, provides a sensor function making it possible to detect small rates of rotation.

The present experimental program is directed toward evaluating the performance of a hydraulic vortex rate sensor over a wide range of operating temperatures($-10^{\circ}F$ to $160^{\circ}F$) and pressures (100 psi - 3000 psi). A variable-geometry capability was incorporated in the design and fabrication of the experimental model so that the effects of the vortex chamber diameter, passage gap heights, and signal pick-off location on the signal output of the device could be evaluated.

1. INTRODUCTION

The present study was undertaken to establish the feasibility of a high-pressure (3000 psi) hydraulic vortex rate sensor for application in a helicopter hydraulic stability-augmentation system. The feasibility of low-pressure fluid stabilization systems has been demonstrated. The primary component that requires development for implementation in a high-pressure system is the vortex rate sensor. The high-pressure hydraulic vortex rate sensor offers the advantage of having an on-board built-in supply of hydraulic fluid which is used in the primary hydromechanical flight control system of the vehicle. A small amount of hydraulic fluid under high pressure can be diverted from the main system to the vortex rate sensor, used to perform a sensing function, and returned to the main hydraulic system.

The fluid systems approach incorporating the high-pressure hydraulic vortex rate sensor offers improved reliability, maintainability, and reduced cost over conventional electromechanical systems. Hence, a program of research, supported by the U.S. Army Aviation Materiel Laboratories, was conducted at Singer-General Precision, Inc., to demonstrate through the design, fabrication and laboratory test evaluation of a breadboard model the ultimate feasibility and performance characteristics of a high-pressure hydraulic vortex rate sensor to meet specific system requirements.

The vortex rate sensor device under consideration consists basically of an ideal sink flow between two coaxial closely spaced discs with a single outlet at the center of the discs. Figure 1 is a schematic representation of the device. The vortex rate sensor is mounted on the vehicle, and any angular motion of the vehicle imparts an angular rotation to the device. The induced angular rotation of the vortex rate sensor about its axis of symmetry is transmitted to the fluid through viscous coupling between the working fluid and the wall surfaces of the sensor in contact with the fluid. Thus a vortex flow is created. The circumferential velocity of a fluid particle increases or "is amplified" as the particle approaches the outlet sink, since the velocity ideally is inversely proportional to the radial distance from the axis of the sink outlet. Viscous effects influence the behavior of this vortex flow and must be considered in the design of an angular rate sensor. A suitable signal pick-off device that senses this circumferential velocity, either in the form of a pressure differential or a flow differential, provides a sensor function making it possible to detect small rates of rotation.

The present experimental program is directed toward evaluating the performance of a hydraulic vortex rate sensor over a wide range of operating temperatures($-10^{\circ}F$ to $160^{\circ}F$) and pressures (100 psi - 3000 psi). A variable-geometry capability was incorporated in the design and fabrication of the experimental model so that the effects of the vortex chamber diameter, passage gap heights, and signal pick-off location on the signal output of the device could be evaluated.

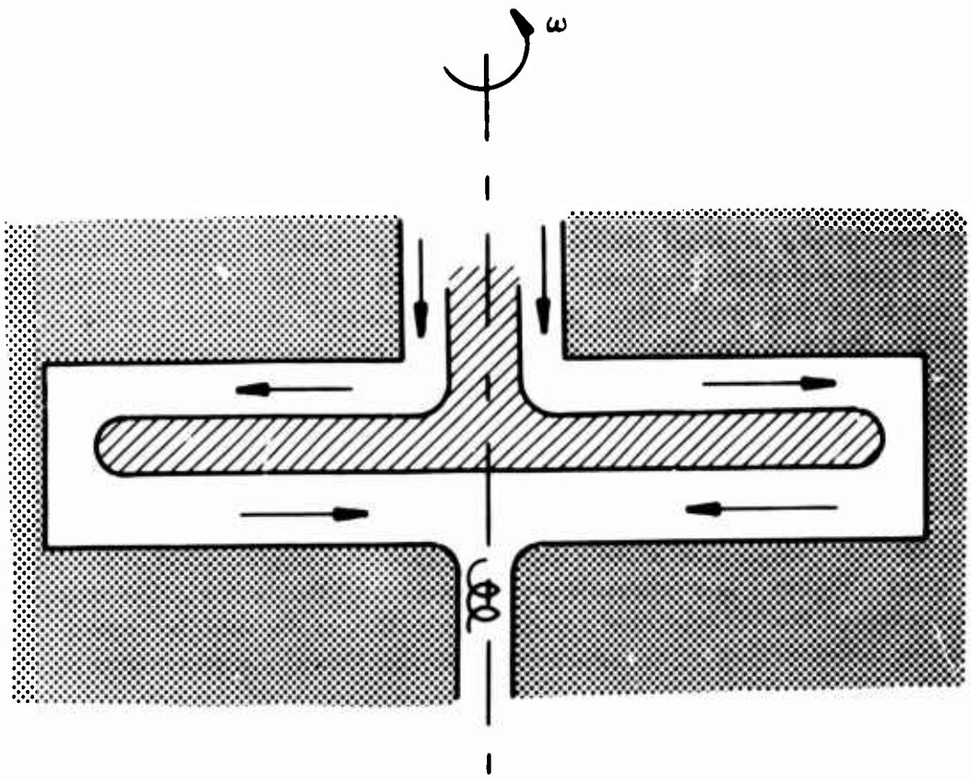

Figure 1. Schematic of Vortex Rate Sensor.

In addition, a limited theoretical trade-off analysis was performed to determine the functional relationships between the output signal and geometric and flow parameters. Based upon this analysis, three chamber diameters were fabricated.

2. EXPERIMENTAL EQUIPMENT

To conduct the experimental investigation of the high-pressure hydraulic vortex rate sensor, sophisticated peripheral equipment was used to supply hydraulic fluid at controlled pressures, flows, and temperatures. The principal components are the hydraulic power supply and test console, which, when interconnected, require only an electrical power source and shop air to be operational. This model, shown in Figure 2, is manufactured by Sprague Engineering.

The hydraulic power supply is contained within a common frame and provides micronically filtered, temperature-controlled test fluid at operating pressures up to 5000 psig and controlled flows to 50 gpm to the test console. Test fluid storage is provided by a 115-gallon reservoir which serves the two stations.

Micronic fluid filtration is provided by filters in the supply system. The four high-pressure filters have integral differential pressure switches which give a red light indication on the test stand control panel when a clogged filter condition exists. A low-pressure filter is installed in the boost system to provide filtration of fluid before it reaches the main pump. A sight tube and bleed valve assembly are connected to the low-pressure filter to permit bleeding of any entrained air from the system.

The main pump volume control and pump compensator are remotely controlled from the test console. The pump is supercharged by a boost pump which supplies fluid from the main reservoir at low pressure to the inlet port of the main pump. Boost pressure to the main pump is controlled by a low-pressure relief valve set to relieve boost pressure at approximately 75 psig.

Fluid cooling is provided by a 2-pass heat exchanger. Fluid temperature is controlled by a temperature control valve installed in the water inlet line with the temperature pick-up mounted in the boost system.

For safety in operation, a pressure switch is installed in the main pump motor. The motor will not continue to operate if boost pressure is insufficient. Figure 3 shows the test console which provides the hydraulic fluid at controlled conditions. The test console consists of a common frame with an all-steel cabinet: 6.5 feet high, 20 feet long, and 3.5 feet wide with a stainless steel work sink. The work sink drains test fluid spillage into a 30-gallon sump reservoir. The reservoir is equipped with a float switch which when activated will start a centrifugal pump. The fluid is then pumped through two 10-micron filters and returned to the main reservoir on the hydraulic power supply.

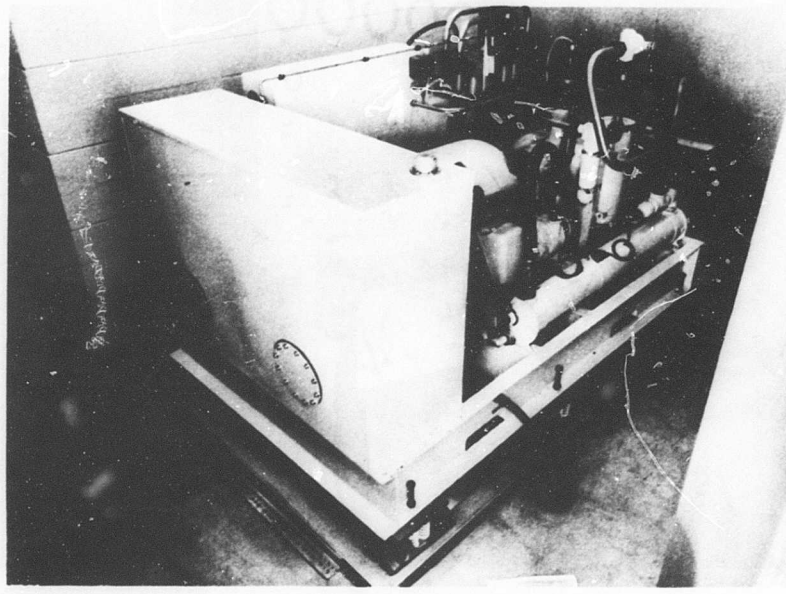

Figure 2. Hydraulic Power Supply.

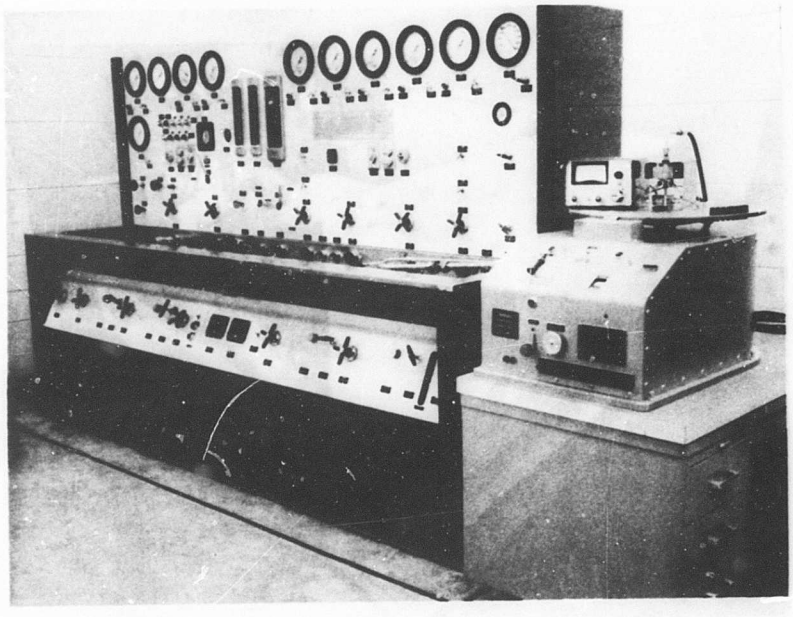

Figure 3. Test Console.

The hydraulic power supply system includes a piston-type accumulator which has an operating pressure of 6000 psig. The accumulator is equipped with a pressure gage and a panel-mounted shutoff valve for isolating the accumulator from the main system.

A hand pump is installed in the main system to provide static pressures from 0 to 15,000 psig. The three panel-mounted flowmeters provide sufficient range for flow tests up to the delivery capacity of the main pump. Return flow through the flowmeters is controlled by shutoff valves on the control panel. A relief valve is provided to protect the flowmeters from overpressure. When pressure to the flowmeters exceeds 100 psig, the valve relieves pressure through a panel-mounted sight flow indicator and back to the main reservoir.

The solenoid-operated bypass valve is normally in the bypass position when power is off; when power is turned on, the valve is automatically closed. A toggle switch on the control panel provides control for bypassing fluid for test operations. A manual bypass valve is also provided for throttling bypass fluid.

Pressure-reducing valves in each of the pressure circuits provide controlled pressure in test operations. The valves are adjustable from 100 to 5000 psig.

Flow is measured with three turbine flowmeters which are matched in flow rates to three direct-reading flowmeters. The turbine flowmeters can be used singly by interconnecting a pressure and return port with the selected turbine flowmeter and opening the flowmeter bypass valve. To incorporate the direct-reading flowmeter, the selected turbine flowmeter is interconnected to the like-numbered direct-reading flowmeter.

Flow can be measured in volumetric or gravimetric units merely by selecting a sampling time so that the unit flow rate through the flowmeter will result in a reading of some integral power of ten on the counter.

Two basic formulas are useful for determining the sampling time, one for volumetric and the other for gravimetric flow rate units.

For Volumetric Units of GPM:

$$T = \frac{60}{K} \times M$$

where T = Time (duration of sample) in seconds.

K = Sensing element constant in cycles per gallon.

M = Multiplier to obtain proper power of ten. It depends upon the full-range flow reading.

The following table indicates specifications of control functions and operational ranges of the power supply and test console.

SPECIFICATIONS OF POWER SUPPLY AND TEST CONSOLE	
Item	**Specification**
Test Medium	MIL-H-5606 Oil
Capacity	50 gpm max. @ 3000 psig 30 gpm max. @ 5000 psig
Static Pressure	15,000 psig (Approx.)
Overall Dimensions:	
Cabinet	
Height	78 inches
Length	120 inches
Width	42 inches
Remote Power Supply	
Length	88 inches
Width	55 inches
Test System Components:	
Main Pump	50 gpm @ 3000 psig @ 1800 rpm 30 gpm @ 5000 psig @ 1800 rpm
Drive Motor	100 HP, 1800 rpm, 440 v, 3ϕ, 60 c
High-Pressure Filters	
Item 111	2 ea. 10 micron nominal
Item 119	2 ea. 5 micron nominal
Accumulator	Piston type, 6000-psig operating pressure, 200-cu. in. oil volume
Pulsation Dampener	6000-psig operating pressure, 50-cu. in. oil volume
Pressure-Reducing Valve	Adjustable 100-5000 psi
Temperature Controller	Set at 110°F

Item	Specification
Boost System Components:	
Pump	55 gpm @ 35 psi @ 1700 rpm
Heat Exchanger	2-pass, rated to dissipate 35 HP of heat with 30 gpm of cooling water
Filter	10 micron nominal
Relief Valve	Adjustable, set @ 75 psig
Instrumentation:	
Flowmeters	Direct reading, calibrated at 100°F using MIL-H-5606 hydraulic oil
	0.04-0.5 gpm range
	0.42-5.05 gpm range
	4.2-50.5 gpm range
Pressure Gages	0-160 psi range (2)
	0-6000 psi range (7)
	0-20,000 psi range (1)
Temperature Gage	50°-300°F range
Differential Pressure Switches	32 ± 4

The Genisco rate table (Model C181) is 36 inches long, 24 inches wide, and 20 inches high. It operates at 105-115 volts, 60 cycles, and is single phase. The table capacity is 100 pounds, and it provides continuously variable angular rate from 0.01 deg/sec to 1200 deg/sec. The table rate is controlled by a simple rate control handwheel on the console panel.

The heart of the experimental equipment, the high-pressure hydraulic vortex rate sensor, was designed and fabricated to meet the rigorous test requirements of this study. The housing of the rate sensor is made from aluminum. The rate sensor is a variable-geometry configuration capable of withstanding hydraulic pressures greater than 6000 psi. The breadboard model allows evaluation over a range of useful parameters such as pancake chamber diameter, pancake chamber gap height, and viscous coupling gap. The pancake chamber diameter can be varied from 3 inches to 6.5 inches by simply interchanging parts. Diameters of 3 inches, 3.5 inches, 5 inches, and 6.5 inches were tested. A fixed-geometry 4-inch-diameter vortex rate sensor was also fabricated. The pancake chamber gap height for any diameter of the variable-geometry rate sensor was designed to be continuously variable from 0 to 1 inch. The viscous coupling gap is also continuously variable. Figure 4 shows the experimental model with the signal pick-off probe dials mounted on the underside. Also shown is the model mounted on the rate table. A schematic of the configuration is shown in Figure 5. Fluid enters the rate sensor from the supply at I and flows through the channel, J, into the viscous coupling gap, the dimension of which is h', and turns 180 degrees into the pancake chamber of radius R and pancake chamber gap height h. The fluid exits through the sink of fixed radius r_E at the center of the pancake chamber. The signal pick-off probes and dials for changing the pick-off probe position within the sink are also shown. The pick-off probe positions are varied by rotating the dial K.

The viscous coupling gap, h', and the chamber gap height, h, are varied by turning the screws A and B clockwise or counterclockwise. O-ring seals prevent leakage around critical areas in the rate sensor as the geometric parameters are varied. The diameter of the sink outlet, located at the center of the chamber, can be varied by removing the section E. The dial settings are calibrated in degrees so that at a zero-degrees reading on the dial, the pick-off probes are touching. At a reading of 720 degrees on the dial, the pick-off probes are farthest apart. The fluid that does not enter the pick-off probes exits through the sink tube and returns to the control console. Figure 6 shows a schematic of the signal pick-off probes. The pick-off assembly consists basically of two pick-off probes connected by long stems to the dial assembly. Signal flow passes through the probes, and the differential pressure between the pick-off probes induced by an angular rate imparted to the rate sensor is sensed by a Pace transducer. The Pace transducer is a variable reluctance pressure-measuring instrument which converts the deflection of a diaphragm into an electrical signal (voltage). For most testing, a 1-psi diaphragm was used.

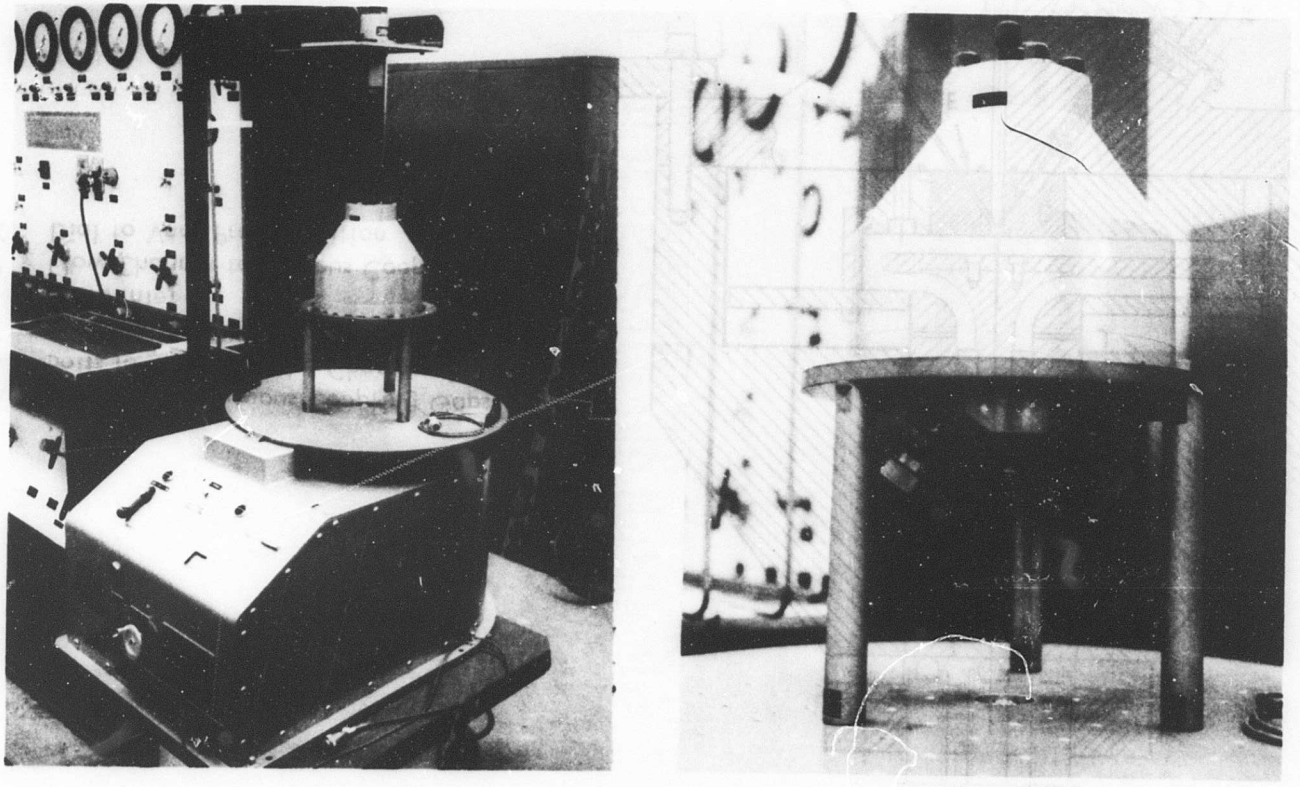

Figure 4. High-Pressure Hydraulic Vortex Rate Sensor Test Apparatus.

A Bolt to Vary Viscous Coupling Gaps
B Bolts to Vary Pancake Chamber Gap Height
E Sink Outlet Member
I Fluid Inlet
J Flow Channel to Viscous Coupling Gap
K Dial to Vary Probe Position

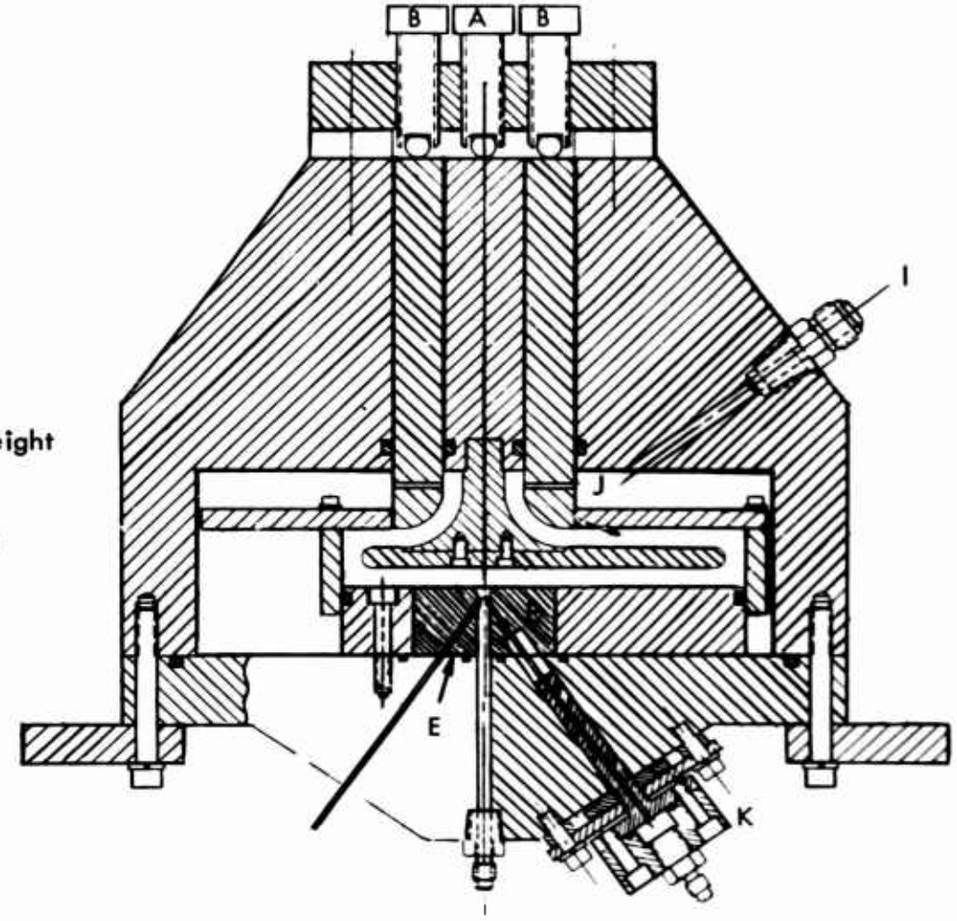

Figure 5. Schematic of Variable-Geometry Vortex Rate Sensor.

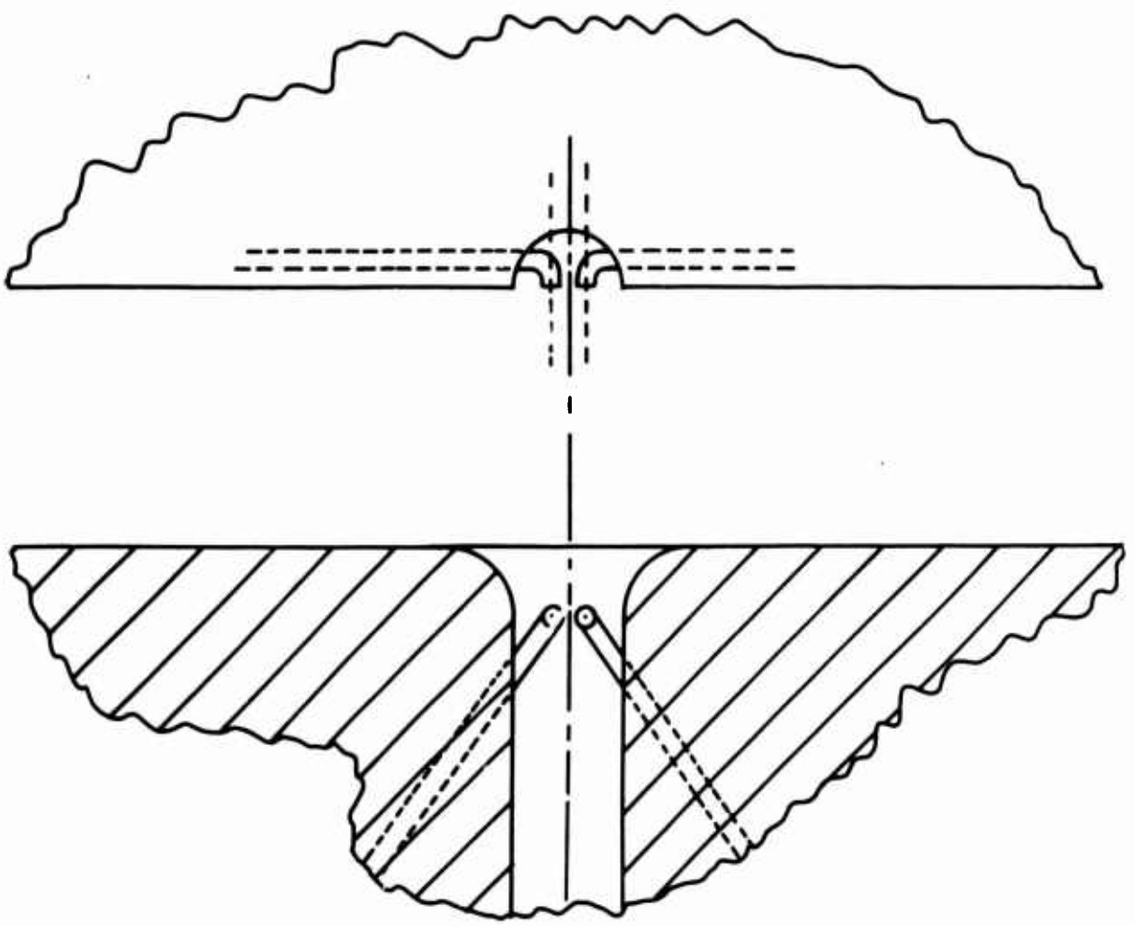

Figure 6. Signal Probe Configuration.

Figure 7 shows the components of the experimental vortex rate sensor assembly including the housing, the discs which form the viscous coupling surfaces, the rings which form the diameter of the chamber, and the cylindrical rods which are used to vary chamber gap height and the viscous coupling gap.

Figure 8 shows the components of the signal pick-off assembly. In Figure 9, the entire experimental assembly and peripheral equipment, with the exception of the supply pump, is shown. Figure 9 is a closeup of the vortex rate sensor, the rotary union, the supply and return lines for the working fluid, the Pace transducer, and the regulating valves. Figure 9 shows the hydraulic and electronic equipment in its operational state. The rotary union consists of a "piggyback" arrangement of two unions, each with independent sealing elements. It is well suited for applications requiring widely varying pressures. It operates at a maximum hydraulic pressure of 3000 psi and a maximum speed of 250 rpm.

The working fluid is MIL-H-5606 oil. This oil is well suited for operation in the severe pressure and temperature conditions required for the experiments. It must flow at temperatures well below $0^{\circ}F$, and it cannot break down at high temperatures after long operation. Two important properties of the MIL-H-5606 are shown in Figure 10 and 11: the viscosity vs temperature and specific gravity vs temperature, respectively. It is seen in Figure 10 that the viscosity increases by two orders of magnitude as the oil temperature decreases from $300^{\circ}F$ to $-50^{\circ}F$.

In addition, a fixed-geometry vortex rate sensor, shown in Figure 12, was fabricated in the preliminary testing program. The only geometrical parameter on this sensor that is variable is the pancake chamber gap height. However, two signal pick-off configurations, a conventional cylindrical element and a signal probe, can be interchanged by removing the sink section which is an insertable element. The major portions of the device were fabricated from AISI 440C stainless steel. The principal individual elements, including the interchangeable sink outlet, are shown in Figure 13. A schematic of the entire configuration is shown in Figure 14, and a sketch of the cylindrical signal pick-off element is shown in Figure 15. Two 0.008-inch-diameter holes are located 0.025 inch from each side of the transverse axis of symmetry of the cylinder. These holes are oriented at 45 degrees with respect to the cross-sectional plane of the sink passage and are both located along the same cylinder generator line.

Figure 16 shows the orientation outlet of the pressure signal pick-off probes in the sink. The orientation of the probes within the sink differs from the probe orientation in the sink of the variable-geometry rate sensor.

The differential signal output pressure was measured with a Pace Type PeD variable reluctance diaphragm-type transducer and a Pace Model CD25 transducer indicator. The maximum frequency response of this transducer is approximately 1000 cycles/sec.

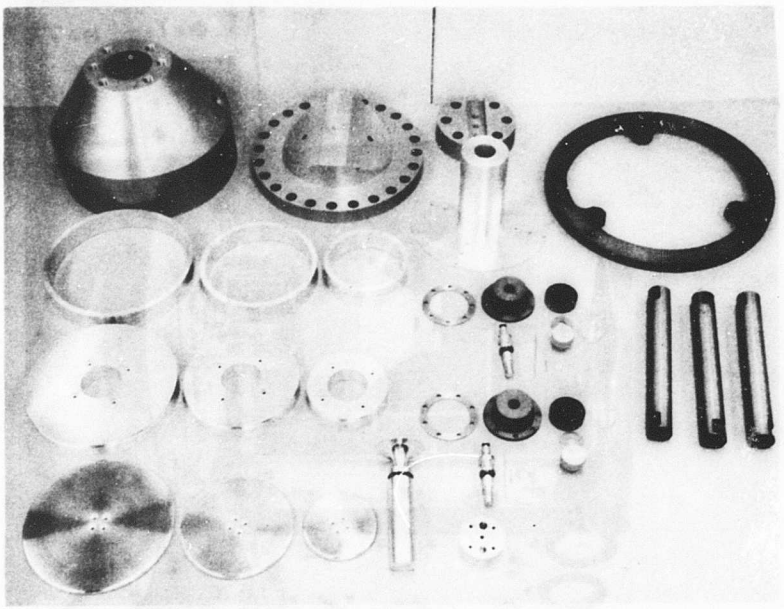

Figure 7. Experimental Test Apparatus Components.

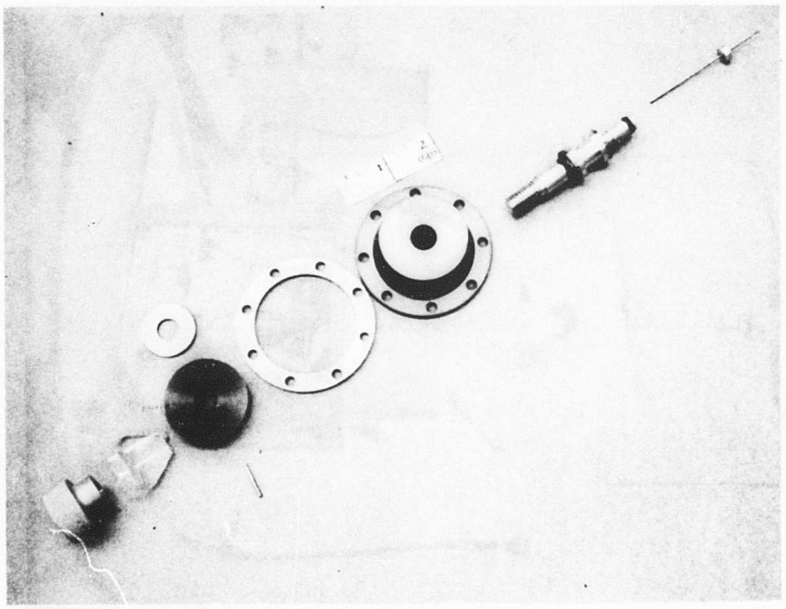

Figure 8. Signal Pick-off Components.

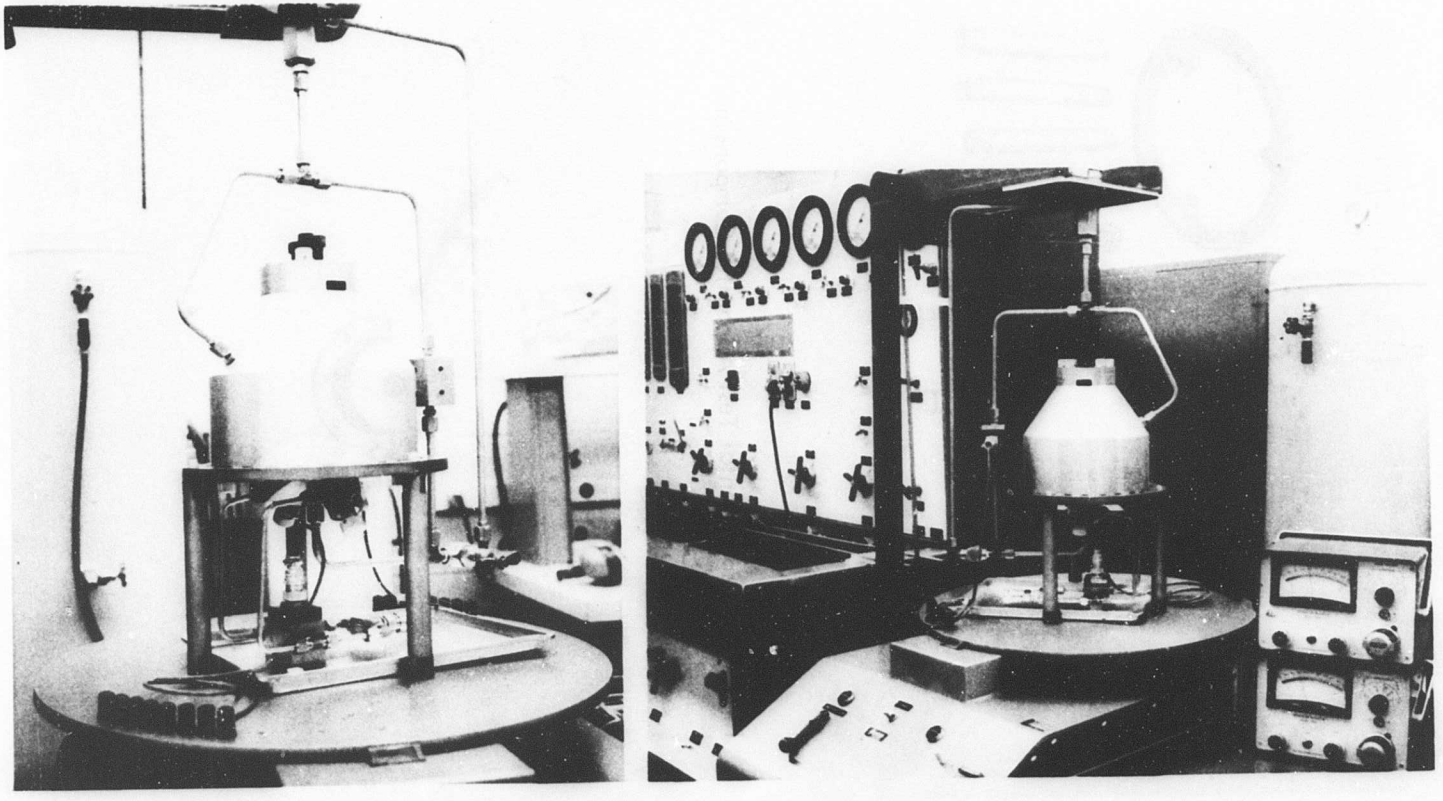

a. b.

Figure 9. Variable-Geometry Vortex Rate Sensor and Peripheral Equipment.

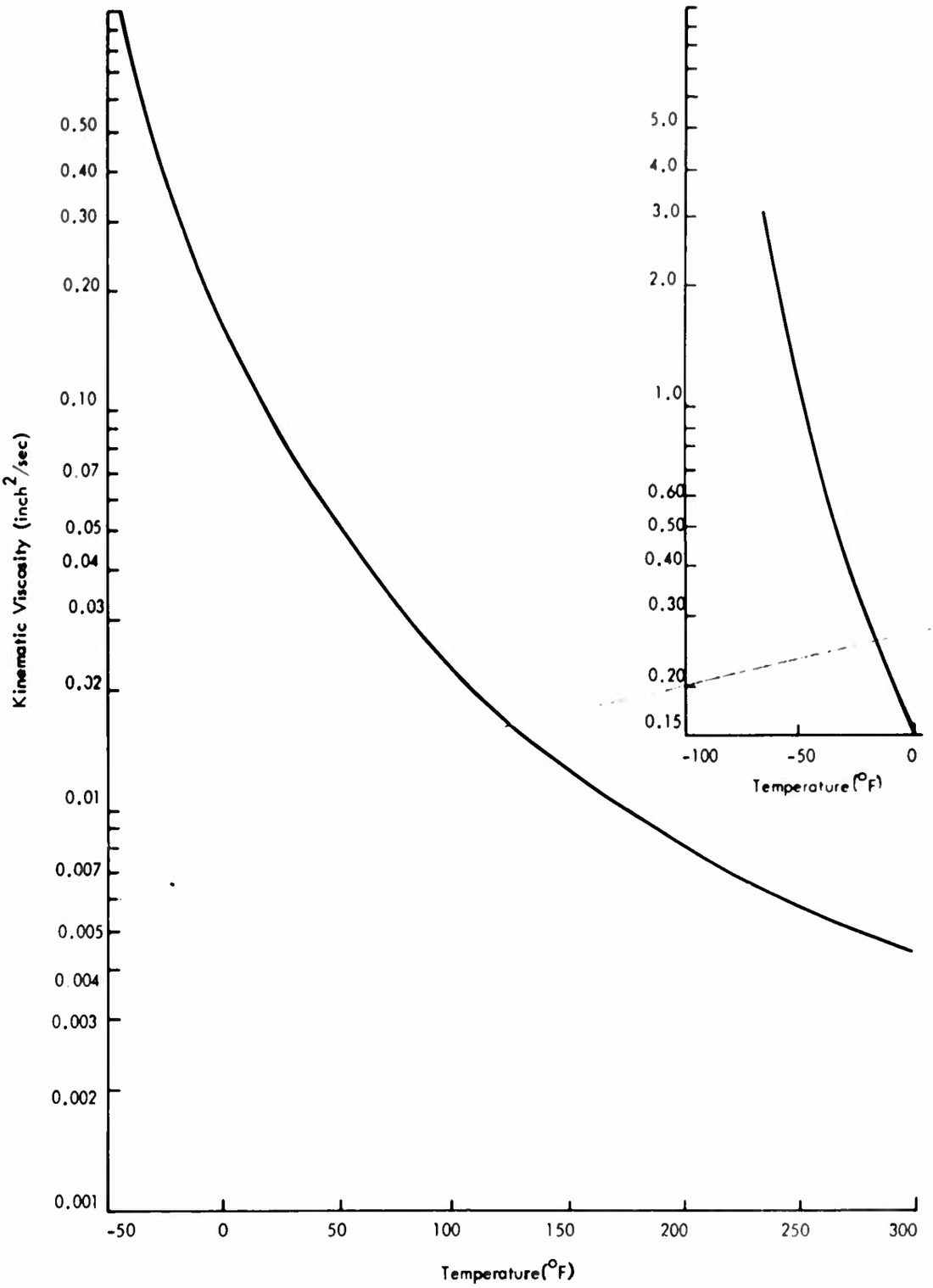

Figure 10. Kinematic Viscosity vs Temperature (MIL-H-5606 Oil).

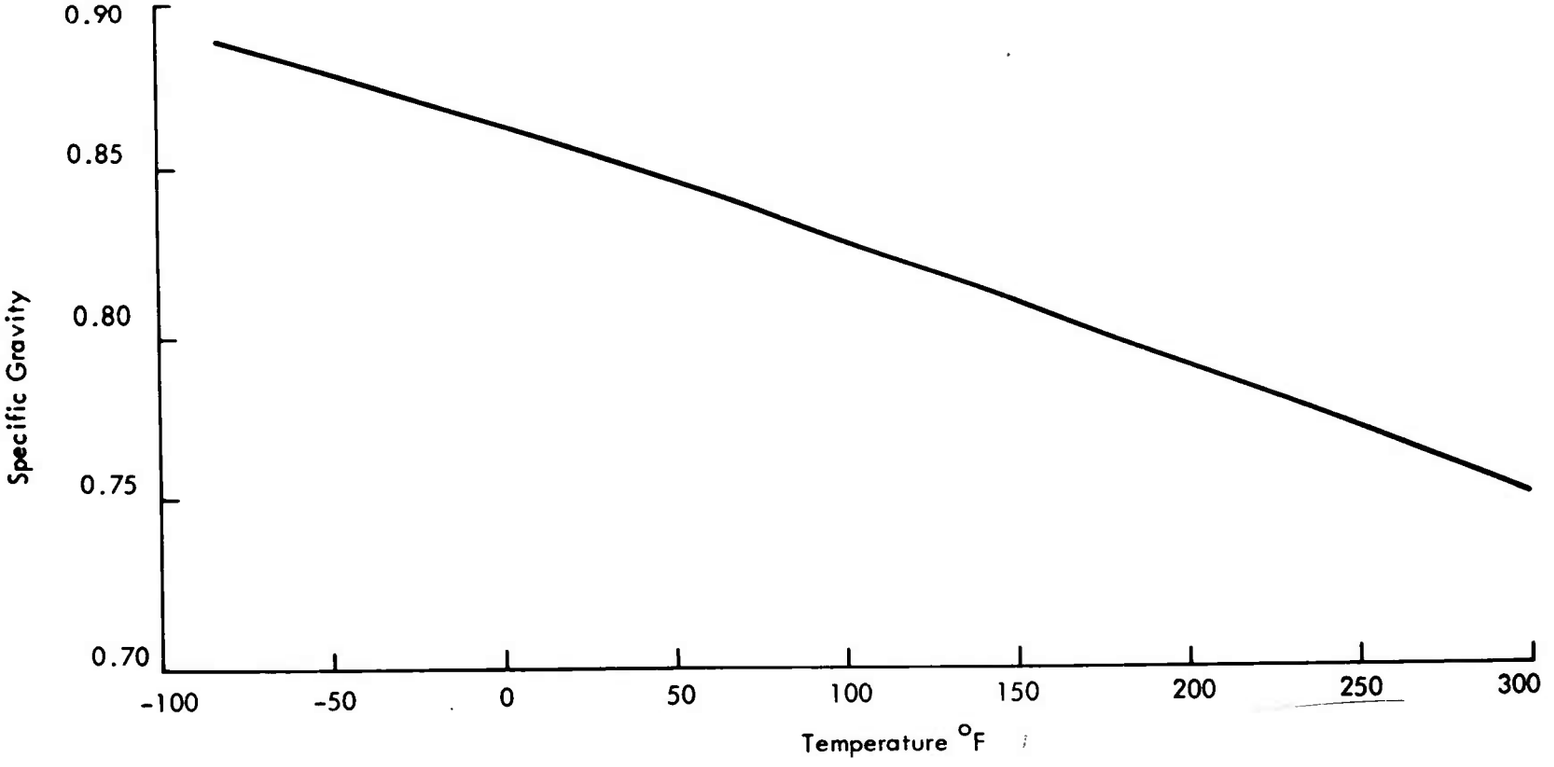

Figure 11. Specific Gravity vs Temperature (MIL-H-5606).

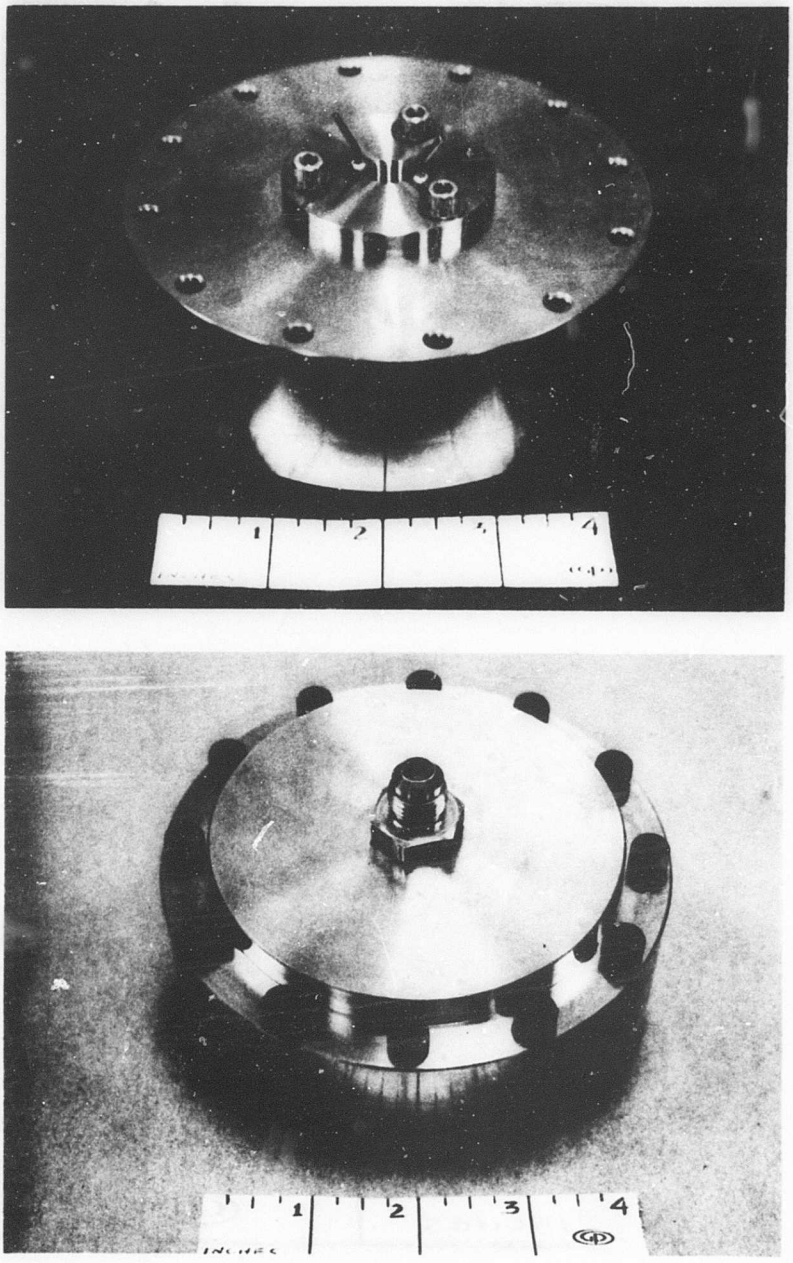

Figure 12. Assembled Fixed-Geometry Vortex Rate Sensor.

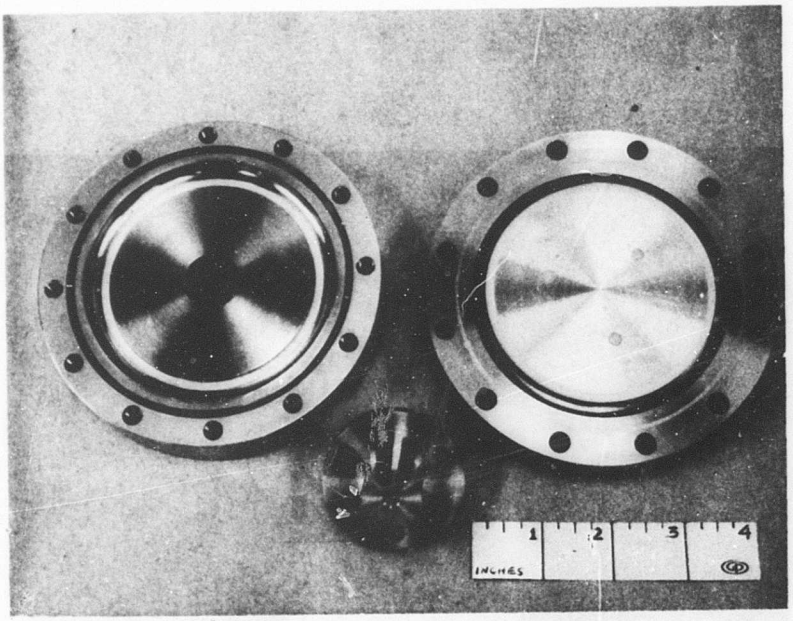

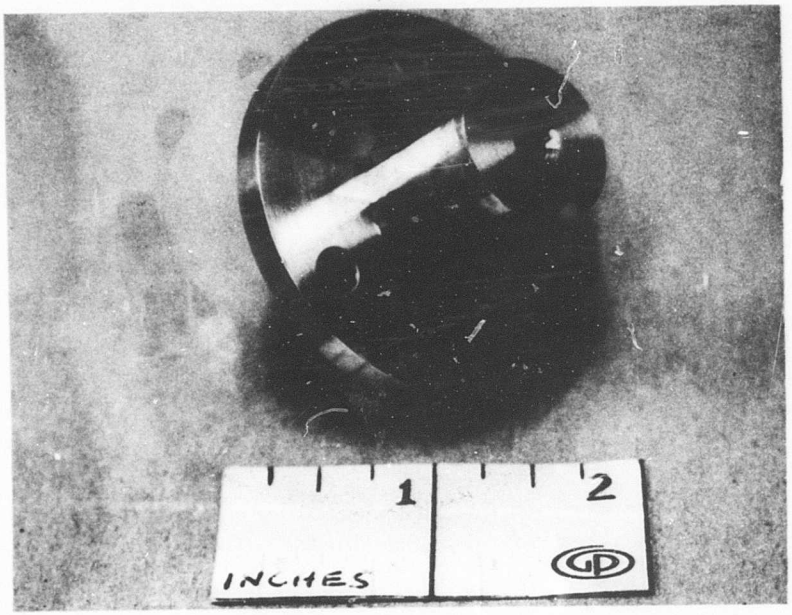

Figure 13. Details of High-Pressure Hydraulic Vortex Rate Sensor.

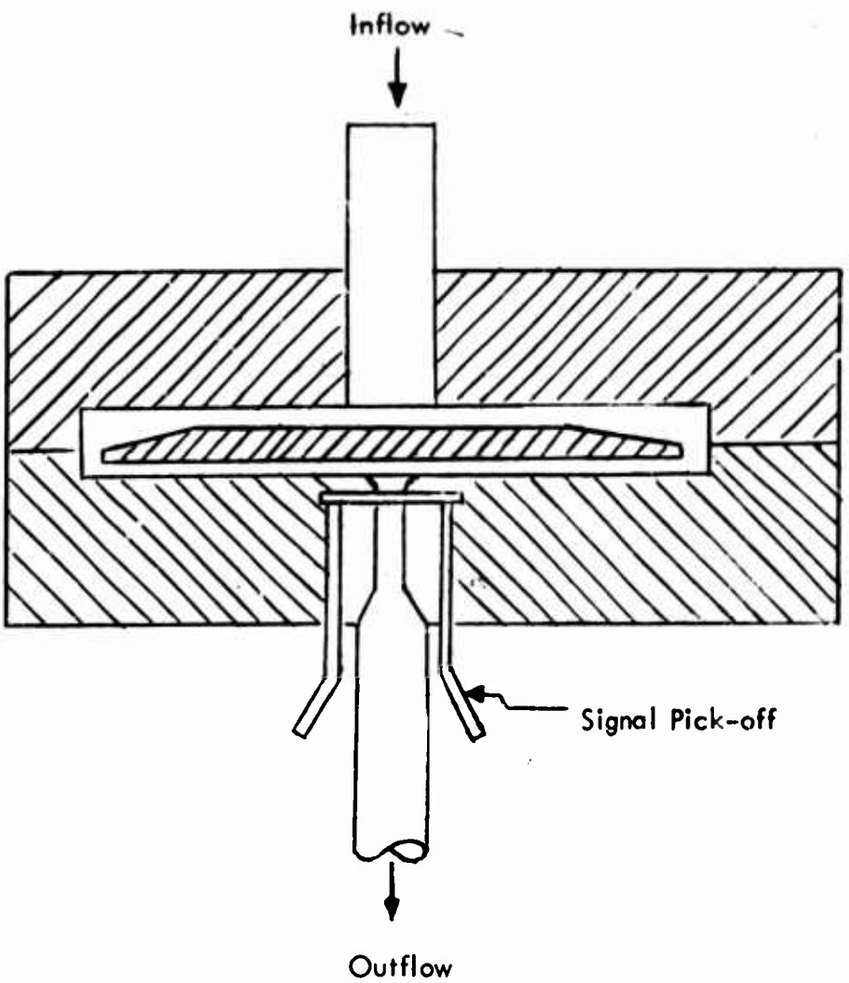

Figure 14. Schematic of Fixed-Geometry Vortex Rate Sensor.

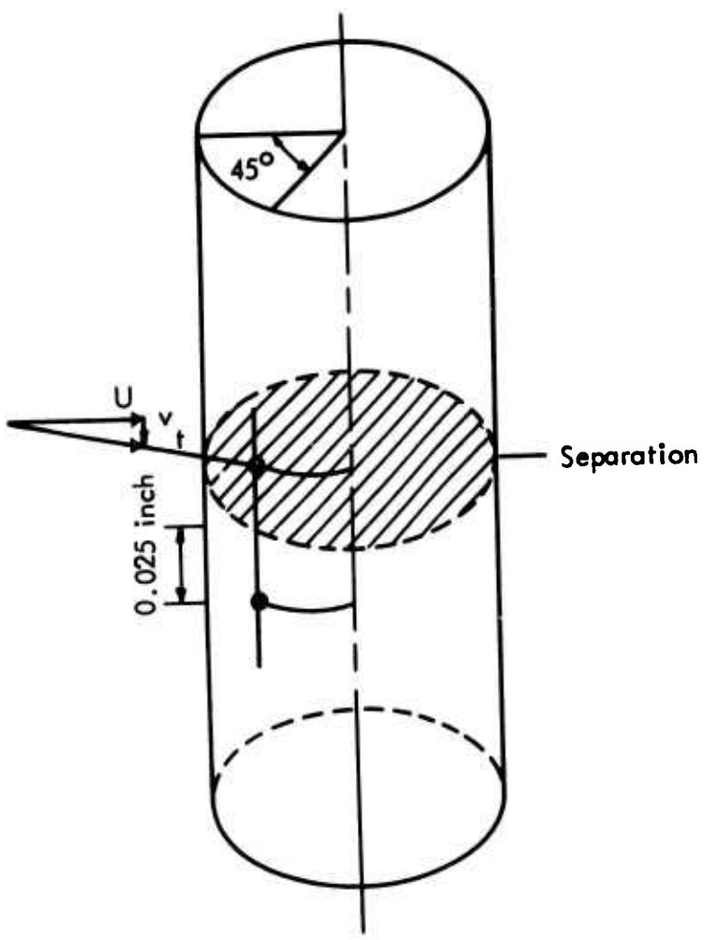

Figure 15. Cylindrical Signal Pick-off Element.

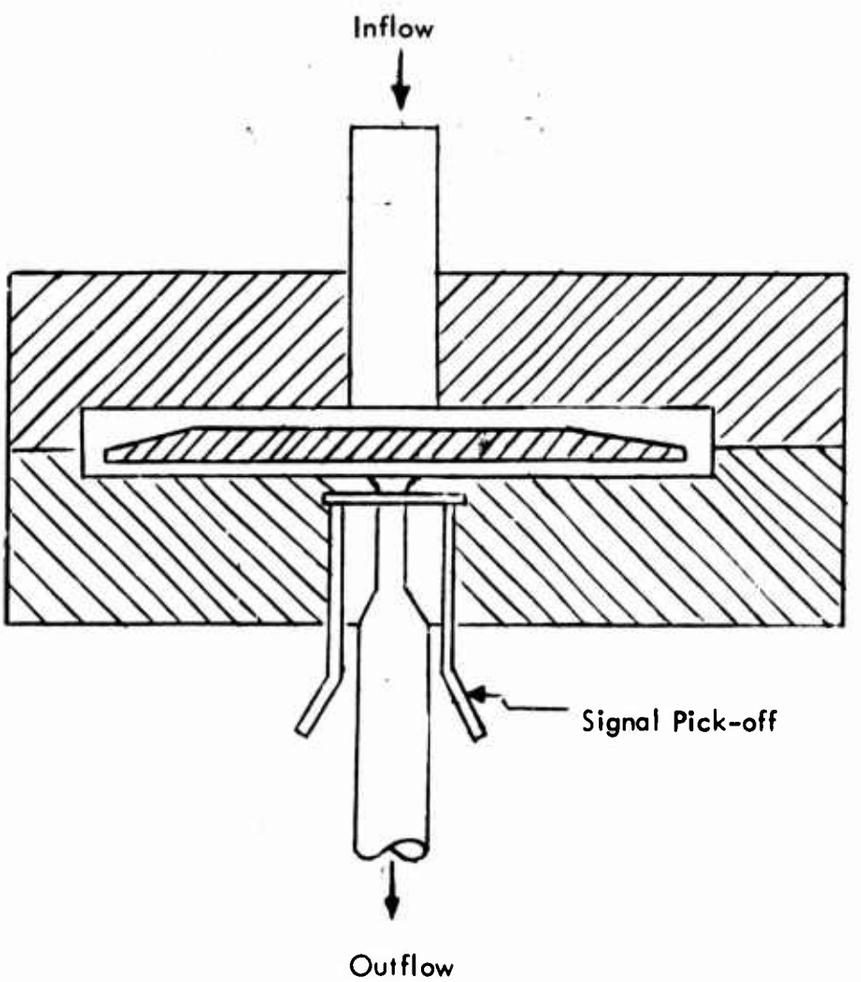

Figure 14. Schematic of Fixed-Geometry Vortex Rate Sensor.

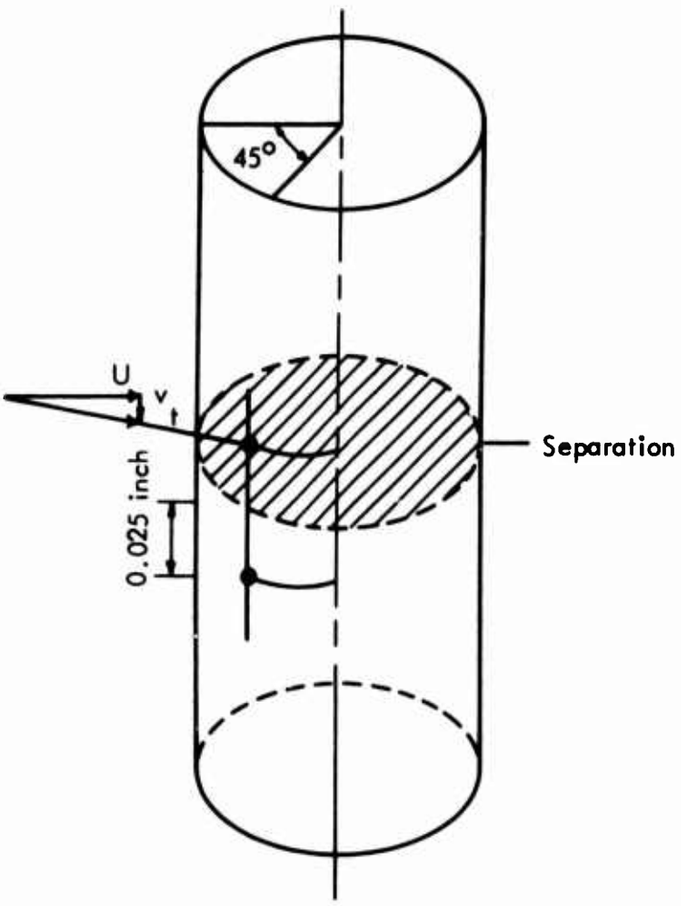

Figure 15. Cylindrical Signal Pick-off Element.

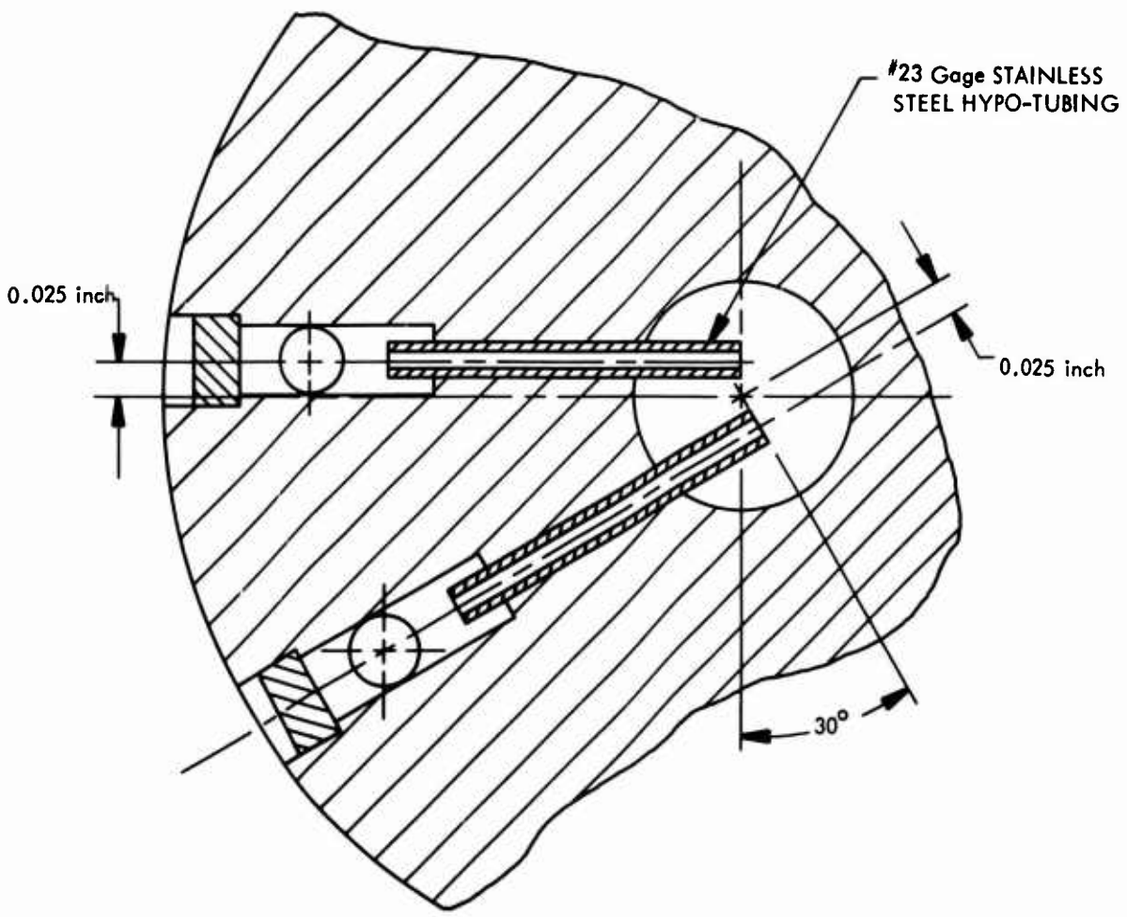

Figure 16. 4-inch Sensor Modified Signal Pick-off Arrangement.

Noise (pressure fluctuations) was measured with a Kistler Model 603A quartz pressure transducer and a Model 504 electrostatic charge amplifier. The output of the charge amplifier was connected into a General Radio Type 1568-A sound analyzer having a high-resolution 1 percent bandwidth. The output of this analyzer is mechanically coupled to a graphic level recorder which is contained within the instrument.

3. EXPERIMENTAL RESULTS

The experimental program was divided into two general phases. The first phase consisted of the evaluation of the variable-geometry vortex rate sensor performance in a no-flow or blocked-output condition. The effects of geometric and flow parameters such as Reynolds number on the pressure output signal were evaluated. In the second phase of the investigation, signal output at the pick-offs was obtained for finite load conditions. This finite condition represents a realistic situation in which signal flow and/or pressure is used in an actuation system.

3.1 PHASE I - BLOCKED OUTPUT CHARACTERISTICS

The principal performance parameter which was evaluated in the experimental program was the differential output pressure per degree per second. Two impact pressure signal probes were mounted in the sink outlet of the rate sensor near the turning section from the flat chamber into the outlet. Angular rate was imparted to the rate sensor from the rate table. The resulting amplification of the induced tangential velocity of the working fluid was sensed by the signal pick-offs as a pressure differential between each signal pick-off probe and was converted to an electrical signal by a variable reluctance Pace transducer. For all tests, two angular rates were chosen for convenience and to meet test requirements. These were 5 deg/sec and 50 deg/sec. The flow rate of 0.5 gpm was maintained in all experiments. Based on the trade-off studies that were conducted, three chambers were fabricated: 6.5, 5, and 3.5 inches in diameter.

First, the 6.5-inch-diameter configuration was tested. Figure 17 shows the differential output signal pressure as a function of the pancake chamber gap height for two viscous coupling gaps, 0.025 and 0.100 inch. The curves shown are for angular rates of 5 deg/sec and 50 deg/sec. For convenience the differential output signal pressure per degree per second will be referred to as the "sensitivity" in the remainder of the report. The sensitivity, from Figure 17, is approximately ten times greater for an angular rate of 50 deg/sec than for an angular rate of 5 deg/sec. This result is reflected in the linearity of the device. For example, Figure 18 shows a typical linearity curve; namely, the functional relationship between the differential output pressure signal and the angular rate in both the clockwise and counterclockwise directions. Counterclockwise rotation of the device appears as a negative differential pressure only in a relative sense since it is the opposite of the flow that the signal pick-off probes "see" in clockwise rotation; i.e., the flow pressure is higher in one signal pick-off probe than in the other and vice versa. Above 40 deg/sec the pressure signal begins to "flatten out" and linearity is lost. This is also seen in Figure 17, where the sensitivity falls away from its linear rise much more rapidly at an angular rate of 50 deg/sec than at 5 deg/sec. The maximum signal obtained was about 0.0052 psi/deg/sec at a pancake chamber gap height of 0.45 inch. An important result shown is that the sensitivity is independent of the

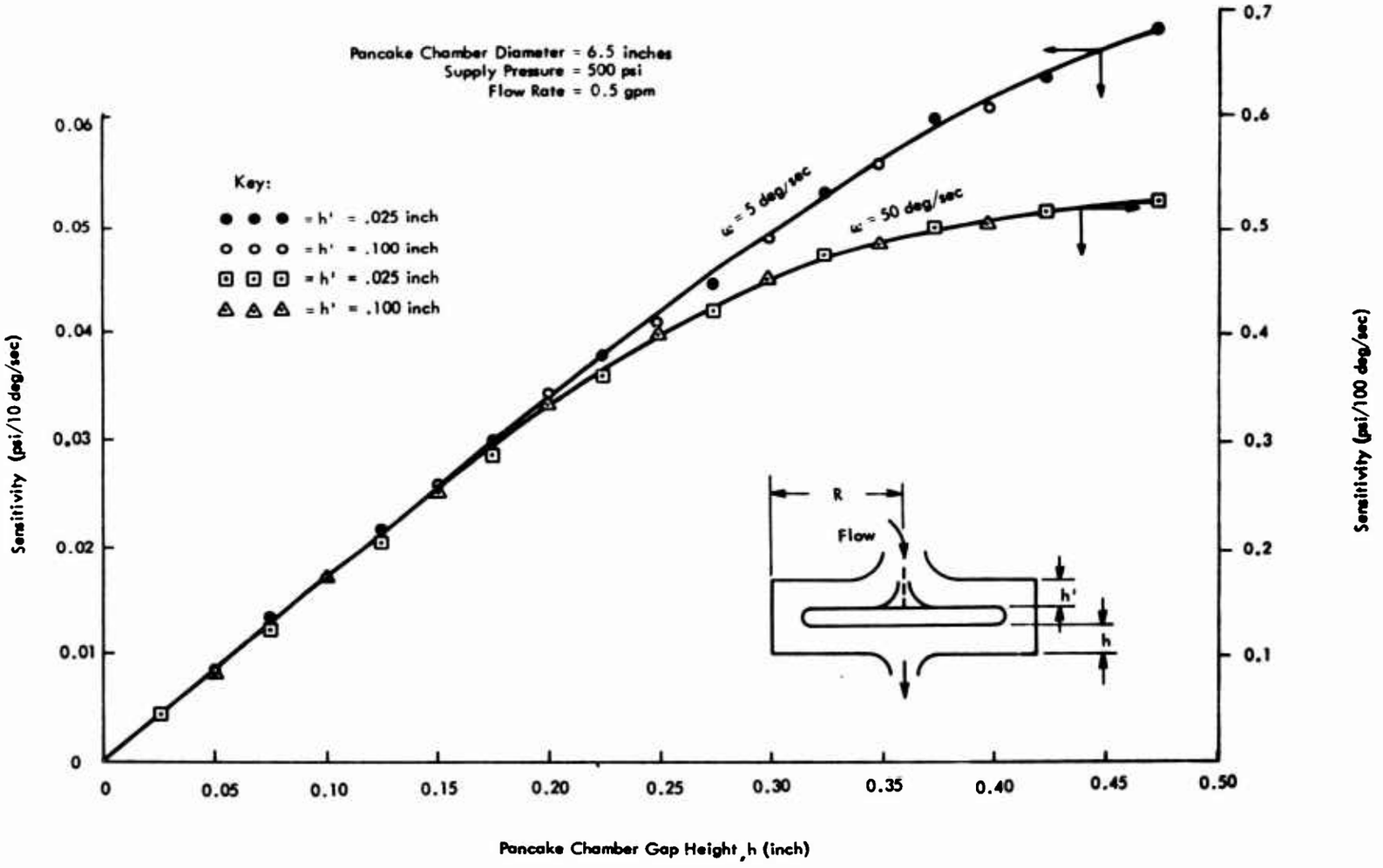

Figure 17. Sensitivity vs Pancake Chamber Gap Height.

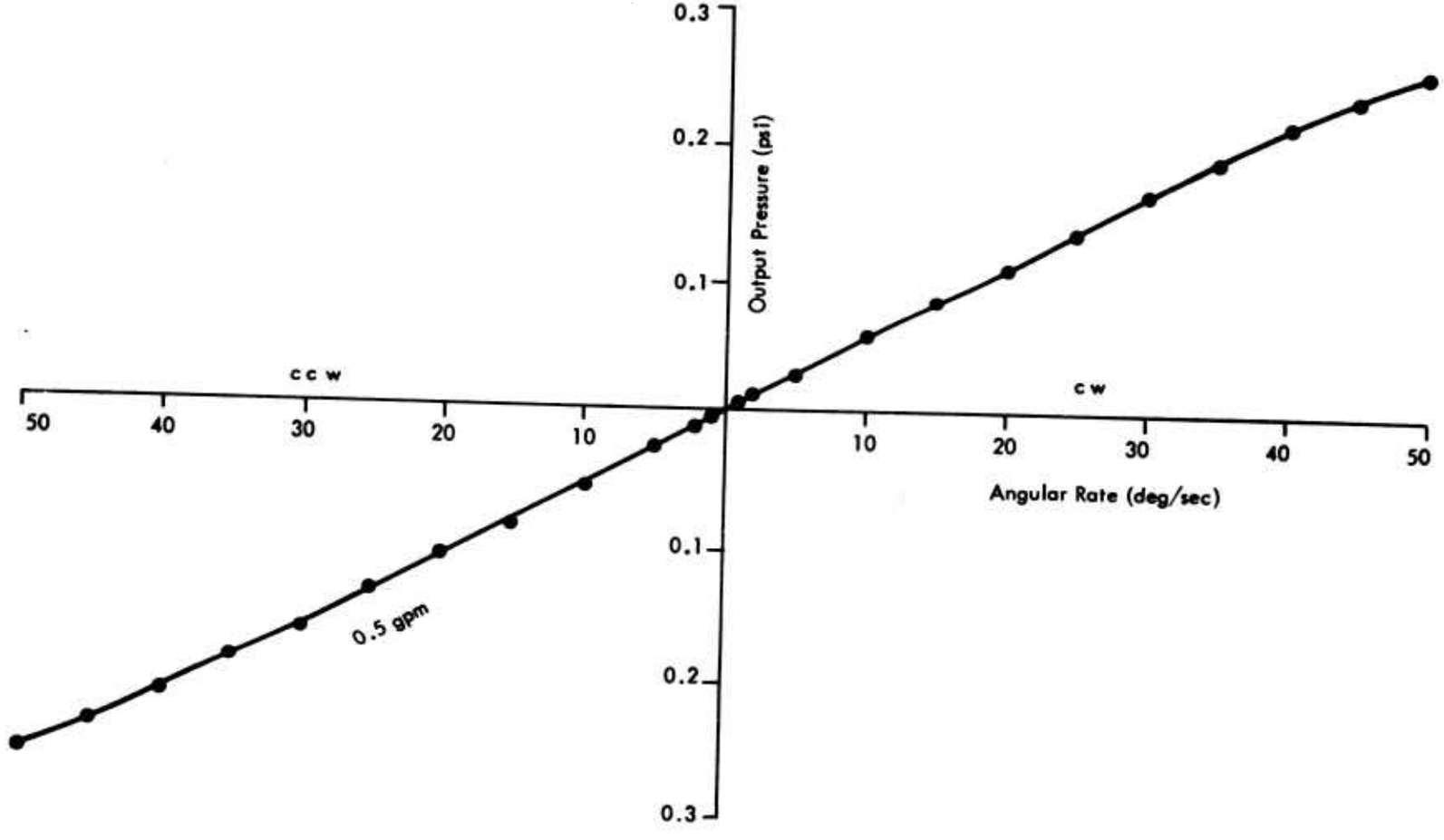

Figure 18. Differential Output Pressure Signal vs Angular Rate.

viscous coupling gaps incorporated into the experiment. The viscous coupling gap was varied from 0.025 inch to 0.1 inch. The temperature of the working fluid supplied to the vortex rate sensor was 85°F.

Second, the 5.0 inch pancake chamber diameter configuration was tested. Figure 19 shows the sensitivity as a function of pancake chamber gap height for three viscous coupling gaps 0.025 inch, 0.05 inch and 0.075 inch. The maximum sensitivity is approximately 0.0052 psi/deg/sec at a pancake chamber gap height of 0.45 inch. In addition, the sensitivity is independent of the viscous coupling gaps that were chosen. The fluid temperature was maintained at 85°F.

Third, the 3.5-inch pancake chamber diameter configuration was tested. Figure 20 shows the sensitivity as a function of pancake chamber gap height for four viscous coupling gaps: 0.025 inch, 0.050 inch, 0.075 inch, and 0.100 inch. The sensitivity again is independent of the viscous coupling gap, h'. The maximum sensitivity is approximately 0.0048 psi/deg/sec at a pancake chamber gap height of 0.45 inch. The fluid temperature was maintained at 85°F.

Fourth, the 3.0-inch-diameter configuration was tested. This is the minimum diameter that can be obtained without an extensive redesign of the sensor. Figure 21 shows the sensitivity as a function of pancake chamber gap height for three viscous coupling gaps: 0.025 inch, 0.050 inch, and 0.100 inch. Again, the sensitivity is independent of the viscous coupling gap h'. The sensitivity is a maximum of 0.004 psi/deg/sec at a pancake chamber gap height of 0.45 inch. The shape of the curve is the same as that for the other diameters, i.e., a monotonic increase in sensitivity with increasing pancake chamber gap height. The fluid temperature was maintained at 85°F.

As the pancake chamber diameter is decreased, the maximum tangential velocity that can be obtained will decrease. In principle, from inviscid flow considerations, conservation of angular momentum predicts that the tangential velocity at an inner radial station behaves like

$$v \sim \frac{RV}{r} \tag{1}$$

where R is the pancake chamber radius and V is the tangential fluid velocity at R. Therefore, the larger the pancake chamber radius R, the greater will be the tangential velocity at a given inner radial station. However, physical size limitations restrict the size of R, and a trade-off must in general be accomplished. In addition, viscous effects modify the relation (1) such that v cannot become unbounded as $r \to 0$, but linearly decreases to zero as $r \to 0$ since viscous forces predominate as $r \to 0$. Figure 22 shows the sensitivity as a function of pancake chamber diameter. The diameters of 6.5, 5.0, 3.5, and 3.0 inches represent the

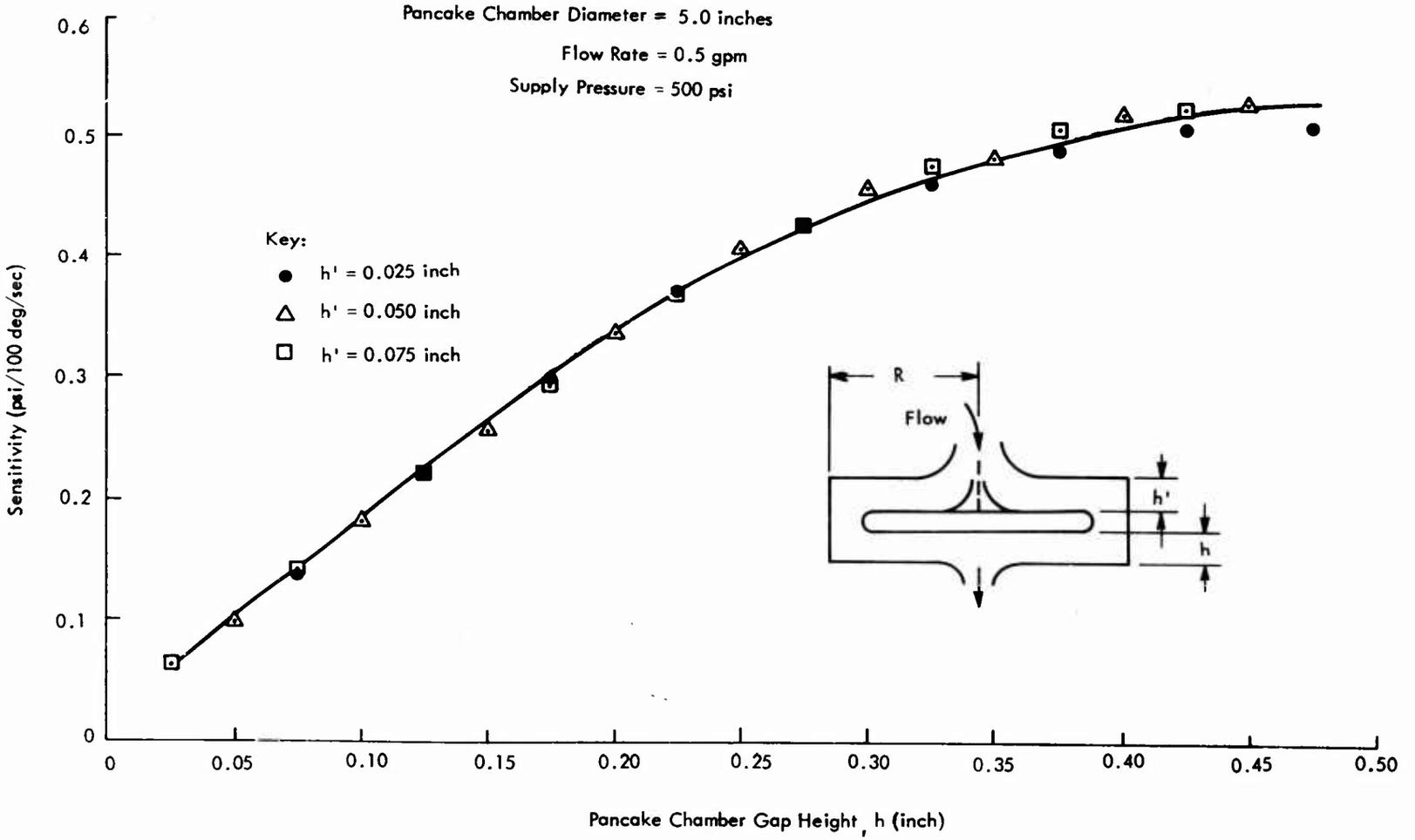

Figure 19. Sensitivity vs Pancake Chamber Gap Height.

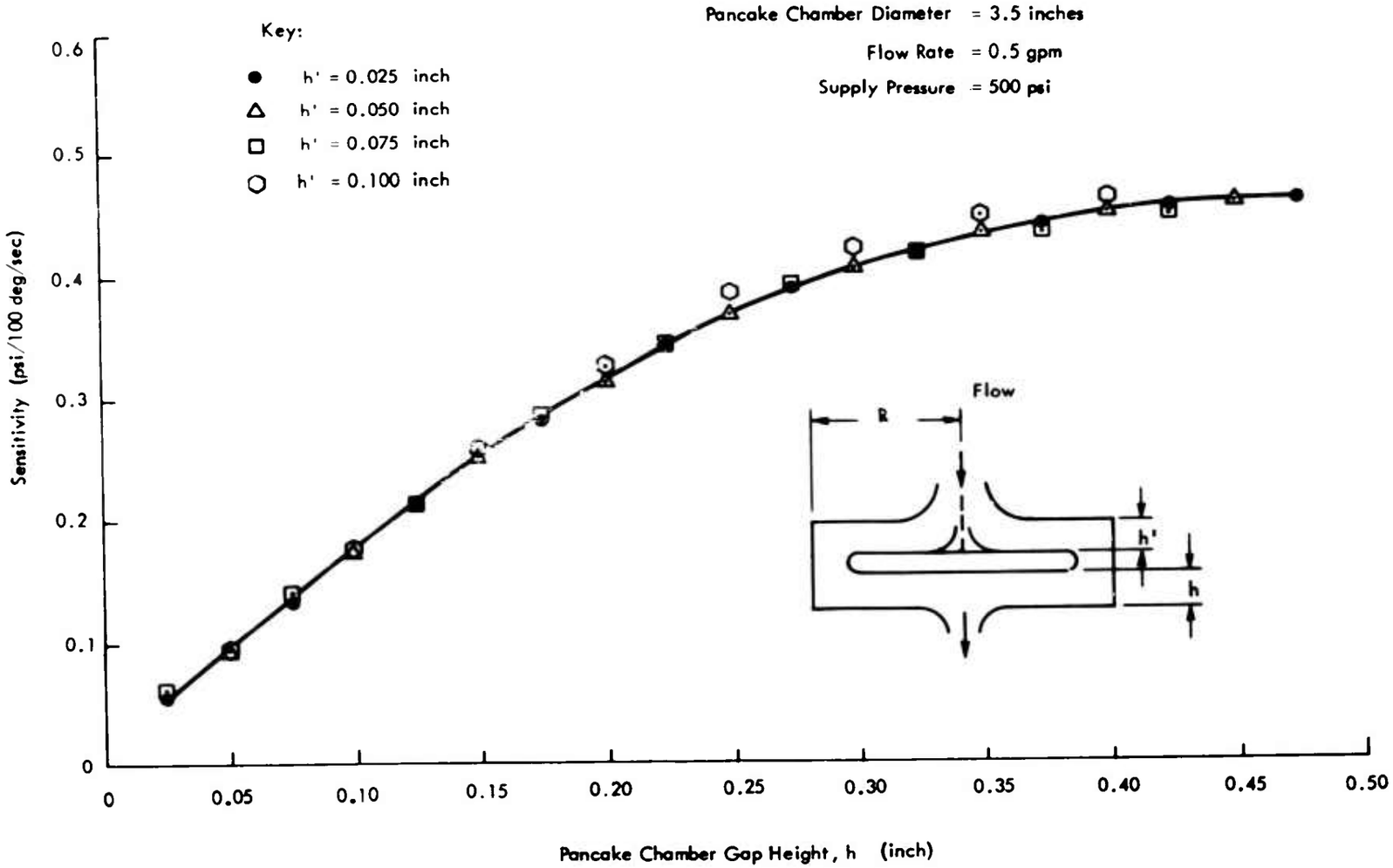

Figure 20. Sensitivity vs Pancake Chamber Gap Height.

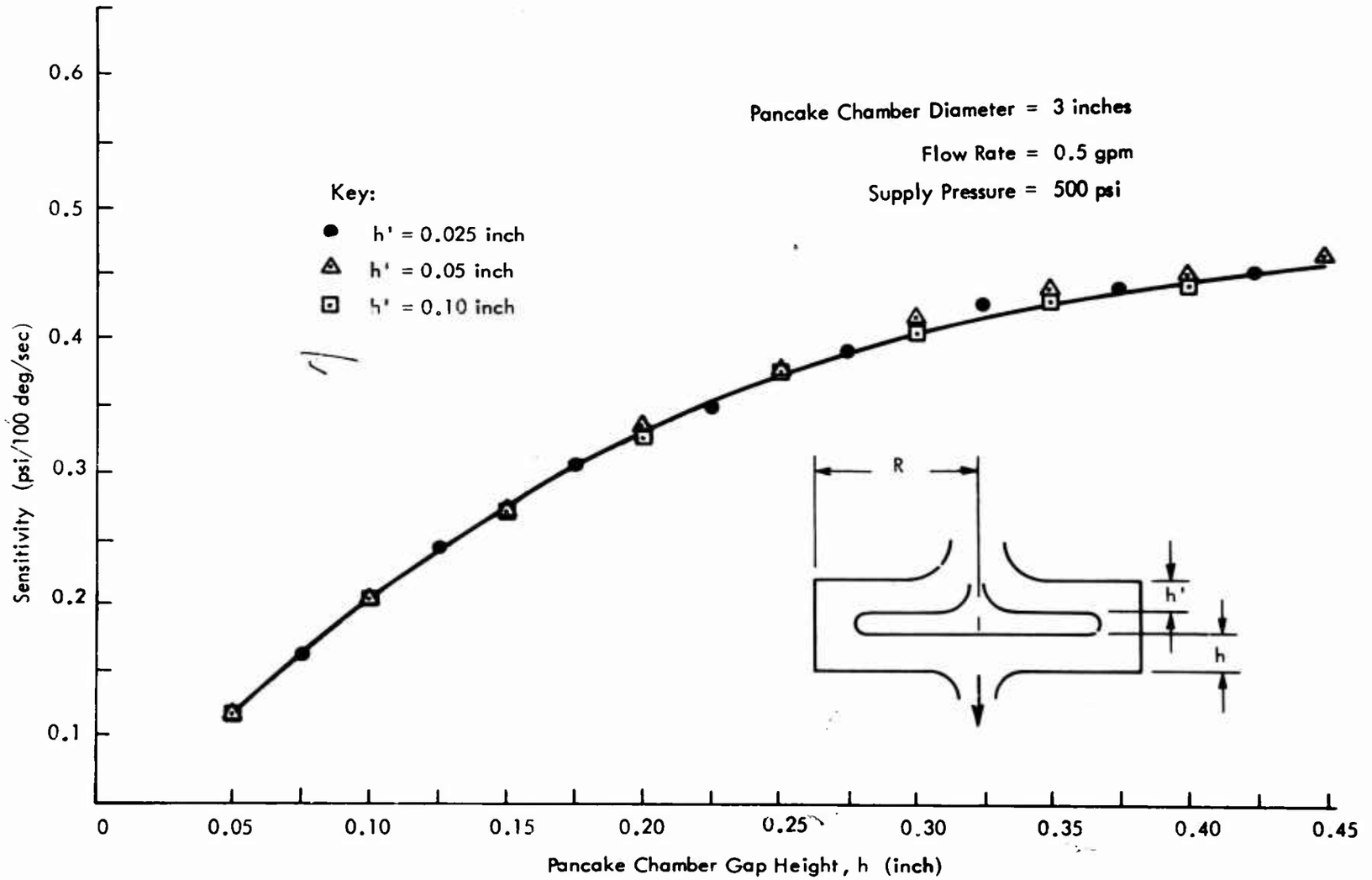

Figure 21. Sensitivity vs Pancake Chamber Gap Height.

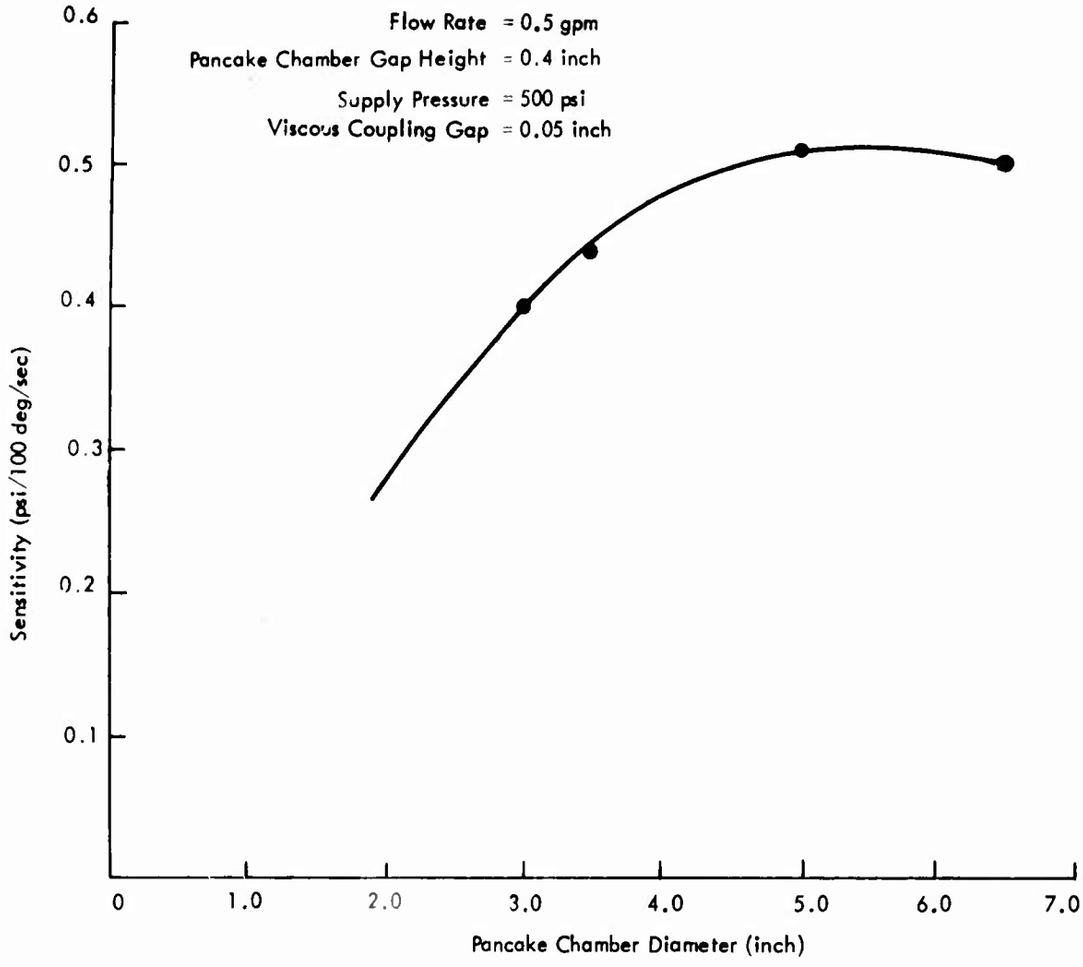

Figure 22. Sensitivity vs Pancake Chamber Diameter.

experimental points. As discussed above, the sensitivity is sharply reduced as the pancake chamber diameter is decreased. There is a 20-percent difference in sensitivity between the 3-inch pancake chamber diameter and 6.5-inch pancake chamber diameter sensor configurations. However, above a pancake chamber diameter of 4.5 inches, the output signal becomes relatively independent of the pancake chamber diameter. The output signal varies by less than 2 percent between pancake chamber diameters of 5.0 and 6.5 inch. This surprising experimental result is quite significant and indicates that viscous action does not influence sensitivity beyond a given pancake chamber radius. The pancake chamber gap height is 0.4 inch and the fluid temperature is 85°F in the results of Figure 22. The position of the signal pick-off probes in the sink region is important in obtaining the maximum possible differential output pressure. Figure 23 shows a typical tangential velocity profile in a vortex flow. The velocity is zero at the walls, increases to a distinct peak, and then falls linearly to zero. The same profile shape is shown on the other side of the centerline due to symmetry. Therefore, it is most advantageous to position the signal pick-off probes so that the maximum differential pressure can be obtained.

To determine experimentally the signal pick-off probe position for maximum signal output, the signal pick-off probe locations were varied over a wide range within the sink outlet. A micrometer dial which indicates signal pick-off probe position in degrees was used. Figure 24 shows the sensitivity as a function of signal pick-off probe position for all four pancake chamber diameters. At zero degrees the signal pick-off probes touch, and at 720 degrees the signal pick-off probes are farthest apart. It is observed that there is no sharp peak in sensitivity, but rather a wide range of outlet radii where the signal pick-off probes could be positioned without sacrificing more than 5 percent in sensitivity. An acceptable range lies between 450 degrees and 650 degrees, representing about 25 percent of the outlet diameter. A possible explanation for the fact that signal pick-off probe position is not critical is the integrating effect the signal pick-off may have due to its size with respect to the outlet diameter.

For a 0.5-inch change in the pancake chamber diameter from 3.5 to 3.0 inches (approximately a 17-percent reduction), there is a 17-percent change in sensitivity. For a 54-percent change in pancake chamber diameter from 6.5 inches to 3 inches, there is a 27-percent change in sensitivity at the peak values. As shown previously, a reduction in sensitivity of only about 2 percent is observed when the pancake chamber diameter is decreased from 6.5 to 5 inches. The bulk of the reduction takes place between 5 inches and 3 inches. The fluid temperature was maintained at 85°F and the pancake chamber gap height chosen at 0.4 inch.

Several experiments were conducted to determine the effect of the working fluid (oil) temperature on the signal output pressure. A rate sensor configuration with a 3-inch pancake chamber diameter was used in all the tests. Since the oil resembles molasses

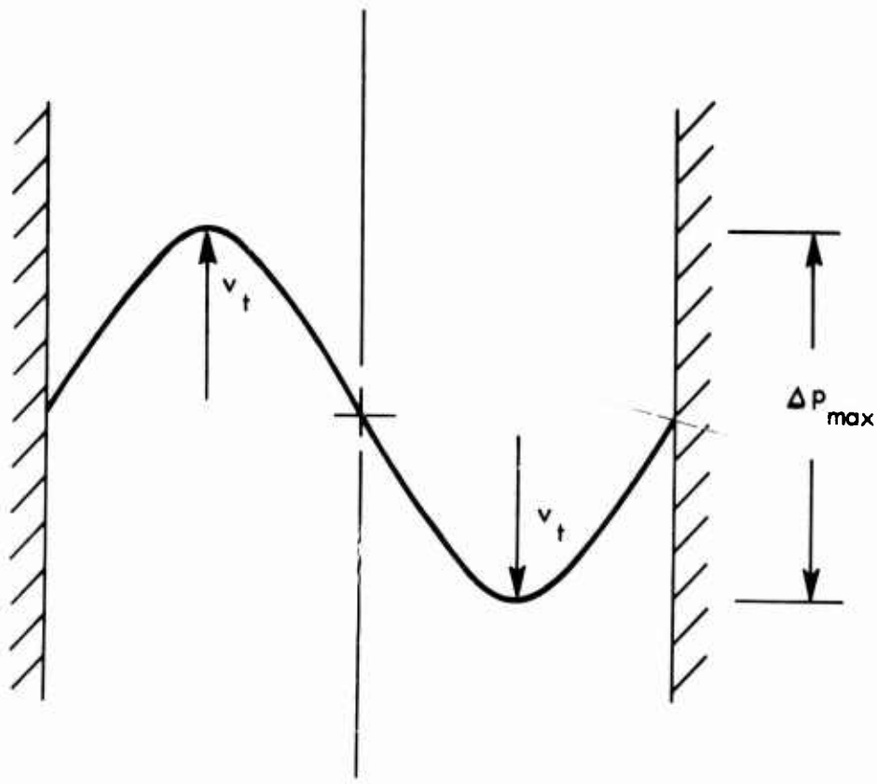

Figure 23. Tangential Velocity in the Sink Outlet.

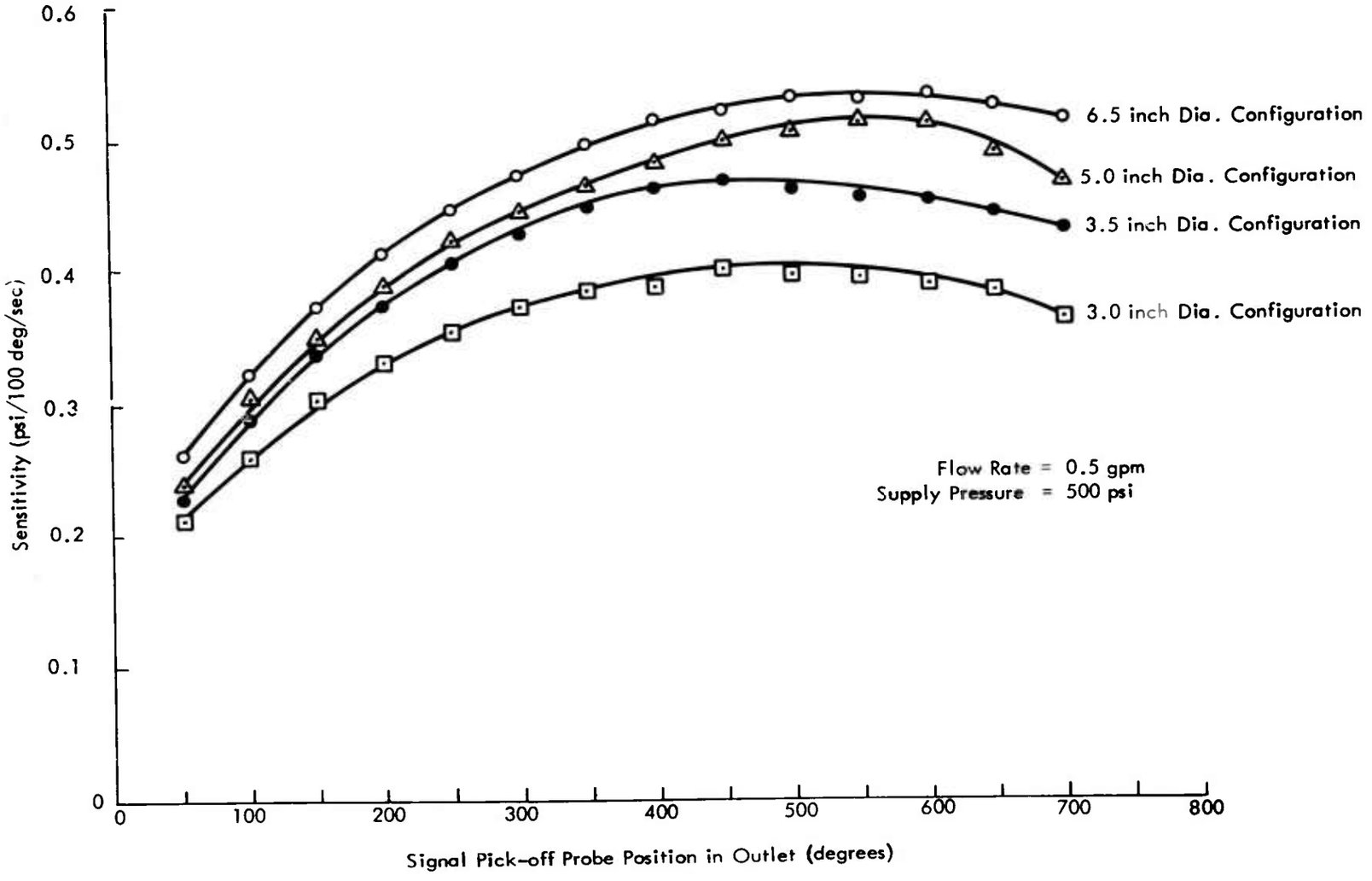

Figure 24. Sensitivity vs Signal Pick-off Probe Position.

at very low temperatures, the signal output will be degraded considerably due to viscous dissipation. Environmental requirements, such as operation in extremely cold weather or extremely hot weather, dictate that the rate sensor must be durable (including working fluid) and must prove to be reliable under any weather conditions.

In the first phase of the environmental testing, the fluid temperature was raised to 155°F. Figure 25 shows the sensitivity as a function of the pancake chamber gap height with a pancake chamber diameter of 3 inches. The maximum output signal is increased by 35 percent over the output signal obtained at a fluid temperature of 85°F. The signal pick-off probe setting was fixed at 400 degrees (which represents a maximum signal output position) and the viscous coupling gap at 0.050 inch. As in the previous results, the sensitivity increases rapidly as the viscous coupling gap height is increased; it then flattens out to a relative maximum.

Figure 26 shows the sensitivity as a function of the signal pick-off probe location within the sink. Again, as reported above, a maximum occurs at a signal pick-off probe setting of 400 degrees. The pancake chamber gap height and viscous coupling gap were set at 0.45 inch and 0.05 inch, respectively.

In the second phase of the environmental study, the fluid temperature was reduced to 23°F by passing the fluid through a coil of tubing immersed in a mixture of dry ice and acetone. The number of coils needed for the low-temperature operation was determined from theoretical heat transfer calculations, as shown in the Appendix. The sensitivity as a function of the pancake chamber gap height is shown in Figure 27. It is observed that there is an order of magnitude decrease in sensitivity relative to that obtained at a fluid temperature of 85°F. It was hypothesized that the signal degradation was due to viscous dissipation. In that case, a Reynolds number effect could be considered to be responsible for the loss of the output signal (sensitivity). In order to test the hypothesis, the Reynolds number was held constant by reducing the mass flow rate to 0.1 gpm at a fluid temperature of 85°F. It was found that the sensitivity was reduced to about the same level, 0.00045 psi/deg/sec, thereby verifying the correctness of the hypothesis. In addition, Figure 27 shows that the sensitivity increases monotonically with increasing pancake chamber gap height, and decreases when the pancake chamber gap height exceeds 0.40 inch.

The sensitivity as a function of signal pick-off probe location was experimentally determined for a fluid temperature of 9°F. Figure 28 shows the functional relationship for a configuration 3 inches in pancake chamber diameter with a pancake chamber gap height of 0.45 inch and a viscous coupling gap height of 0.05 inch. In contrast to previous results, a sharp peak in sensitivity is observed at a signal pick-off probe setting of 400 degrees. This result indicates that the positioning of the signal pick-off probe is very important for low-temperature operation. But no

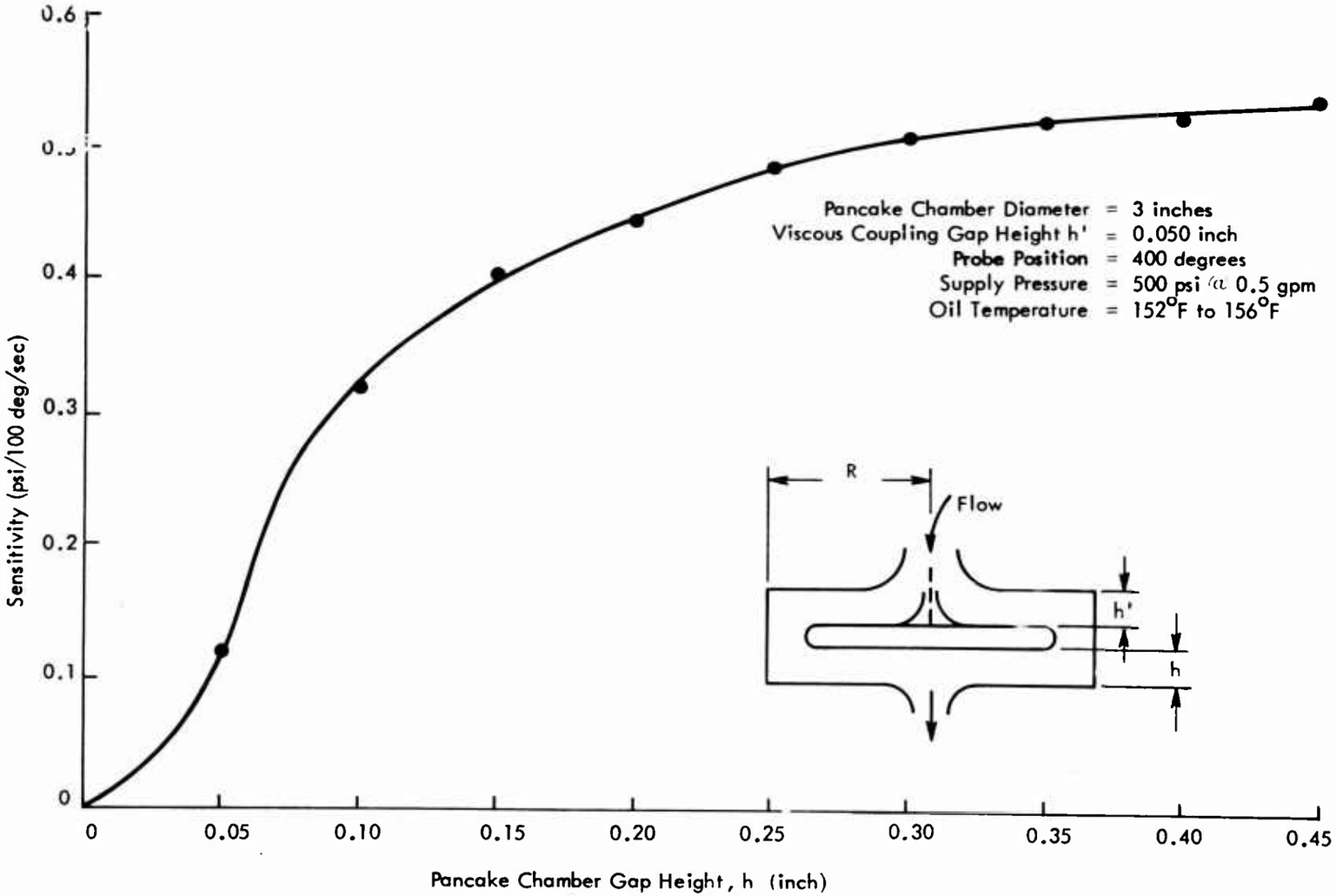

Figure 25. Sensitivity vs Pancake Chamber Gap Height.

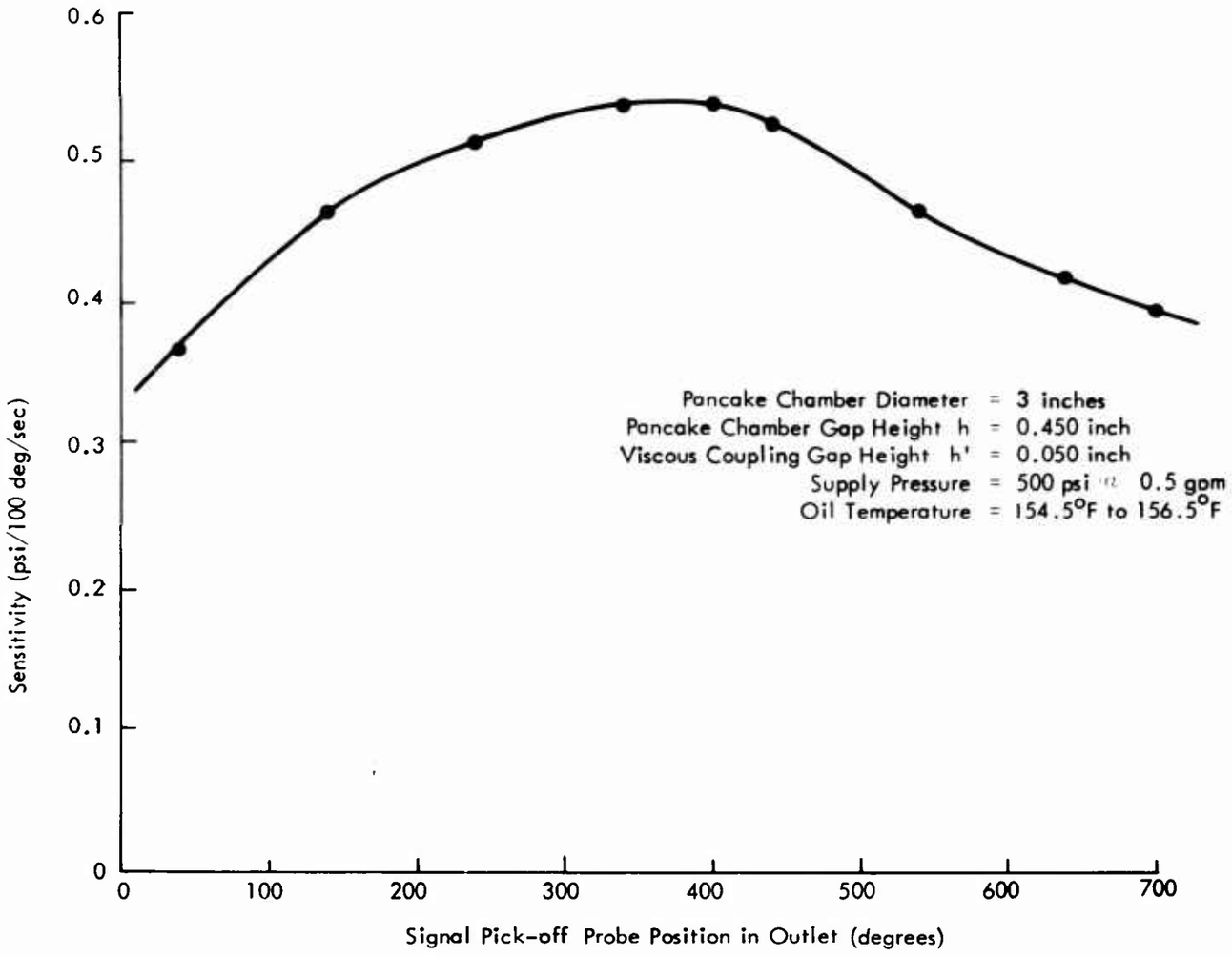

Figure 26. Sensitivity vs Signal Pick-off Probe Position in the Outlet.

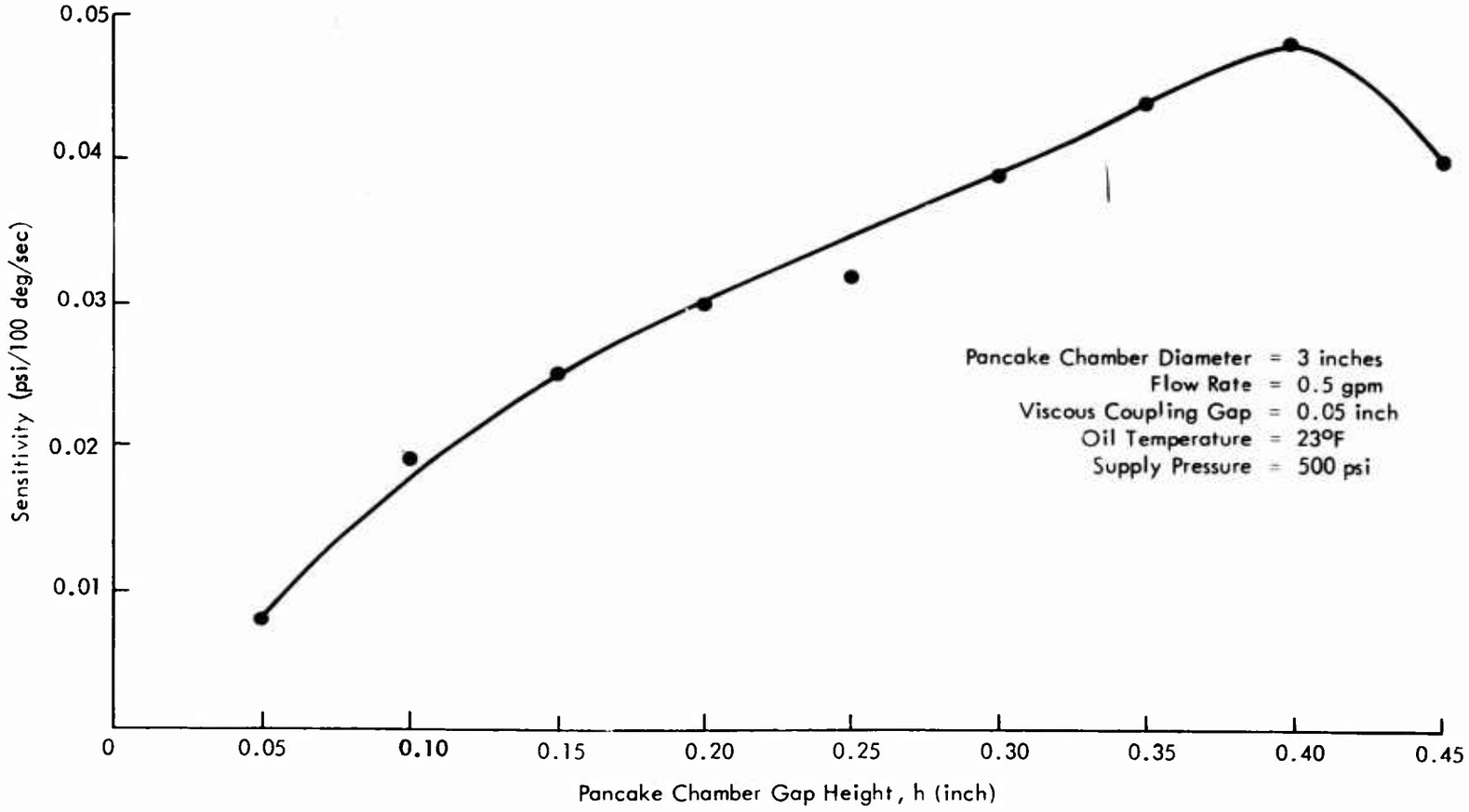

Figure 27. Sensitivity vs Pancake Chamber Gap Height.

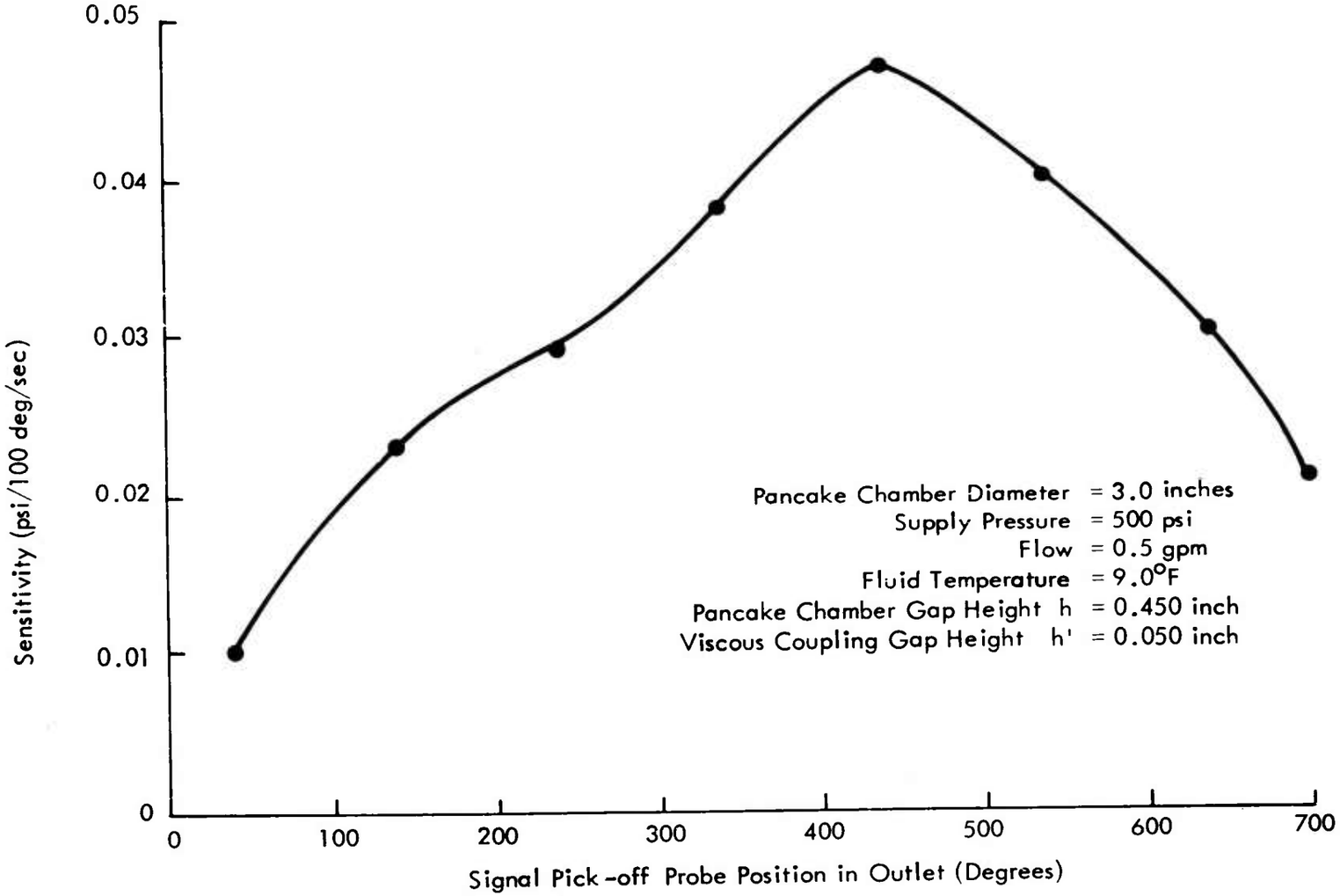

Figure 28. Sensitivity vs Signal Pick-off Probe Position.

difficulty is encountered, since the same signal pick-off probe position maximizes the sensitivity at the other fluid temperatures of 85°F and 155°F. It should also be noted that the maximum sensitivity is almost identical, i.e., 0.00048 psi/deg/sec, at fluid temperatures of 23°F and 9°F. This result is seen from Figures 27 and 28. This indicates that solid body rotation may be taking place below a fluid temperature of 25°F. Therefore, regardless of how much the fluid temperature is decreased below 25°F, the maximum signal output will remain nearly constant.

The supply pressure is an important parameter to be considered in the experimental program. Ideally, it is most desirable to operate the vortex rate sensor at 3000 psi. The primary control system operates in this range. Therefore, for example, for optimum actuation of the rotor pitch control on a helicopter, operation in the range of 3000 psi in the primary and stability-augmentation systems is a design goal. Thus, experimental tests were conducted to determine the influence of supply pressure on the sensitivity of the rate sensor at a fluid flow rate of 0.5 gpm. Figure 29 displays the sensitivity as a function of supply pressure. The fluid temperature was maintained at 85°F, with a pancake chamber gap height of 0.45 inch, pancake chamber diameter of 3 inches, viscous coupling gap at 0.05 inch, and signal pick-off probe setting of 400 degrees. The supply pressure was varied from 100 psi to 3000 psi, and the sensitivity remained almost constant up to 2500 psi and then decreased slightly at 3000 psi. Therefore, all the tests specified above could be run at any convenient supply pressure without signal loss.

For the same geometric configuration, the working fluid temperature was increased to approximately 155°F. It is observed in Figure 30 that as the supply pressure increases from 100 psi to 3000 psi, the sensitivity increases monotonically and linearly from 0.005 psi/deg/sec to 0.0058 psi/deg/sec, representing approximately a 16-percent increase in sensitivity.

The requirements of the stability-augmentation system dictate that 0.5 gpm be available to the high-pressure vortex rate sensor to process signal information. It has been shown that the magnitude of the differential signal output pressure is extremely sensitive to flow rate. In Figure 31 the differential signal output pressure is shown as a function of angular rate. At an angular rate of 20 deg/sec, a flow rate of 0.30 gpm produces a signal output of 0.005 psi. At 0.5 gpm flow rate the signal output is 0.017 psi, or a threefold increase of differential signal output pressure over a 0.3 gpm flow rate. For a flow rate of 1.0 gpm, the differential signal output pressure is 0.07 psi and represents another threefold increase over that obtained for a 0.5 pgm flow rate. In addition, the curves are linear for all flow rates shown over the range of clockwise and counterclockwise rotations that were chosen.

In Figure 32, the dependence of signal output pressure as a function of supply flow is shown for an angular rate of 20 deg/sec at 3000 psi. It is seen that the sensitivity increases exponentially with increasing supply flow rate. Doubling the supply flow

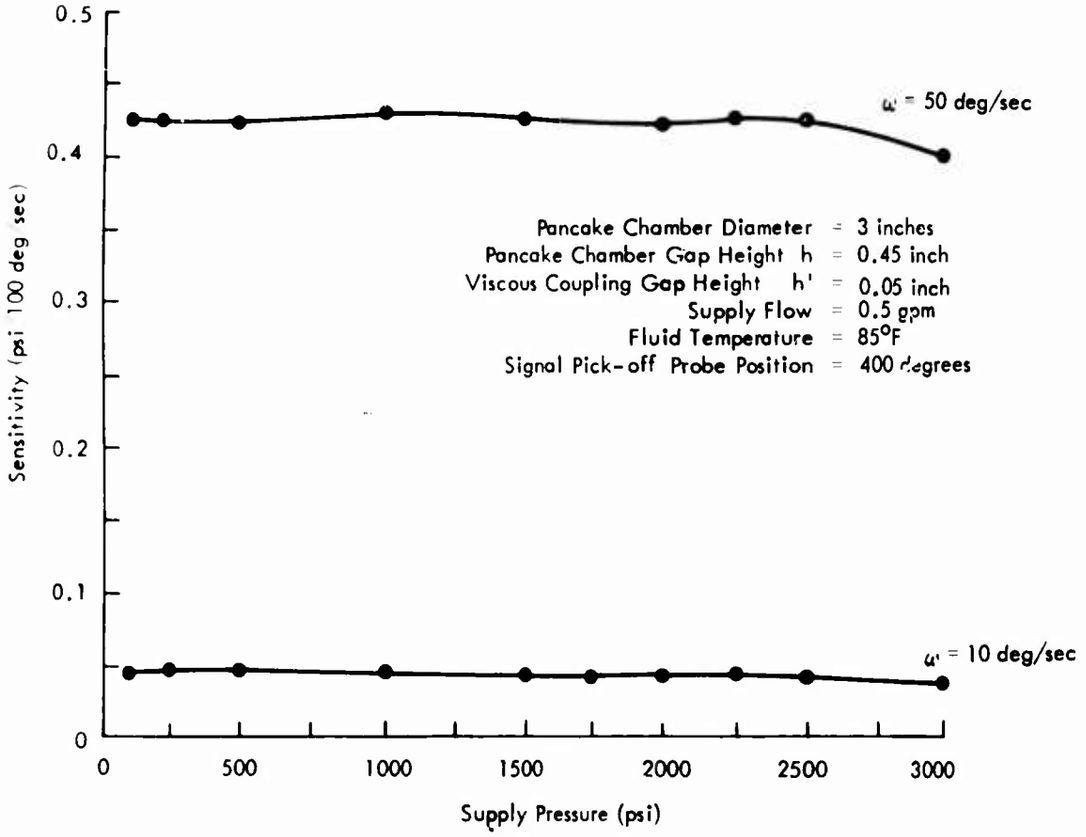

Figure 29. Sensitivity vs Supply Pressure.

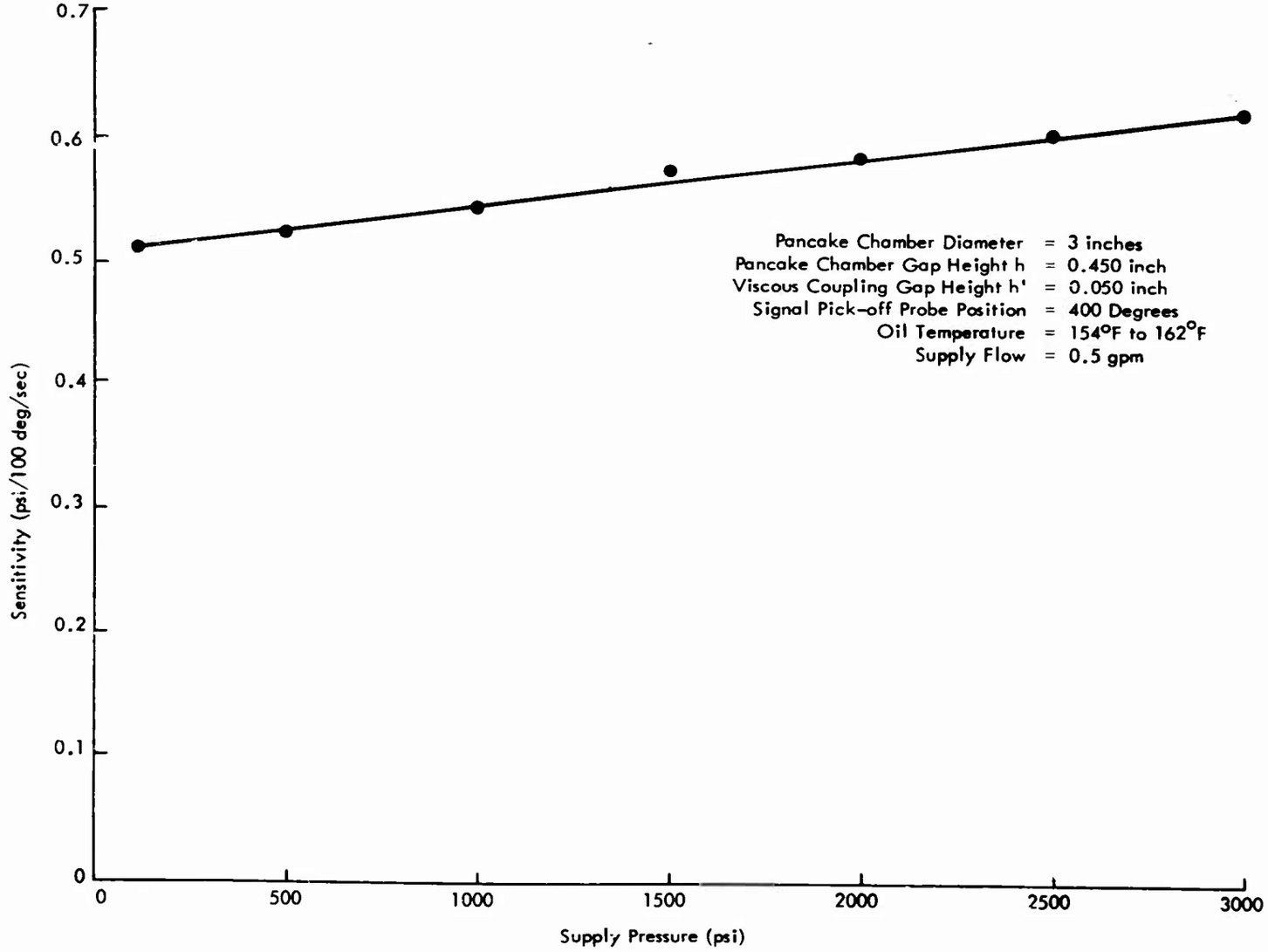

Figure 30. Sensitivity vs Supply Pressure.

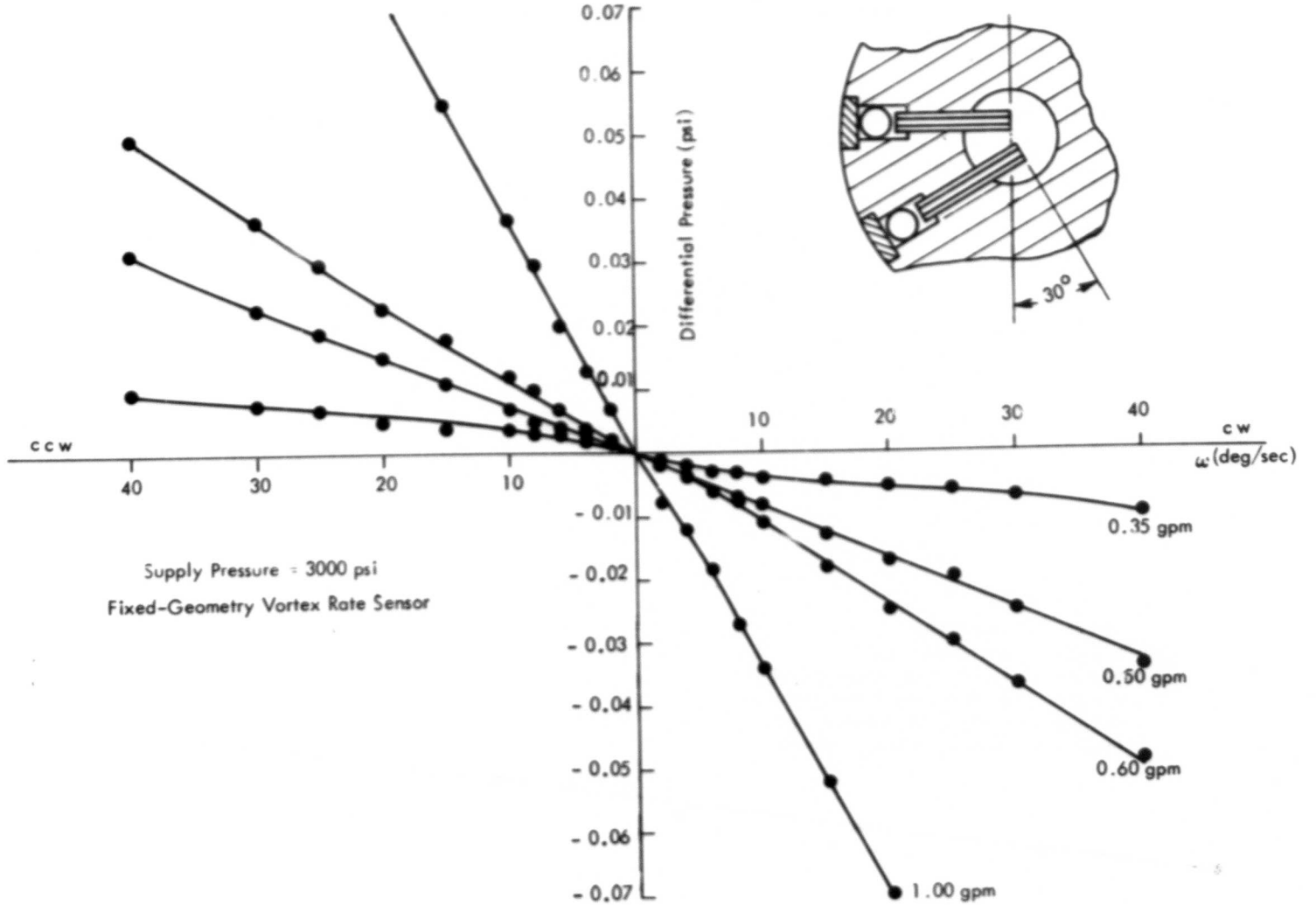

Figure 31. Differential Signal Output Pressure vs Angular Rate.

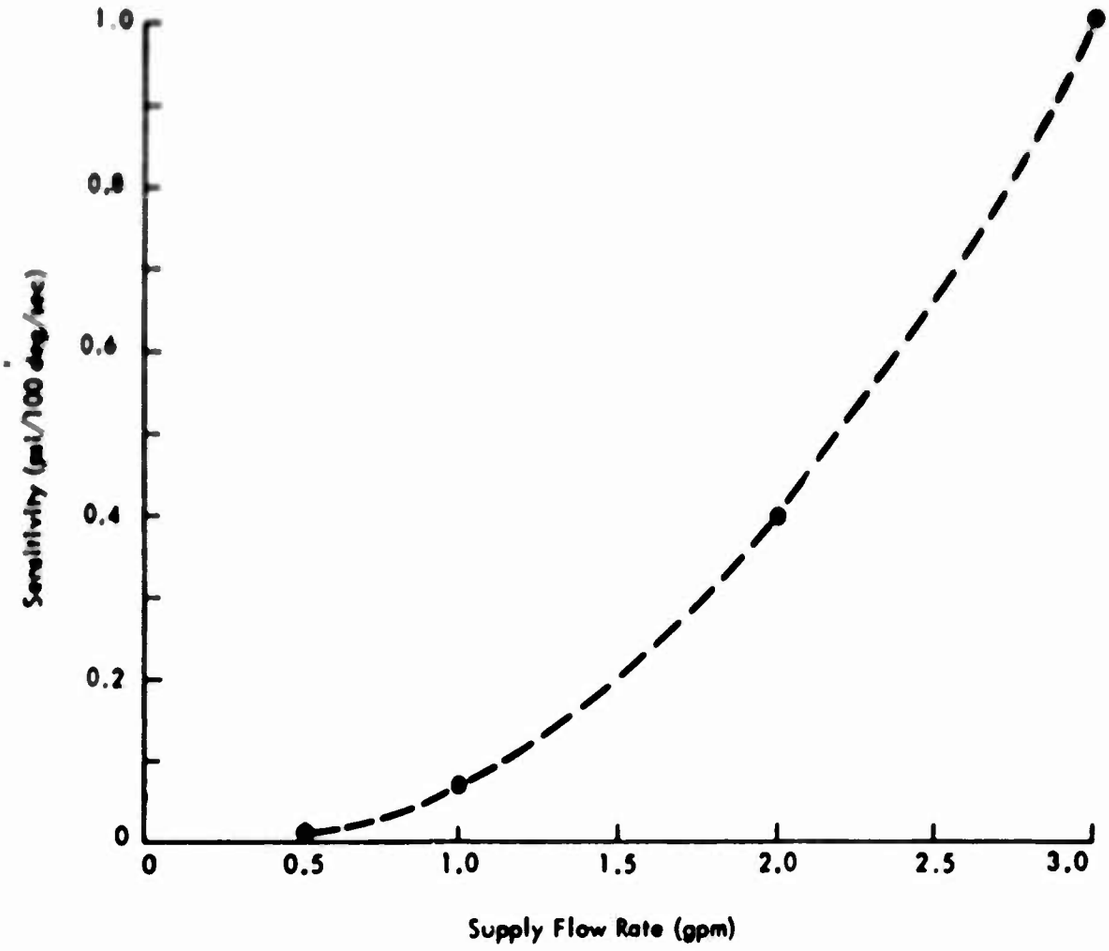

Figure 32. Sensitivity vs Supply Flow Rate.

from 0.5 gpm to 1 gpm results in a fourfold increase in sensitivity. At 3 gpm, the sensitivity is almost 75 times greater than the sensitivity at 0.5 gpm. Thus the flow rate itself, aside from geometrical considerations, is a critical factor in the performance of the rate sensor.

3.2 PHASE II - DYNAMIC RESPONSE CHARACTERISTICS

The second phase of the investigation of the rate sensor performance is critical since the device must be interfaced with other components in the overall stability-augmentation system. The interfacing involves the capability to draw signal flow from the rate sensor pick-offs to drive a hydraulic amplifier, which in turn supplies flow to an actuator to perform a specific controlling function.

Experimental results reported in the first phase of the program were obtained for a blocked output configuration, i.e., no flow was drawn from the signal pick-offs. Therefore, the signal output level was maintained over a wide range of supply pressures and working fluid temperatures. However, when fluid is used to activate another portion of the control system, the output signal level changes substantially from the no-flow condition. If enough flow is drawn, the signal pressure can be reduced to zero. Figure 33 shows a hypothetical pressure-flow characteristic curve which can be used as a criterion to evaluate rate sensor performance. In theory, as flow is increased, the signal pressure should be maintained over a large percentage of the flow range. Then the signal pressure falls to zero.

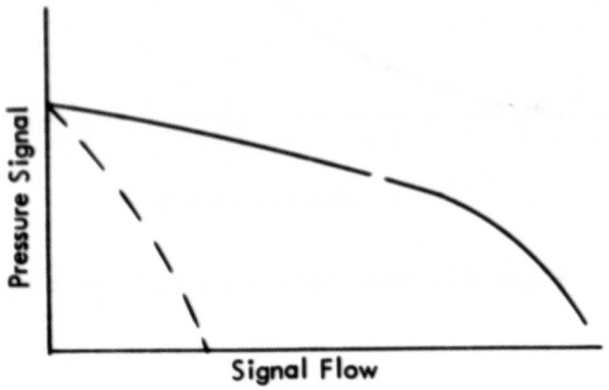

Figure 33. Signal Pressure vs Signal Flow.

But it is possible in a physical situation that the signal pressure will fall rapidly to zero as flow is increased. A hypothetical example is shown by the dotted line of Figure 33. A situation like that is undesirable since the flow output may not be sufficient to interface properly in a control system and still maintain pressure signal. Therefore, the second phase of this investigation was concerned with evaluating the capability of the breadboard model to give high flow rates and to maintain signal pressure over a wide range of supply pressures, fluid temperatures, and geometrical variables such as viscous coupling gap height and pancake chamber diameter.

Initially the variable-geometry vortex rate sensor was tested in the finite output load configuration. The differential output pressure as a function of flow rate from one signal pick-off was obtained. For a 3-inch-pancake chamber diameter configuration, Figure 34 shows that the sensitivity increases as the flow through the signal pick-off increases from zero to 7 cc/min at a supply pressure of 100 psi. Then as the flow increases, the sensitivity falls off rapidly. At a supply pressure of 200 psi, the curve is flat to approximately 8 cc/min and then falls off. A schematic of the experimental configuration, including a flow control valve which maintains 0.5 gpm flow rate, is shown in Figure 35. The data were difficult to obtain due to pressure fluctuations and flow surges which are partly due to the opening and closing of valves.

Unfortunately, these data could never be reproduced. Flow rates of 5-10 cc/min were so small that control at very high supply pressures was impossible to achieve. The outlet legs from the signal pick-offs were modified by incorporating micrometer valves and load orifices in the flow lines. In order to achieve signal stability, the load impedance (the load due to valves, orifices, and piping) in each leg was carefully matched. Then experiments were performed over a wide range of supply pressures to determine the effect on signal stability. Unfortunately, when the supply pressure was changed, or flow rate was increased, the impedance also changed such that signal stability could not be attained.

However, it was suspected that the signal pick-offs themselves were at fault. The reason was that when a finite load configuration was tested, a relative positive pressure signal was recorded regardless of whether the device was rotating clockwise or counterclockwise. All previous results showed that this phenomenon never occurred. The differential pressure output signal was either "positive" or "negative" depending on the direction of rotation of the rate sensor.

To confirm the suspicion that the signal pick-off was faulty, the 4-inch fixed-geometry rate sensor with impact pressure signal pick-off probes was tested in a finite load configuration. The sink outlet in the variable-geometry sensor could not be changed because of the signal pick-off design. The signal pick-off probes were bent within the sink so that the pick-off holes faced the tangential flow and were oriented at 90 degrees with respect to the outlet flow. Since the tubes were cemented in place; they could not be removed and replaced without a redesign of

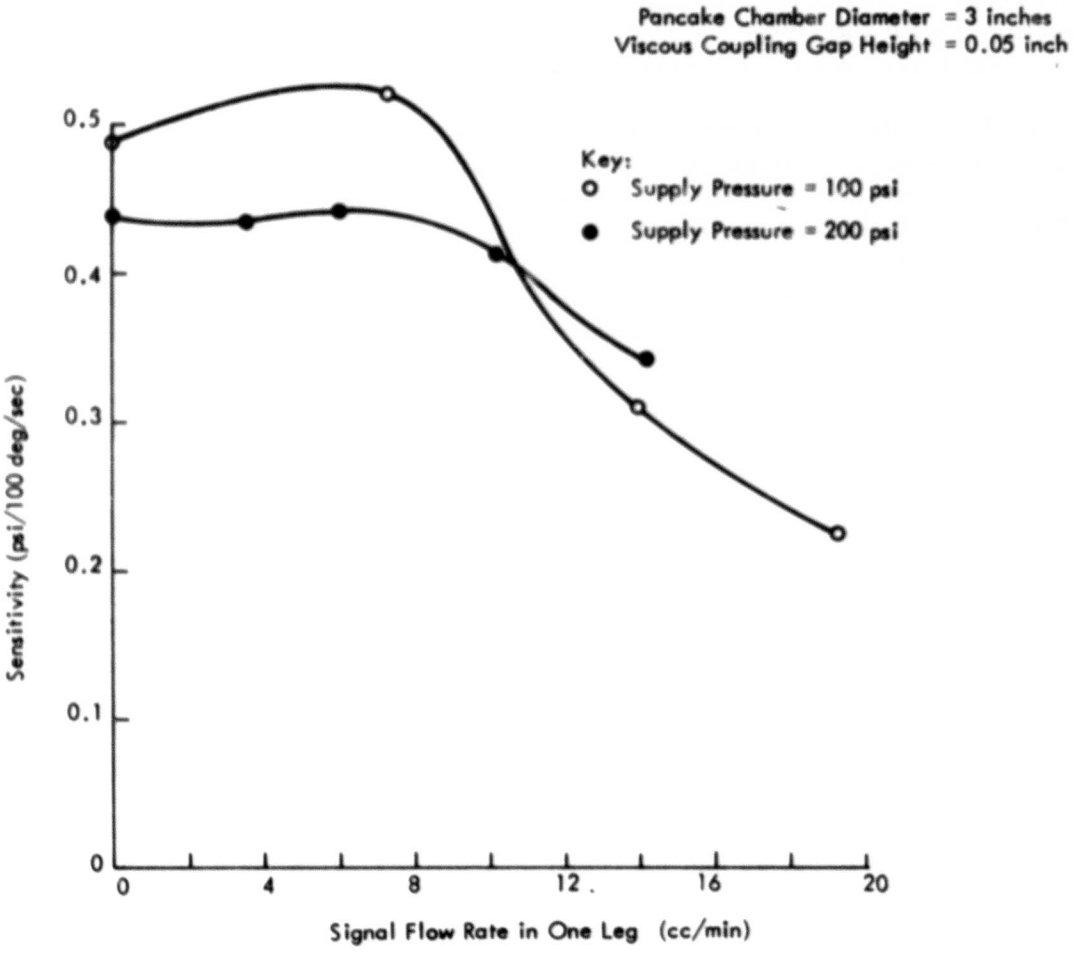

Figure 34. Sensitivity vs Signal Flow.

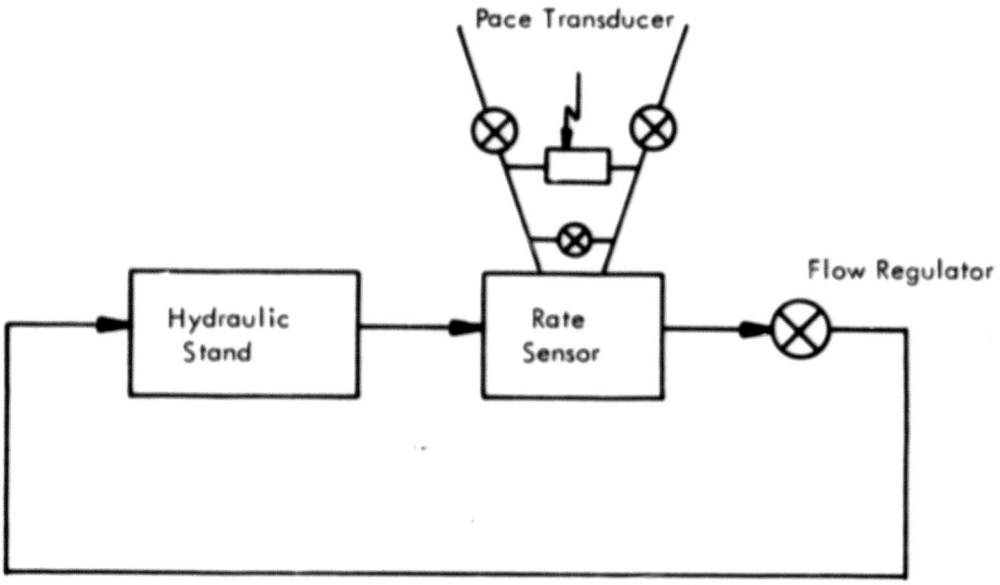

Figure 35. Schematic of Flow Configuration.

the signal pick-off configuration. Rather than redesign the signal pick-off assembly of the variable-geometry sensor, the experimental program was redirected to run the test on the fixed-geometry sensor.

It must be emphasized that all the data obtained with the variable-geometry sensor in the blocked-output mode are still valid since the signal pick-off impedance is always infinite regardless of the direction of rotation of the device or supply pressures.

Figure 36 shows a schematic of the experimental apparatus associated with the measurement of the functional relationship between the differential output pressure and the output flow. A flow regulator upstream of the vortex rate sensor insures the delivery of 0.5 gpm at all times to the vortex rate sensor. A pressure gage and flow regulator, R2 , are located downstream of the vortex rate sensor. The input pressure to the vortex rate sensor is 3000 psi at a 0.5 gpm flow rate. The vortex rate sensor acts as an impedance in the line. A pressure drop takes place across the vortex rate sensor. The flow regulator, R2 , is not intended to regulate the upstream flow because the output pressure from the vortex rate sensor would be partially dictated by the flow control downstream, which is totally undesirable. The purpose of the flow regulator downstream is to act as a load impedance on the vortex rate sensor. The pressure of the fluid downstream of the flow regulator, R2 , is nearly atmospheric: most of the pressure drop takes place across flow regulator R2. The pressure drop across the vortex rate sensor is a function of the supply pressure. The governing impedance in the vortex rate sensor is the sink outlet because of its small size. At 3000-psi supply, the pressure drop across the vortex rate sensor is approximately 500 psi.

The signal pick-off lines consist of three micrometer needle valves and a Pace transducer. The Pace transducer measures the differential signal pressure taken between each impact signal pick-off probe. The single valve connected to both lines is used to relieve the differential pressure on the diaphragm of the Pace transducer so that it is not damaged due to pressure surges in the flowing condition. The remaining two valves control the quantity of flow issuing from each pick-off probe.

Initially the 4-inch fixed-geometry sensor (FGRS) was tested using a pancake chamber gap height of 0.050 inch. A porous coupler was incorporated into the vortex rate sensor, resulting in a reduction of the pancake chamber diameter to 3 inches. This is due to the fact that the porous coupler must be mounted properly for the high-pressure application. The porous coupler consisted of a sintered material. The porous coupler improves the signal output because the efficiency of the coupling between surfaces and the fluid is increased. However, the coupler did cause some minor pressure signal fluctuations indicative of increased noise levels.

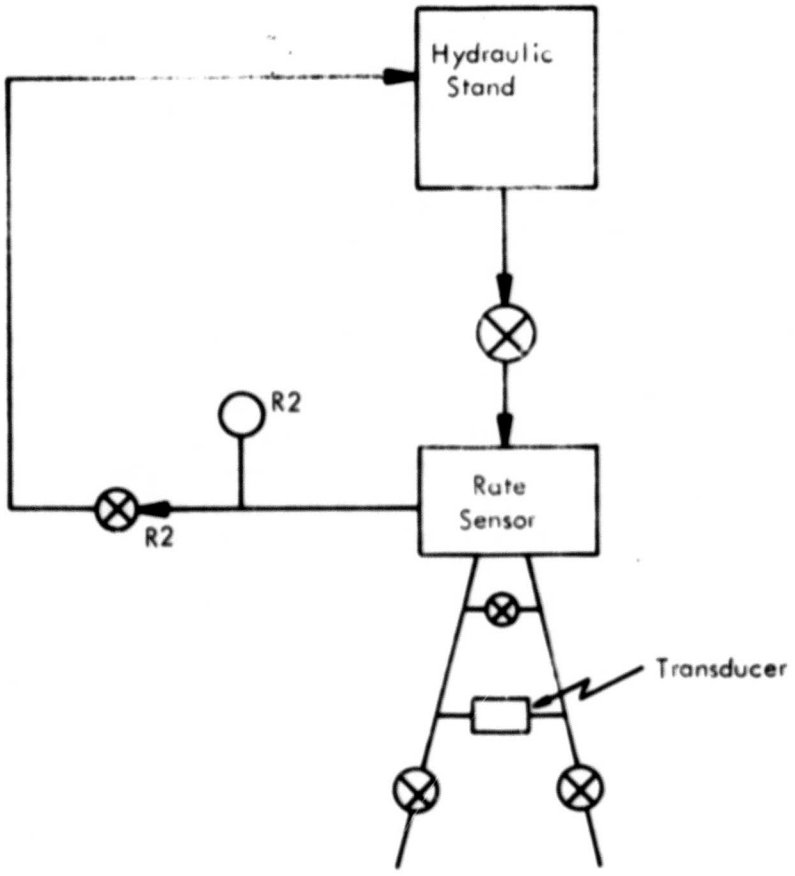

Figure 36. Schematic of Test Setup .

Figure 37 shows the relationship between the sensitivity and the supply flow rate at a supply pressure of 200 psi. The low supply pressure was chosen initially to gain confidence that the vortex rate sensor could perform under conditions already established by other researchers. From Figure 37, it is observed that the sensitivity increases very rapidly as the supply flow rate is increased from 0.5 to 1.4 gpm. The magnitude of the sensitivity at 1.4 gpm is almost 20 times its value at a 0.5 gpm flow rate. At 0.5 gpm the sensitivity is 0.0008 psi/deg/sec. The low signal output level occurs because the pancake chamber gap height is only 0.05 inch. All previous experiments reported herein have shown that the sensitivity increases rapidly with increasing pancake chamber gap height and attains a relative maximum at pancake chamber height h = 0.45 inch. Therefore, without modifying the existing rate sensor to obtain larger gap heights, the output signal levels can be predicted from previous experiments.

The pancake chamber gap height was increased to 0.12 inch with only a minor modification of the internal assembly. Currently, spacers are used to vary the pancake chamber gap height between 0 and approximately 0.120 inch.

A series of experiments was conducted at several supply pressures and supply flow rates with a pancake chamber gap height of 0.12 inch. First, the sensitivity as a function of signal flow rate through one pick-off leg was obtained for a supply pressure of 200 psi and a supply flow rate of approximately 0.5 gpm. Figure 38 shows the pressure flow curve for these conditions. It is observed that the sensitivity increases as the signal flow rate through one leg of the signal pick-off increases up to approximately 90 cc/min. Then the signal falls rapidly to zero for larger signal flow rates. In Figure 34 it was shown that the same trend occurred at P_s = 100 psi in the variable-geometry rate sensor, which consisted of a pancake chamber diameter of 3 inches and a pancake chamber gap height of 0.45 inch. From Figure 38, the maximum sensitivity is 0.004 psi/deg/sec at a signal pick-off flow rate of approximately 90 cc/min.

The supply pressure was increased to 1000 psi while the supply flow rate was maintained at 0.5 gpm. Figure 39 shows the sensitivity as a function of signal flow rate through one pick-off leg. It is observed that the sensitivity increases as the signal flow rate through one pick-off leg increases. No tendency to decrease is shown by the sensitivity curve as signal flow rate increases. It must be noted that the pressure drop across the vortex rate sensor increased as the signal flow rate through the signal pick-off increased. For example, in the blocked-output mode, Δp = 120 psi. At a flow rate of 250 cc/min, Δp = 180 psi. The increased pressure drop affects the vortex flow within the vortex rate sensor. The pressure drop in the vortex flow as the radius decreases to zero is a mechanism for the development of a tangential velocity component. In order to increase the tangential velocity in magnitude, the pressure drop must be increased. Thus, as more flow is drawn through the signal pick-offs, the pressure drop increases above its previous value, the tangential velocity component increases, and the signal pressure increases. It is noteworthy

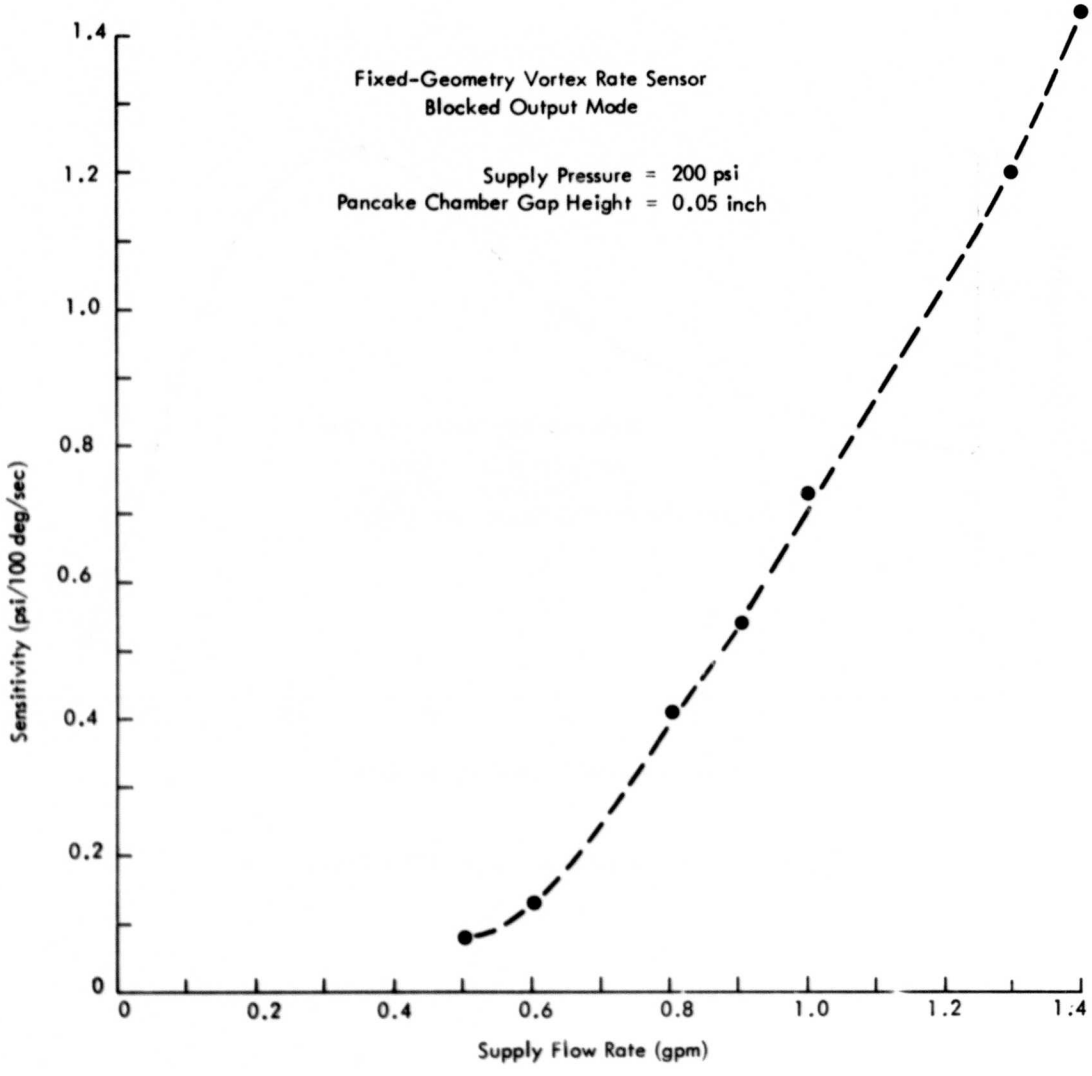

Figure 37. Sensitivity vs Supply Flow Rate.

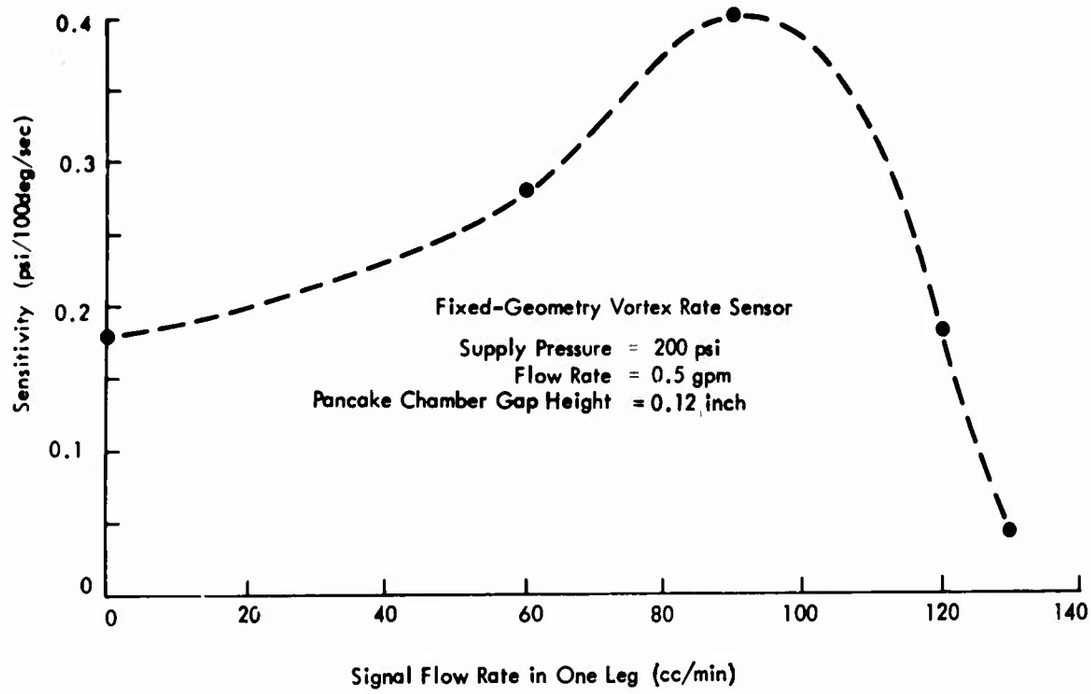

Figure 38. Sensitivity vs Signal Flow Rate.

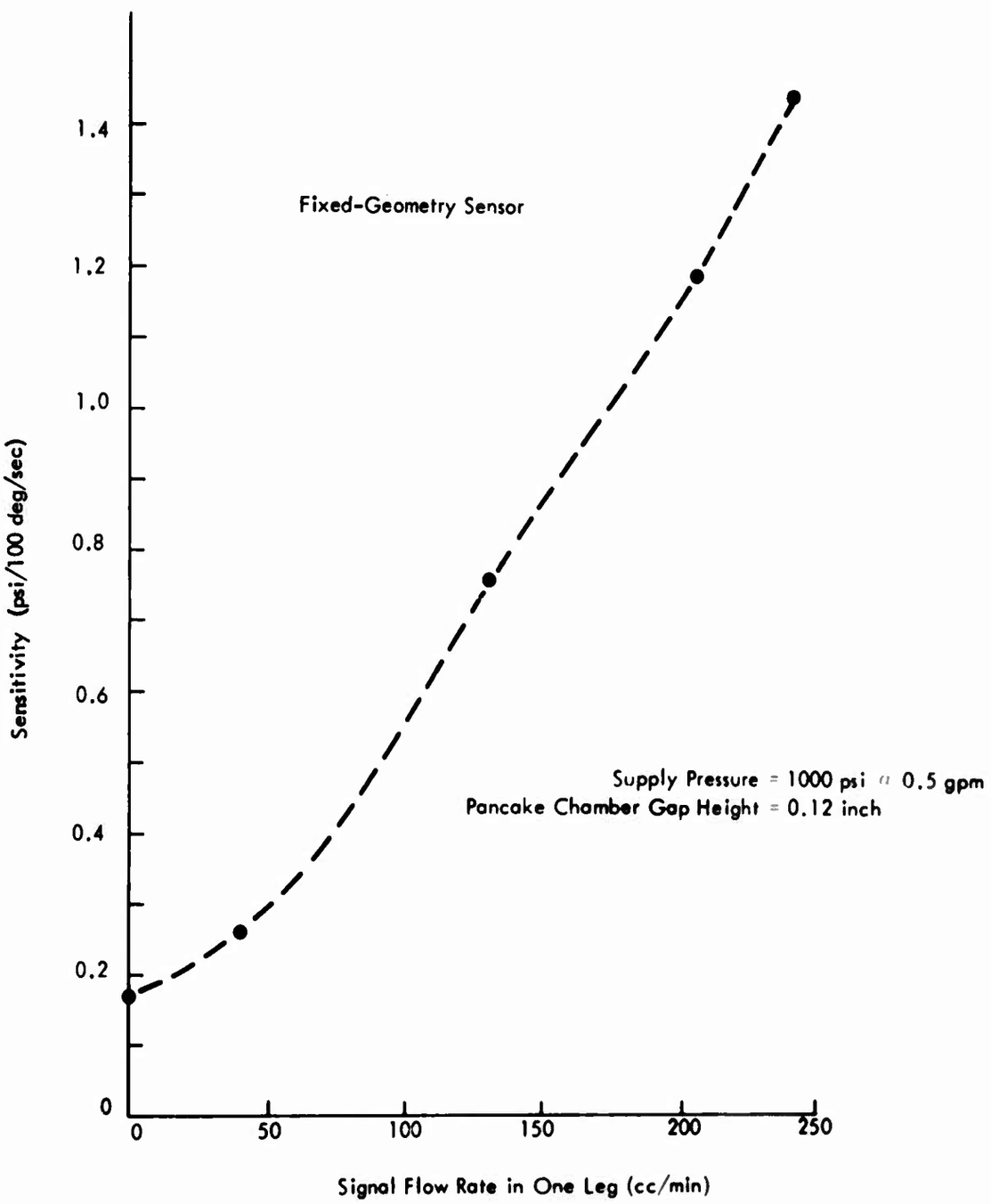

Figure 39. Sensitivity vs Signal Flow Rate.

that this result was exhibited at lower pressures in only one instance. From the pressure-flow load curve of the variable-geometry vortex rate sensor (see Figure 34), the sensitivity increased as the flow was increased to 10 cc/min; then the sensitivity decreased toward zero for higher flow rates. However, the sensitivity increase at 1000 psi supply pressure is much more pronounced. In addition, the signal flow rate has significantly increased to approximately 250 cc/min, an order-of-magnitude increase over the results shown in Figure 34.

Figure 40 shows the sensitivity as a function of flow rate through the signal pick-offs at supply pressures of 2000 psi and 3000 psi. Again, the same trend is exhibited as in the previous case. The magnitude of the output signal is nearly the same for all three supply pressures, although it decreases as the supply pressure increases.

The signal flow at which the sensitivity begins to decrease could not be obtained readily because at the higher signal flow rates the signal pressure fluctuated and surged to such an extent that no reliable or repeatable data could be obtained.

Finally, in all cases, the difference in flow rate between the signal pick-offs could not be measured with any confidence because the magnitude was so small.

3.3 NOISE CHARACTERISTICS

One of the important parameters governing the performance of a vortex rate sensor is the signal-to-noise ratio. Unfortunately, noise at an input to the device is amplified simultaneously with the pressure signal. The noise levels can be high enough to swamp the signal output. Consequently, the vortex rate sensor will respond to a noise signal regardless of whether the angular rate input is present or not. By making the signal-to-noise ratio large enough and incorporating a threshold operating point, the vortex rate sensor will not respond to random noise input.

In the experimental program, prior to obtaining data from the vortex rate sensor, the noise produced by the test stand itself was obtained to establish a reference noise level at a pressure of 3000 psig. For this evaluation, the vortex rate sensor was removed from the supply line, and a Kistler transducer was connected directly into the pressure line from the test stand. A typical frequency spectrum for this test condition is shown in Figure 41.

Figure 42 shows the noise spectrum of the instrumentation, which includes the charge amplifier associated with the Kistler transducer and the wave analyzer. The zero noise level is -30 db. The average noise level is approximately -20 db in the frequency range between 20 and 20,000 cps. At the frequency levels between 20 and 200 cps, large fluctuations about the average are observed. Maxima occur between -5 and -10 db.

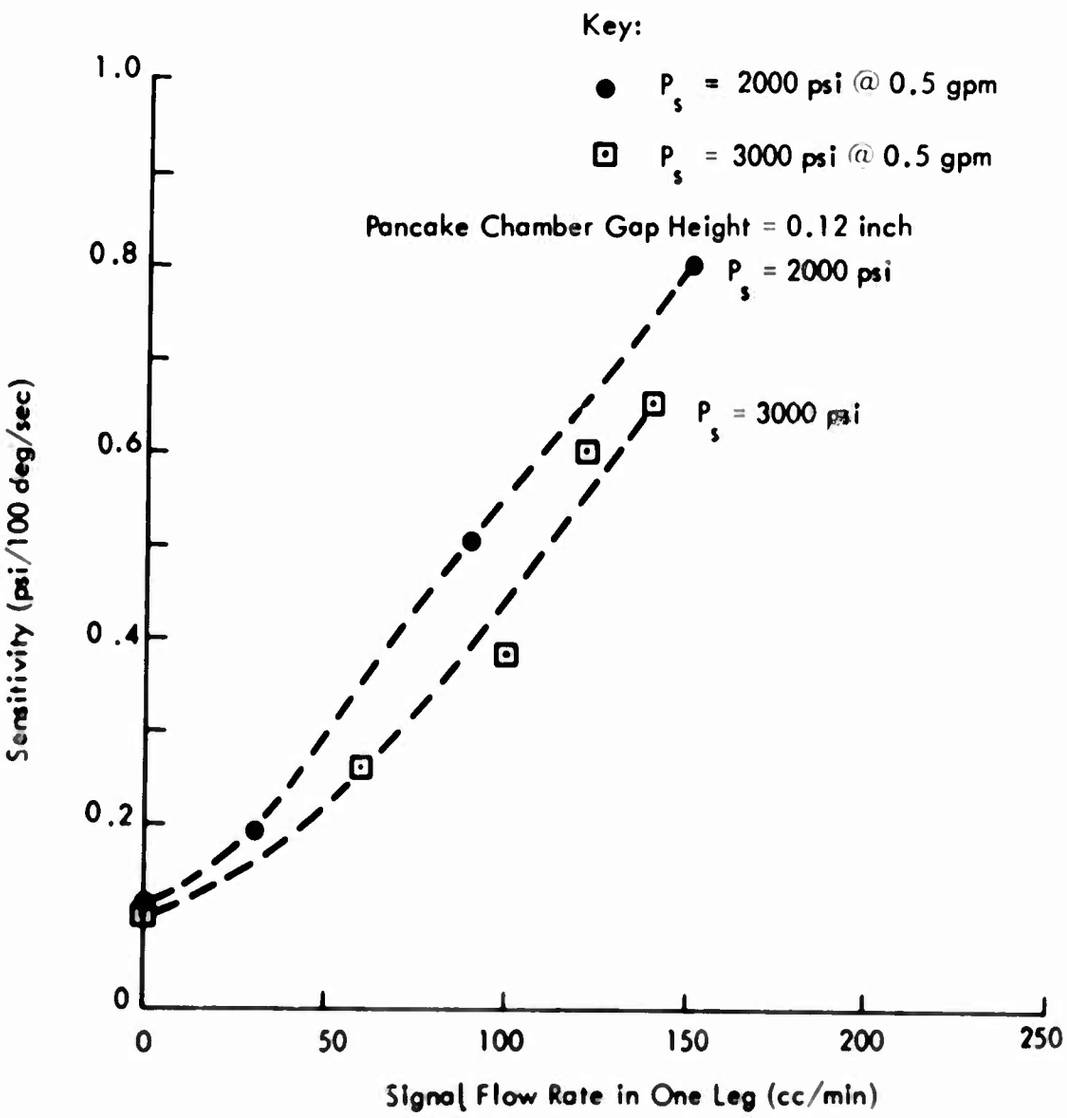

Figure 40. Sensitivity vs Signal Flow Rate.

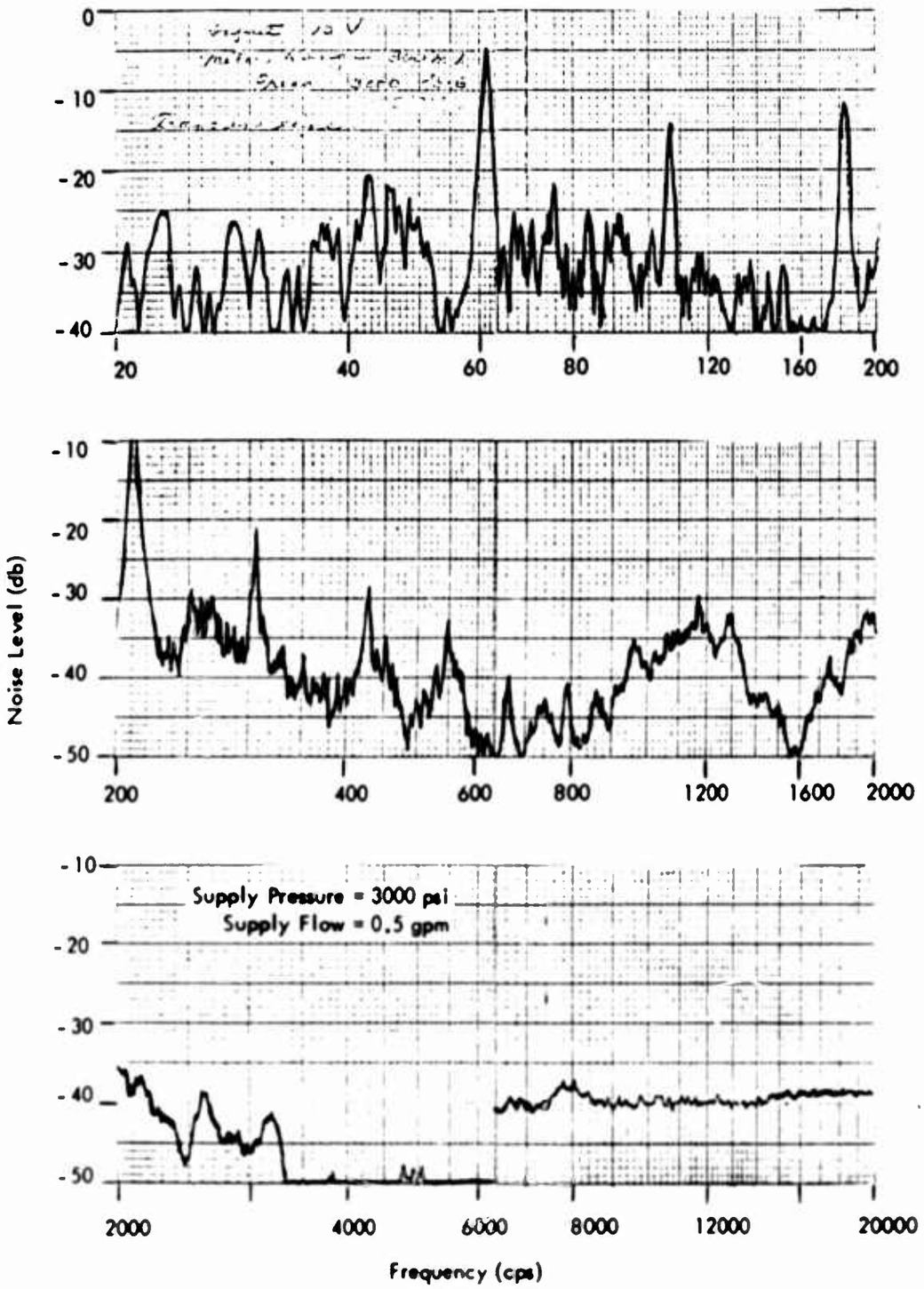

Figure 41. Test Stand Noise Spectrum.

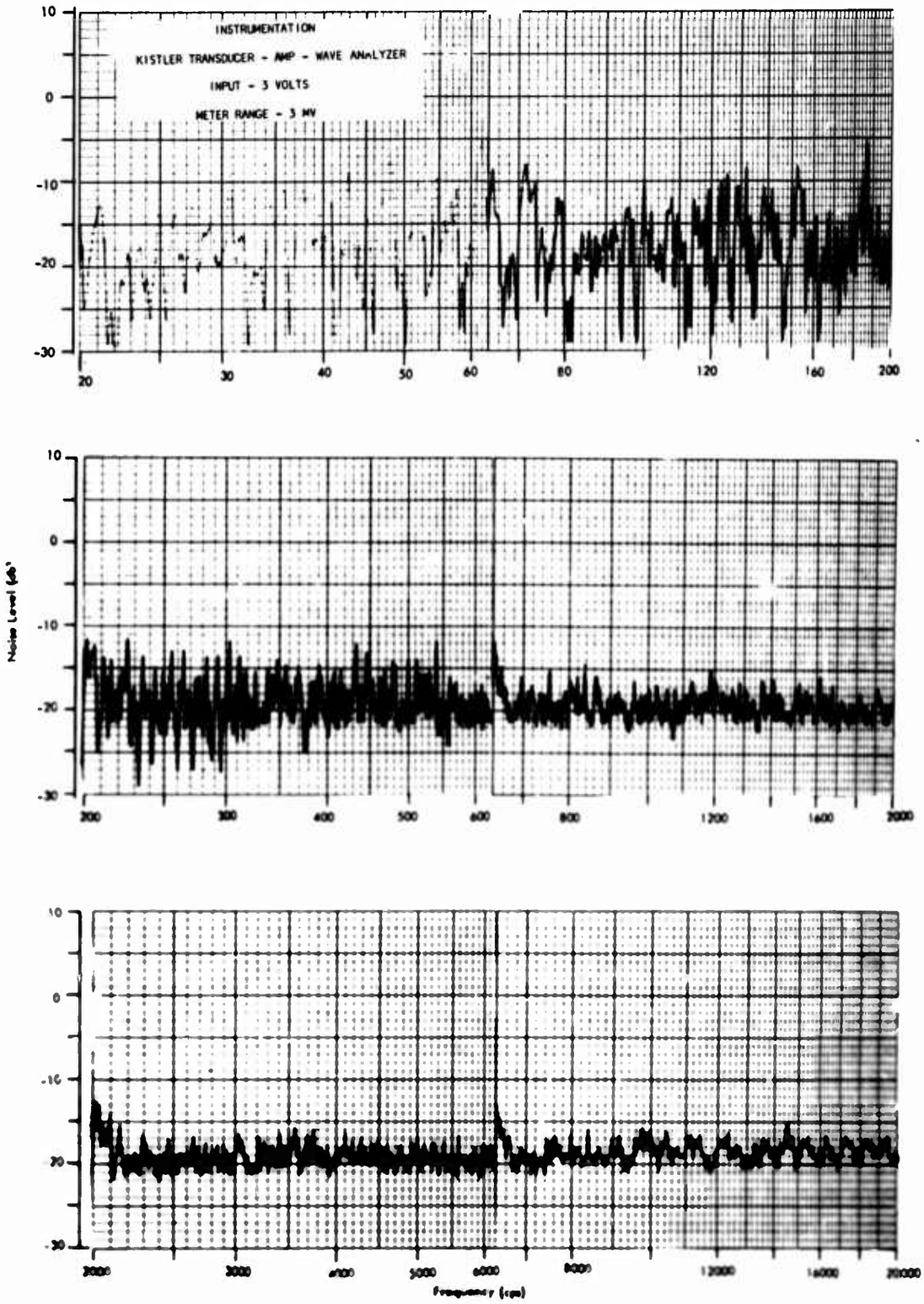

Figure 42. Instrumentation Noise Spectrum.

Figure 43 represents the noise spectrum of the entire experimental apparatus including the test stand, vortex rate sensor, and instrumentation at a supply pressure of 3000 psi and a supply flow of 0.5 gpm, with no angular rate in the blocked-output mode. In the frequency range between 20 and 60 cps, the average noise level is approximately -5 db. A sharp spike occurs at 31 cps and is equal to +15 db. In the frequency range between 60 and 20,000 cps the average noise is approximately -20 db. This is the same level as the instrumentation noise. However, between 20 and 200 cps, the noise level does not differ significantly from instrumentation noise except at 30 cps, where a sharp spike (equivalent to +15 db) is observed.

In Figure 44, the noise spectrum is shown for the same conditions as in the previous case except that a flow rate of 70 cc/min is drawn from each signal pick-off. The chart indicates that between 200 and 20,000 cps, the noise spectrum is the same as for no flow. At 210 cps, a spike does occur with a peak at approximately -2 db for both the no-flow (Figure 43) and the flow (Figure 44) modes. Between 20 and 60 cps, the average noise level is -5 db, while the peaks occur at a level of +5 db for several frequencies. For a condition of no flow through the pick-offs (Figure 43), a sharp peak occurred at 30 cps and equalled +15 db. However, the average was approximately -5 db. Therefore, the average noise level remains the same when flow is drawn from the pick-offs. Between 60 and 200 cps, the noise levels shown in Figure 44 do not increase significantly over the previous case. At 120 cps, a sharp spike in the noise spectrum occurs. The noise level is at least +15 db. The average noise level in this frequency range is approximately -12 db. This represents an increase of 3 db over the case of no flow through the pick-offs in this frequency range.

Figure 45 shows the noise spectrum for the same conditions as represented by Figure 44 except that an angular rate of 2 deg/sec was imparted to the rate sensor. For substantially larger angular rates, slip rings were needed, and these damped out the noise response. In the frequency range between 200 and 20,000 cps, no change from the previous results was detected. The average noise level is approximately -10 db. However, sharp peaks occur at 210 cps and at 430 cps. These represent noise levels of +10 db and +3 db respectively, which are 2 to 3 db greater than the peaks observed in the previous case. Between 60 and 200 cps, the average noise level is approximately -12 db. The sharp peak at 120 cps in the previous case (Figure 44) does not occur, but a smaller peak (approximately -1 db) is shown. Thus the average noise level does not increase with small angular rates. Between 20 and 60 cps, the peak noise levels occur at several frequencies and equal approximately +5 to +10 db. This represents a 5 db increase over the previous case. Therefore, it appears that all the increased noise levels with flow and angular rate appear in the frequency range between 20 and 200 cps. An additional comparison of the results of Figure 43 and 45 shows that the noise levels are nearly the same in the frequency range between 20 and 200 cps when flow is drawn from the signal pick-offs and angular rate is imparted to the vortex rate sensor.

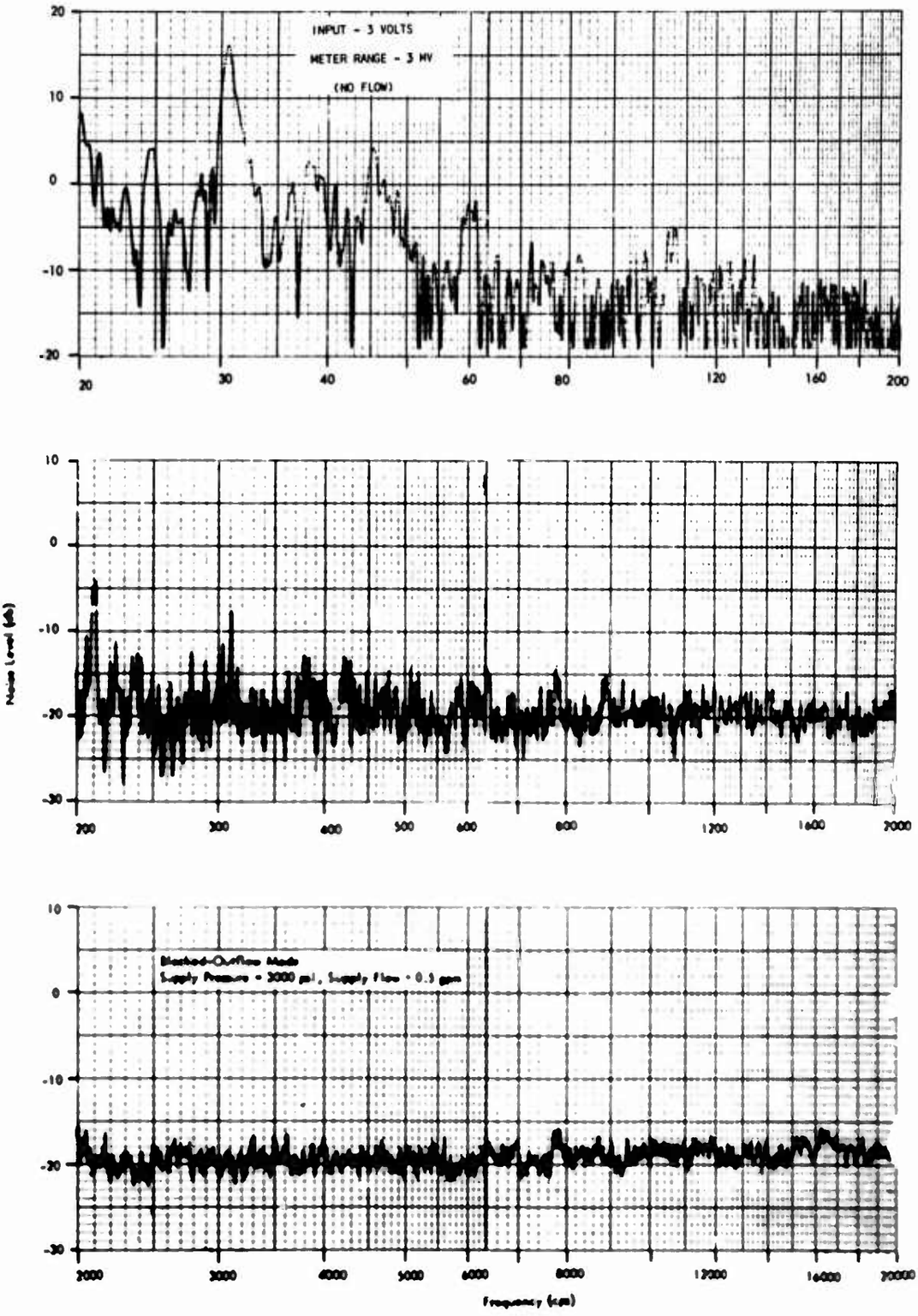

Figure 43. Experimental Apparatus Noise Spectrum.

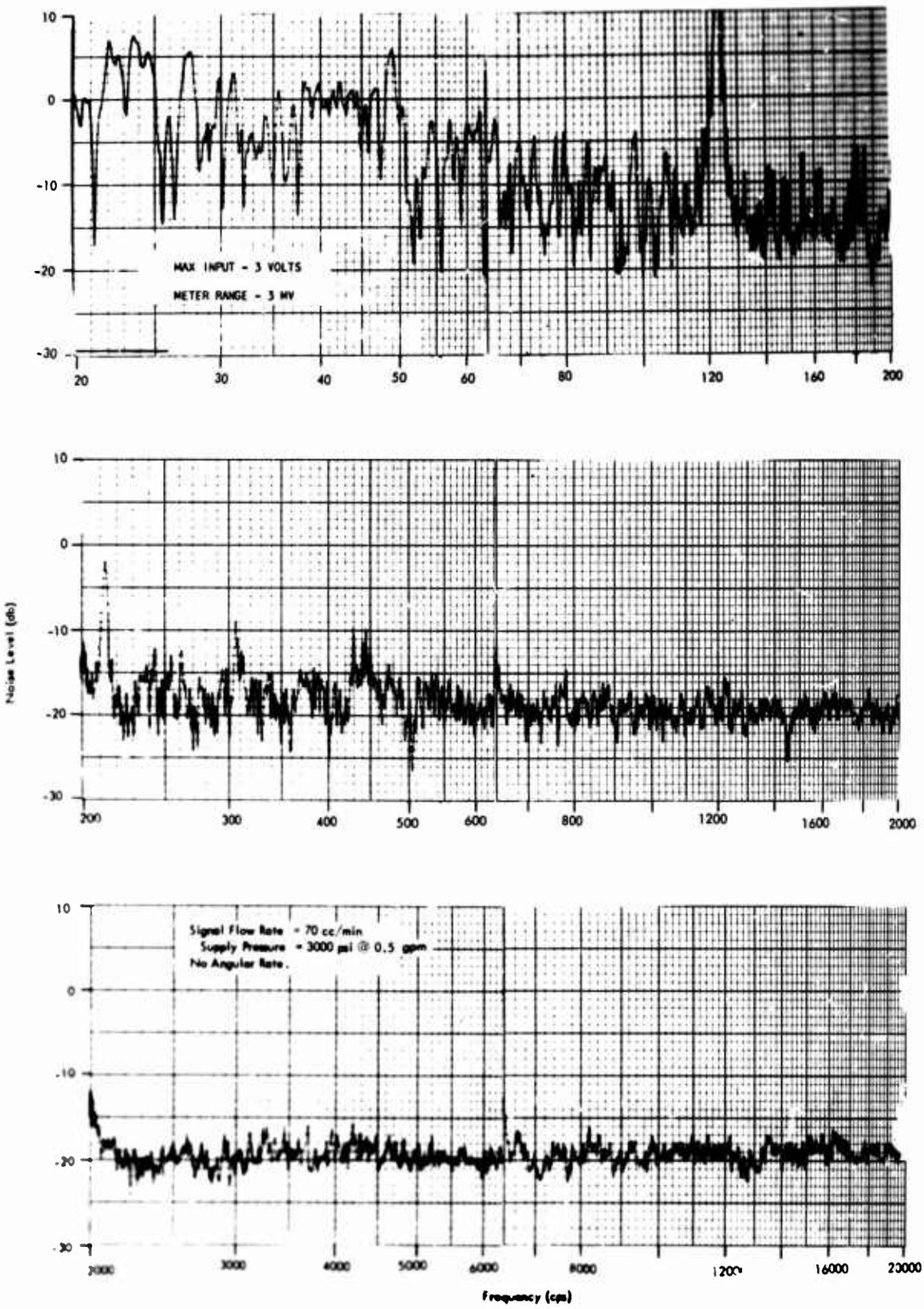

Figure 44. Noise Spectrum with Signal Flow.

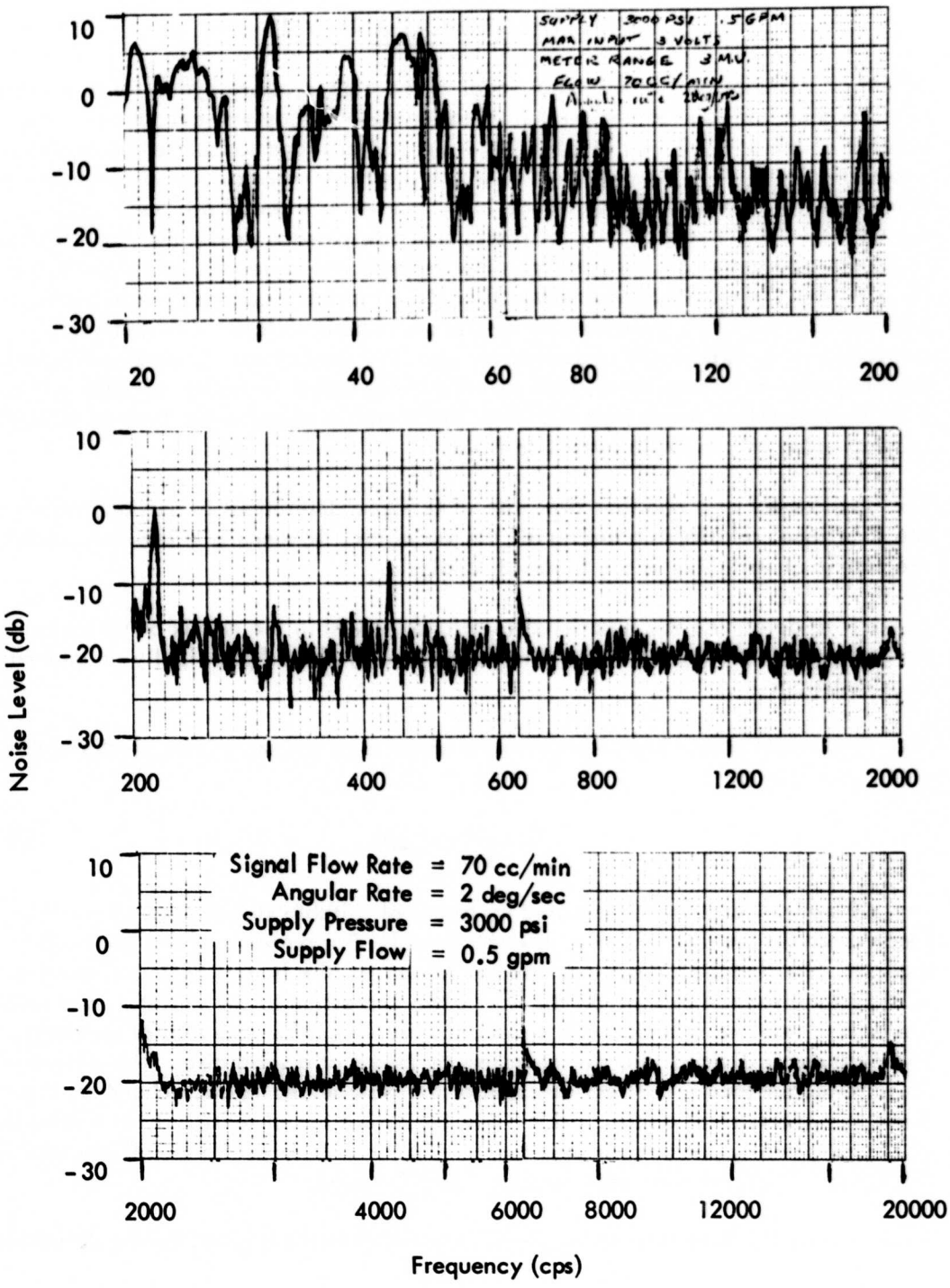

Figure 45. Noise Spectrum with Angular Rate.

4. THEORETICAL ANALYSIS

Before an experimental breadboard model of the high-pressure hydraulic rate sensor was designed and fabricated, an analytical trade-off study was conducted. The purpose of the analysis was to establish design criteria and to isolate the important geometrical and fluid flow parameters which are most important in an optimum design. Some specific elements of importance in the vortex rate sensor are the coupler, signal pick-off element and its location, and flow passage geometries. Critical performance parameters are sensitivity, time response, noise levels, and signal-to-noise ratio. From the results of the trade-off study, a variable-geometry vortex rate sensor was fabricated so that experimental results could be correlated with analytical predictions over a wide range of geometries and flow conditions. Several performance design goals were established, such as vortex rate sensor operation at 3000 psig over a fluid temperature range from -25°F to 160°F with a signal delay time of 10 milliseconds using MIL-H-5606 hydraulic fluid.

The requirement of a constant flow rate of 0.5 gpm determines in part and restricts the functional relationship among all the variables. In essence it serves to reduce the matrix of variables in the trade-off analysis.

In order to determine the functional relationships within the matrix of variables, several equations were derived. The derivations are based principally on geometrical considerations.

The differential output signal pressure, referred to as the sensitivity, is defined as

$$S = \frac{\partial}{\partial \omega} (\Delta p) \qquad (2)$$

The differential pressure is measured by means of suitable signal pick-off probes located within the sink of the vortex rate sensor. For purposes of the trade-off analysis, the signal pick-off was assumed to consist of a hollow cylinder mounted with its longitudinal axis perpendicular to the centerline of the outlet. Two holes are drilled into the cylinder wall equidistant from its transverse axis of symmetry. The cylinder is divided into two chambers by means of a solid disc. The differential pressure output then is a direct function of the flow sensed in each chamber. Figure 46 shows the geometrical configuration. For the derivation of sensitivity as a function of V_∞, θ, and α, it was assumed that $\theta_1 = \theta_2$. This type of pick-off was used in the 4-inch fixed geometry rate sensor originally tested.

From elementary fluid mechanics the differential pressure is given by the definition

$$\Delta p = \Delta C_p \left[\frac{1}{2} \rho V_\infty^2\right] \qquad (3)$$

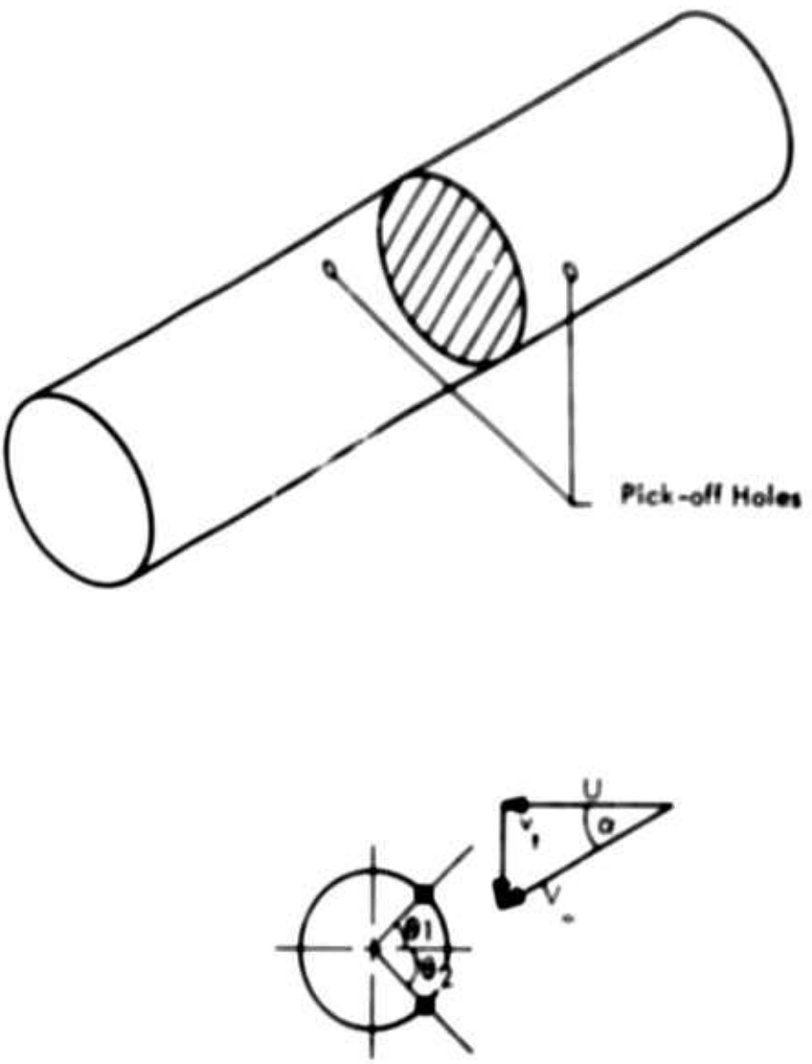

Figure 46. Cylindrical Pick-off Probe.

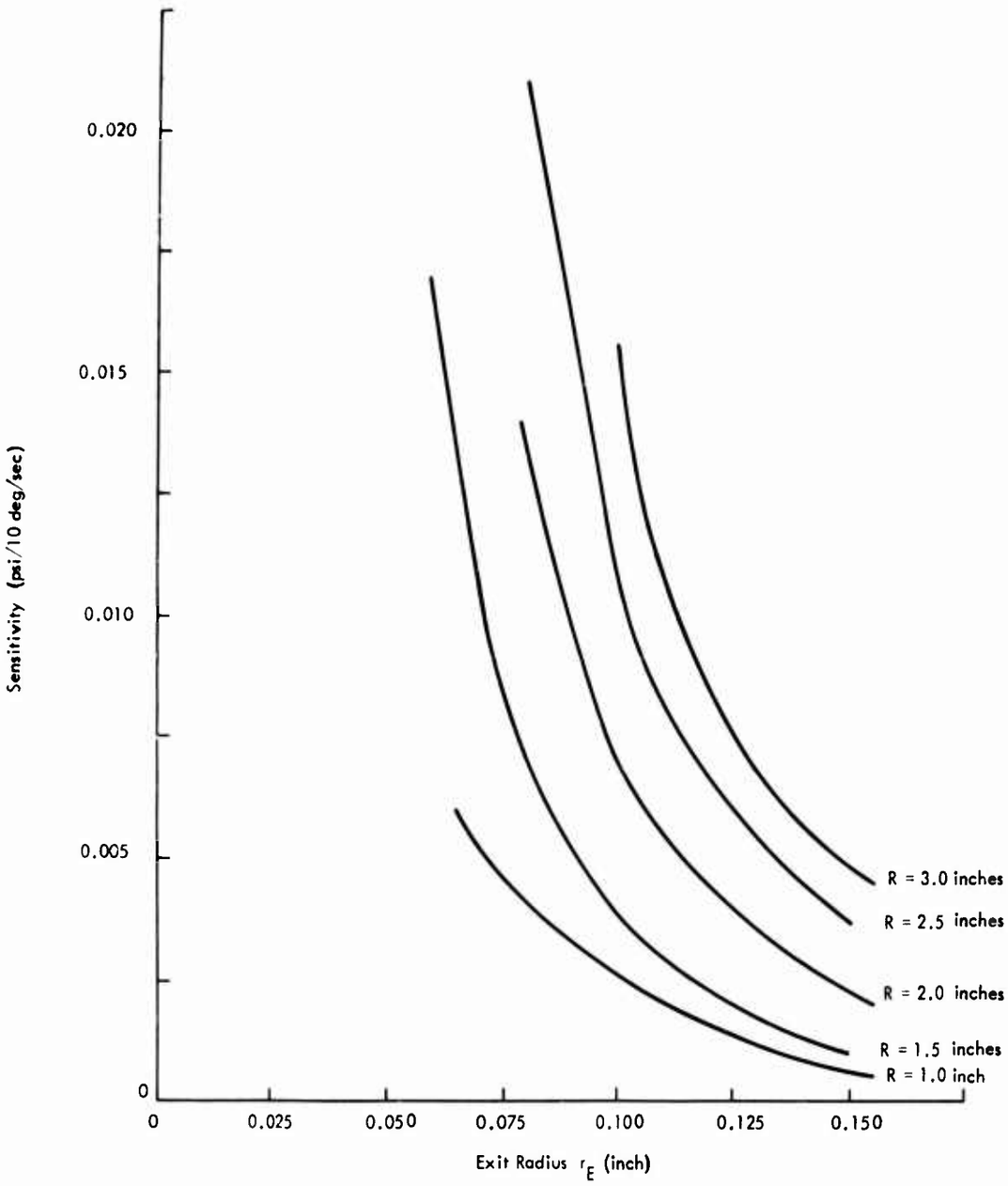

Figure 47. Sensitivity vs Outlet Radius, Angular Rate = 5 Deg/sec.

Therefore, t_d can be expressed completely in geometrical terms since Q is fixed at 0.5 gpm. Thus

$$t_d = \frac{4\pi h R r_E}{Q} \tag{15}$$

or in terms of v_t,

$$t_d = \frac{4\pi h R^3 \omega}{v_t Q} \tag{16}$$

For delay times in the range from 0 to 100 milliseconds, Figure 48 shows the tangential velocity as a function of angular rate for several delay times and pancake chamber radii. The sensitivity is proportional to the square of the tangential velocity component. For a delay time of 100 milliseconds and a threefold change in pancake chamber radius from 0.49 inch to 1.56 inches, the tangential velocity increases from 0.1 ft/sec to 1.1 ft/sec (a tenfold increase), which implies a hundredfold increase in sensitivity. From equation (16), it is also observed that delay time increases as R^3.

Using the basic relations (6) through (8), the deflection angle, α, was determined as a function of angular rate for several pancake chamber gap heights and fixed inlet and outlet radii. The deflection angle indicates the ratio of tangential velocity to outlet velocity. The higher this ratio is, the greater the sensitivity. Figure 49 shows the deflection angle as a function of angular rate for two delay times. As the pancake chamber gap height increases, so does the tangential velocity and, therefore, the sensitivity. It was shown in the experimental results that, indeed, the sensitivity increased rapidly with increasing pancake chamber gap height, corroborating the analytical result of Figure 49.

A flow parameter of great importance in fluidic mechanics problems is the Reynolds number defined by

$$N_{R.} = \frac{UR}{\nu} \tag{17}$$

In the experimental tests it was pointed out that the output signal decreases as the fluid temperature decreases due to viscous dissipation. In essence this is a Reynolds number effect since the kinematic viscosity is a strong function of temperature. The Reynolds number as a function of temperature for several pancake chamber gap heights, h, is shown in Figure 50. From the definition equation (17) and the

Using the analogy of pressure distribution on a cylinder immersed in a fluid flow and Figure 46,

$$\Delta C_p = 4\left[\mathrm{Sin}^2(\theta_1 + \alpha) - \mathrm{Sin}^2(\theta_1 - \alpha)\right] \tag{4}$$

$$V_\infty^2 = W^2 + v_t^2 \tag{5}$$

$$\tan\alpha = v_t/W \tag{6}$$

For continuity and momentum conservation, equations (7) and (8) are respectively,

$$W = \frac{Q}{\pi r_E^2} \tag{7}$$

$$v_t = \frac{\omega R^2}{r_E} \tag{8}$$

Combining equations (2) through (8), an analytical expression for the sensitivity is obtained, i.e.,

$$S = \frac{4\rho Q}{\pi R}\left(\frac{R}{r_E}\right)^3 (1 + 4\,\mathrm{Sin}^2\alpha\cos^2\alpha)\,\mathrm{Sin}\,2\theta_1 \tag{9}$$

For small angle α, i.e., $v_t << W$,

$$S \approx \frac{4\rho Q}{\pi R}\left(\frac{R}{r_E}\right)^3 (1 + \alpha^2)\,\mathrm{Sin}\,2\theta_1 \tag{10}$$

It is observed that the coefficient of $\left(\frac{R}{r_E}\right)^3 (1 + \alpha^2)$ is always known from geometry and fluid density. In addition, the sensitivity behaves basically like $(1/r_E)^3$, which indicates extremely sharp gains in sensitivity as $r_E \to 0$ for fixed R. However, physical limitations impose a minimum size on r_E since a pick-off

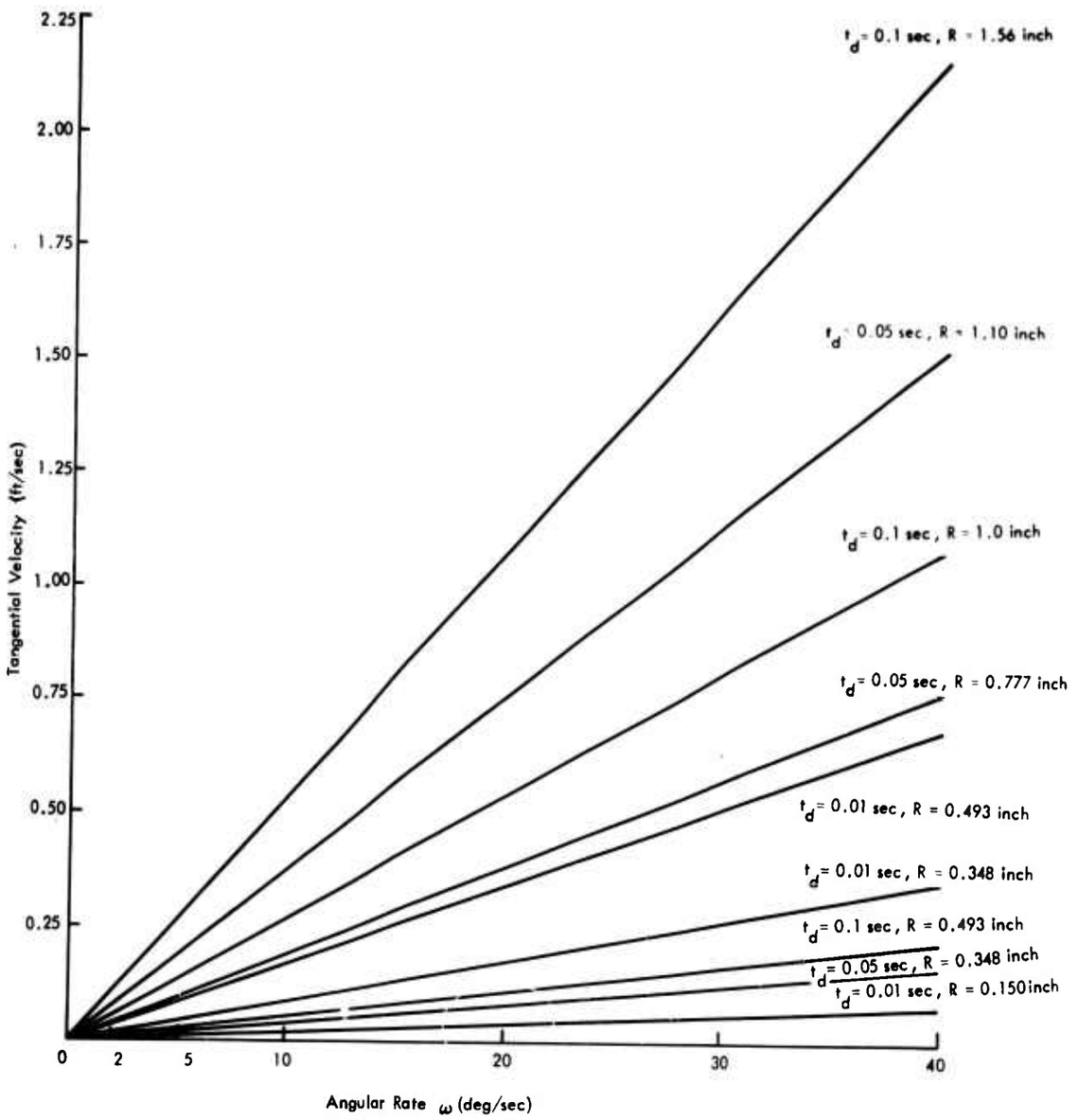

Figure 48. Tangential Velocity vs Angular Rate.

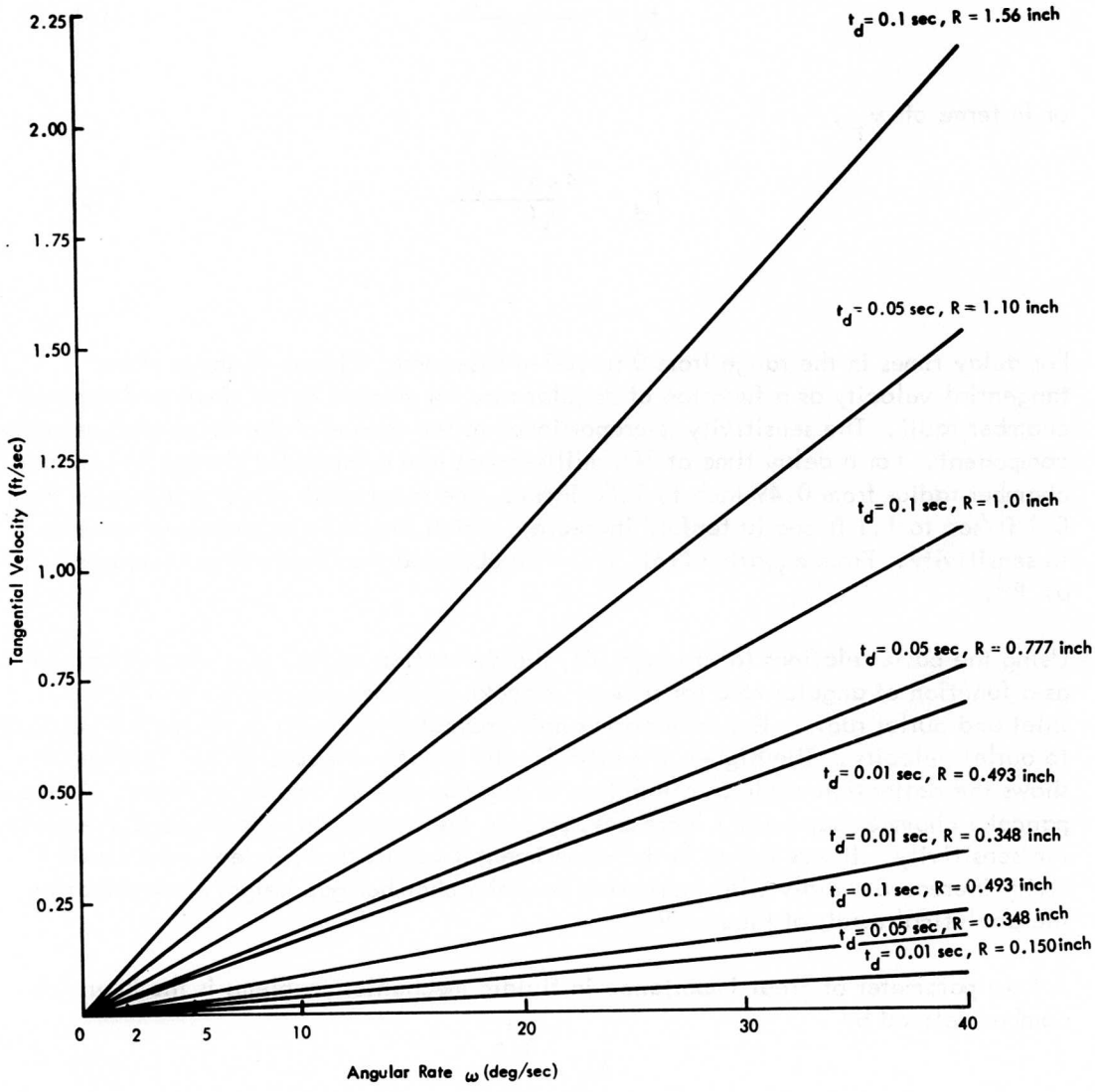

Figure 48. Tangential Velocity vs Angular Rate.

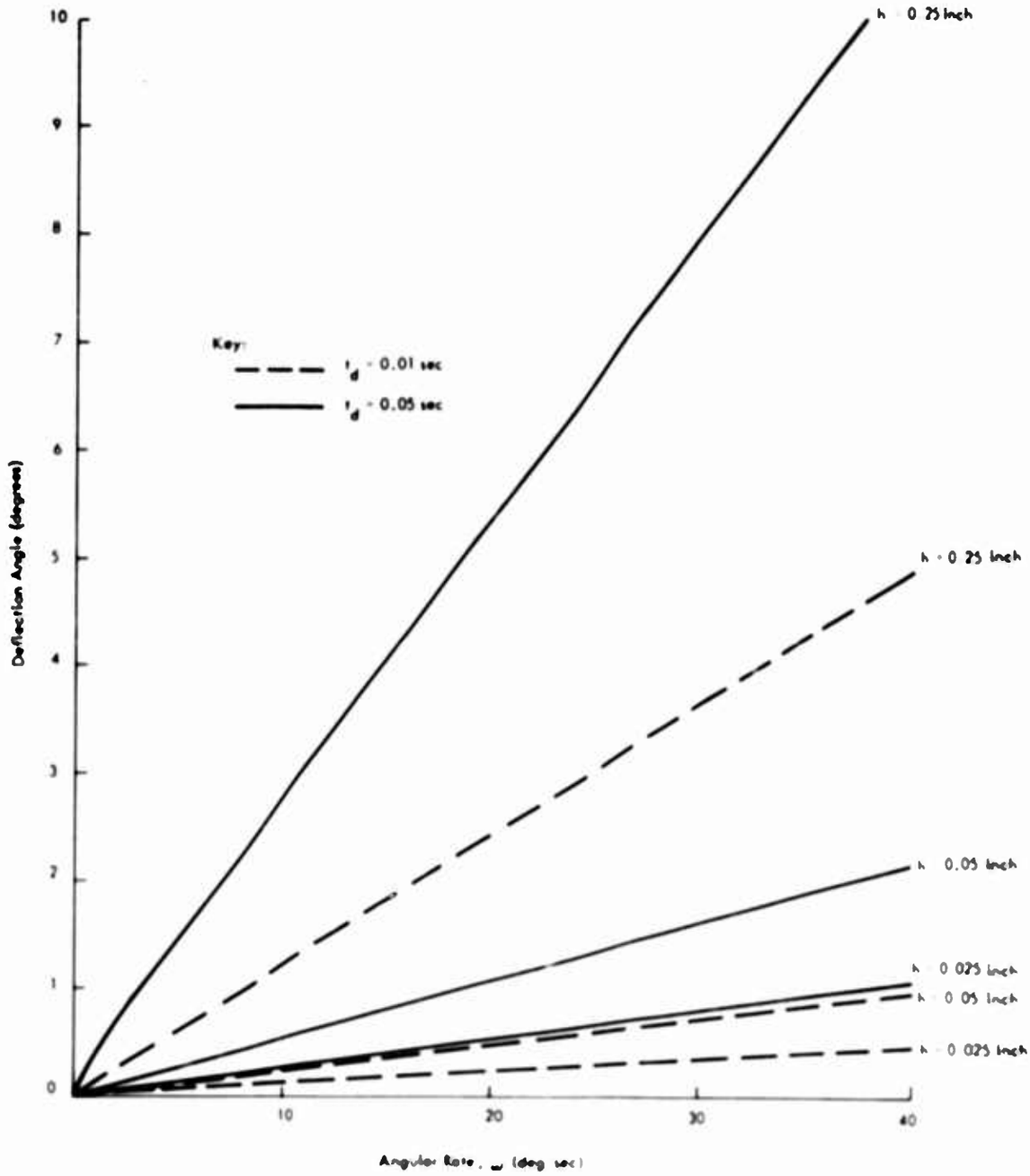

Figure 49. Deflection Angle vs Angular Rate.

continuity relation,

$$Q = 2\pi RUh \tag{18}$$

where Q is always constant (0.5 gpm); it is seen that the product RU varies inversely with h. Therefore, in Figure 50 the Reynolds number decreases for increasing pancake chamber gap height at a fixed temperature. For a fixed pancake chamber gap height, the Reynolds number increases for increasing temperature since ν decreases.

As pointed out in the experimental results, the sensitivity of the vortex rate sensor decreases with decreasing temperature since fluid viscosity increases very rapidly. Furthermore, it has been shown that the sensitivity is proportional to v_t^2. In Figures 51, 52, and 53 the tangential velocity as a function of inlet radius, R, is shown for a delay time of 10 milliseconds at fluid temperatures of -25°F, 100°F, and 160°F, respectively. For an angular rate of 20 deg/sec and $R = 0.5$ inch, the tangential velocity increases by 350 percent (or by 3.5 times) as the fluid temperature is raised from -25°F to 100°F. This represents an order-of-magnitude change in sensitivity. The experimental results showing the signal output change of approximately one order of magnitude for a fluid temperature change from 10°F to 100°F verify this theoretical result. Furthermore, from Figures 52 and 53 it is observed that for a fluid temperature increase from 100°F to 160°F, v_t increases from 0.35 to 0.43 ft/sec. This represents approximately a 34-percent increase in sensitivity. Indeed, approximately a 35-percent increase in sensitivity was observed in the experiments under the same conditions.

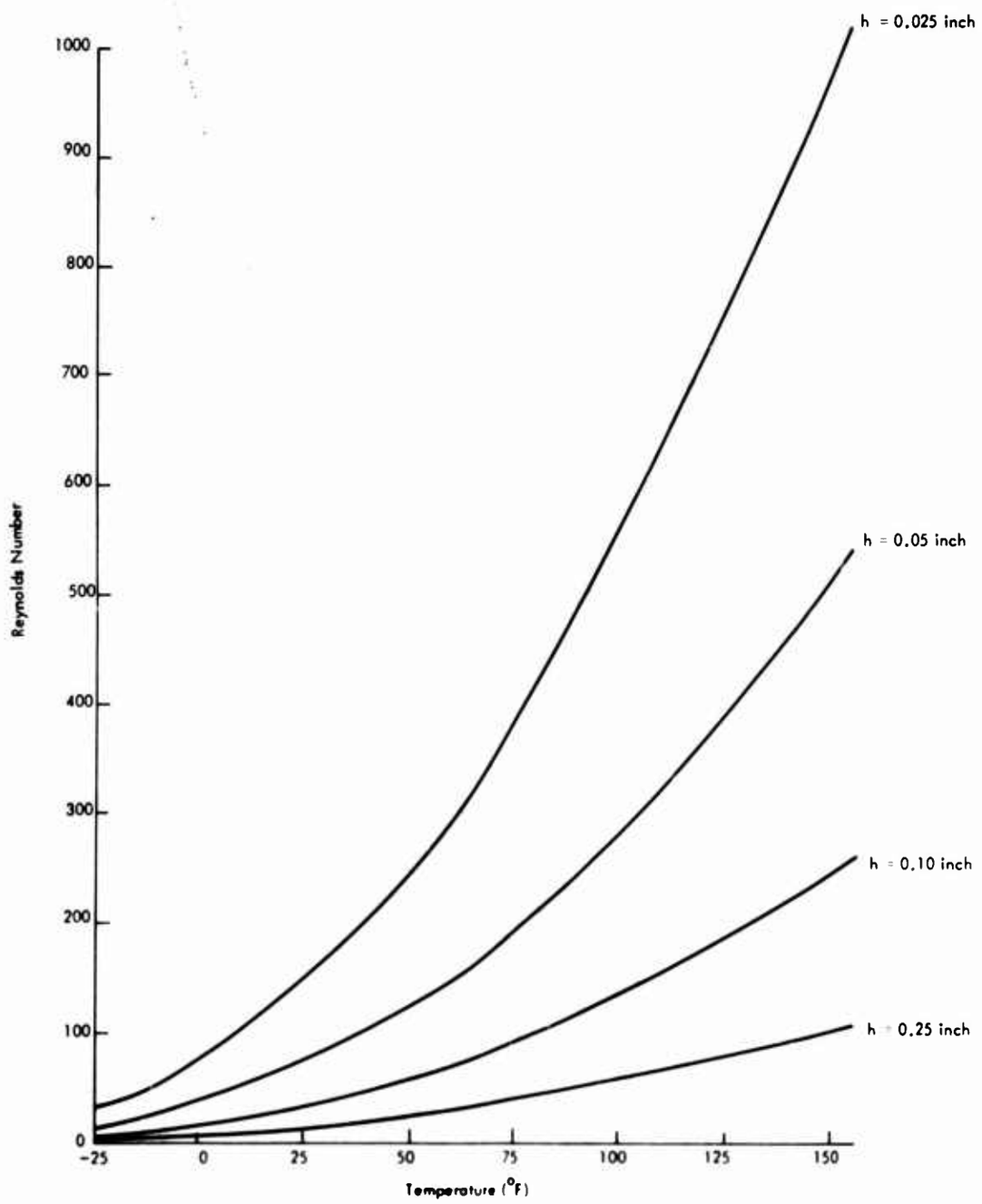

Figure 50. Reynolds Number vs Temperature.

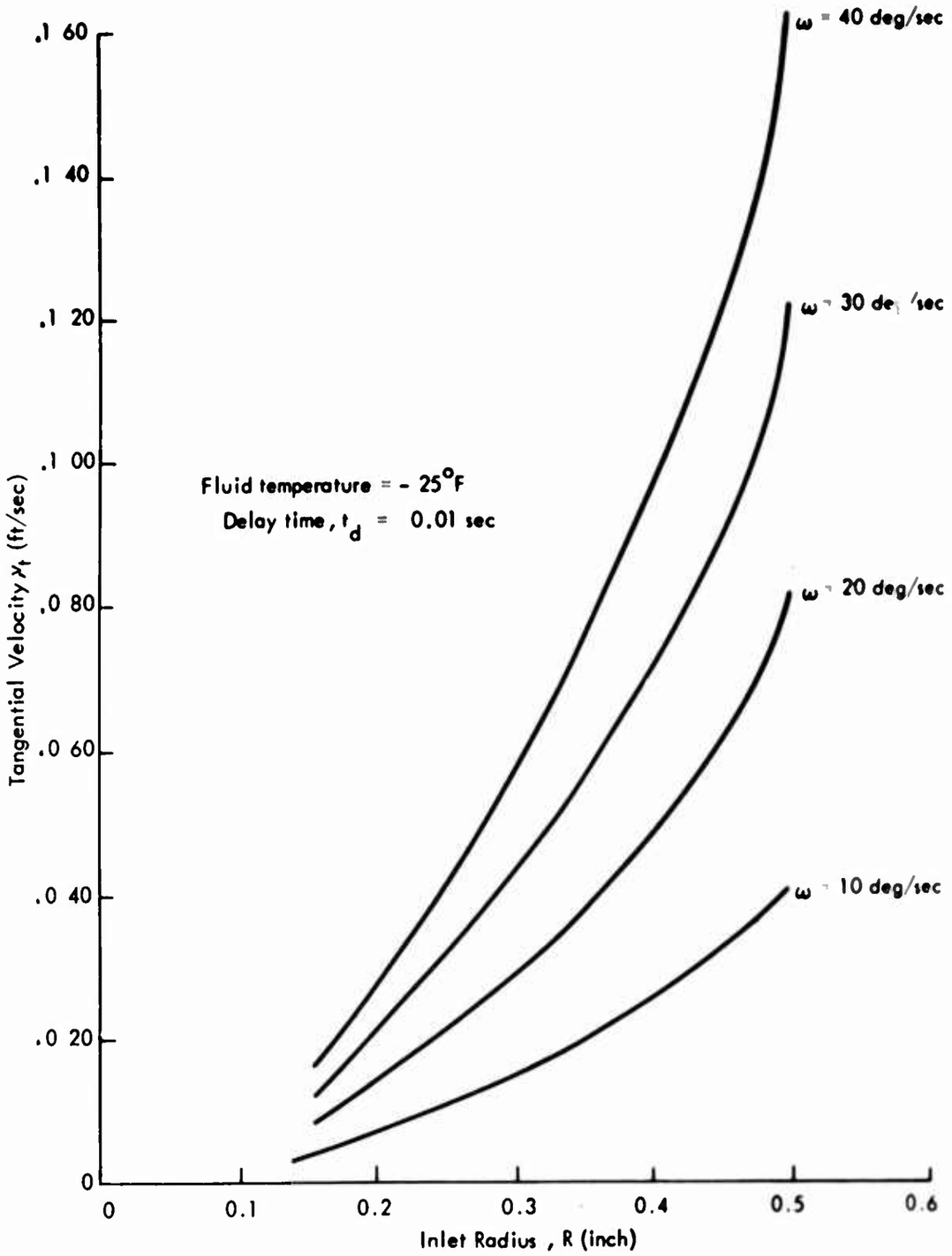

Figure 51. Tangential Velocity vs Inlet Radius.

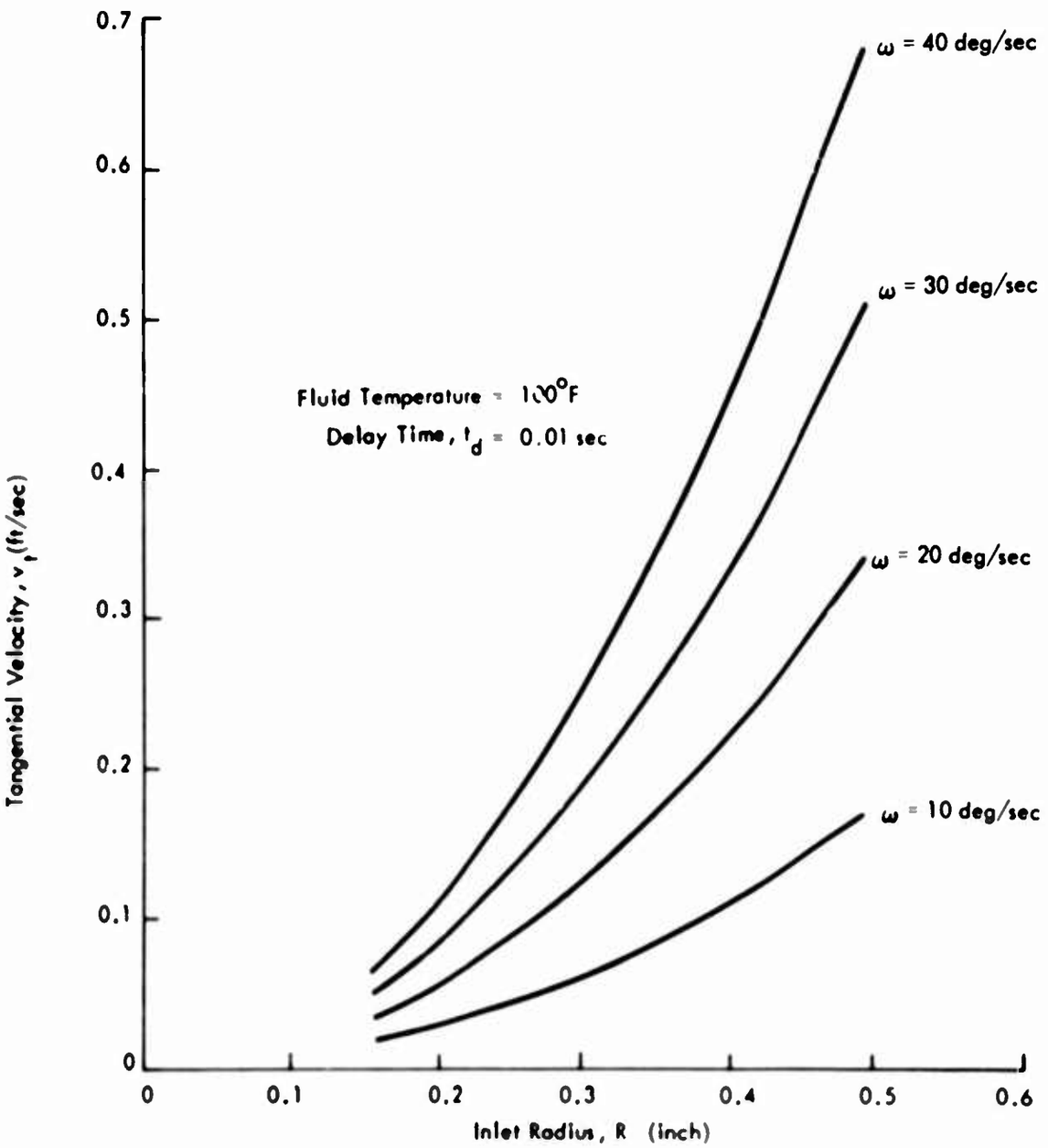

Figure 52. Tangential Velocity vs Inlet Radius.

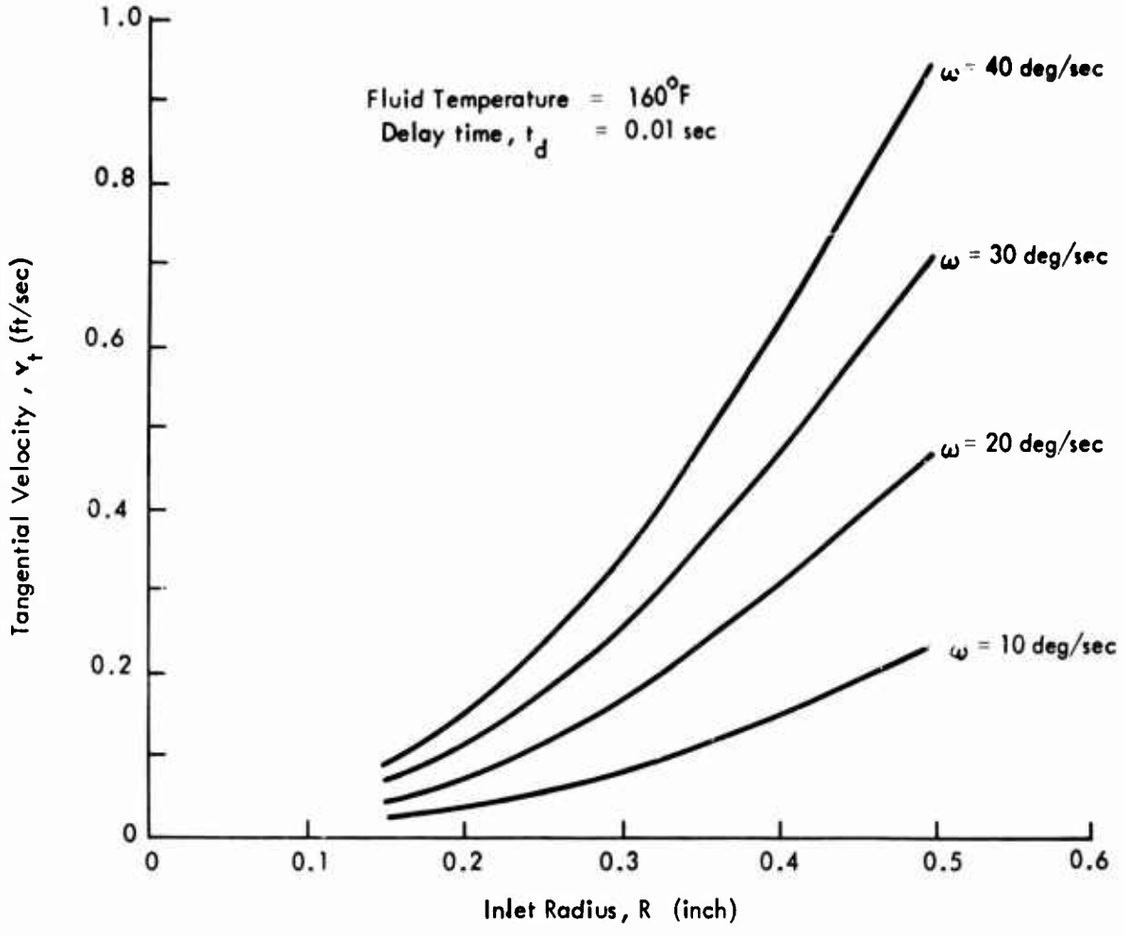

Figure 53. Tangential Velocity vs Inlet Radius .

5. RESULTS AND CONCLUSIONS

The objective of this experimental program was to demonstrate the feasibility and performance characteristics of a high-pressure (3000 psi) hydraulic vortex rate sensor to meet specific requirements. The conclusions resulting from the trade-off study and the experimental program are:

- An optimum geometrical configuration of the vortex rate sensor would consist of a pancake chamber diameter of 5.0 inches and a pancake chamber gap height of 0.45 inch.

- The device exhibits linearity up to an angular rate of 50 deg/sec for all supply flow rates tested.

- The location of the signal pick-off probes within the sink for all pancake chamber diameters is not critical in the determination of signal magnitude. A sharp peak in signal output as a function of signal pick-off probe location within the sink is not exhibited. Rather, a range of locations yields nearly the same output signal at fluid temperature equal to room temperature and at fluid temperatures in excess of 150°F. At a fluid temperature of 9°F, the location of the signal pick-off within the sink is critical. This result is probably due to the high viscosity of the fluid at low temperatures.

- The sensitivity (differential output pressure) in the blocked output mode is independent of supply pressure in the range $100 \leq P_s \leq 3000$ psi at room temperature. At a fluid temperature of 160°F, the sensitivity at 3000 psi was approximately 10 percent larger than at 100-psi supply pressure.

- The maximum sensitivity obtained (among all configurations) was 0.005 psi/deg/sec in a blocked output mode.

- The sensitivity of the vortex rate sensor increases exponentially with an increase in supply flow. The sensitivity at 1.0 gpm is 7 times greater than at 0.5 gpm. At 3.0 gpm, the sensitivity is approximately 75 times greater than at 0.5 gpm.

- The viscous coupling gap size does not affect the sensitivity for any pancake chamber gap heights tested.

- A porous coupler does improve the signal output by a factor of 2, but it also increases the noise levels in the form of increased pressure fluctuations about the mean.

- The temperature of the working fluid, MIL-H-5606 oil, seriously affects the magnitude of the sensitivity. At a fluid temperature of 10°F, the sensitivity is ten times lower than its level at 85°F, and, at 160°F, the sensitivity is approximately 25 percent higher than at 85°F.

- No useful pressure-flow load curves could be obtained in the variable-geometry vortex rate sensor. It was found that the pick-off was at fault. The 4-inch-diameter fixed-geometry vortex rate sensor was used in place of the aforementioned vortex rate sensor, and useful results were obtained. A redesign of the signal pick-off in the variable-geometry vortex rate sensor was not undertaken because of the availability of the fixed-geometry vortex rate sensor.

- For all supply pressures between 100 psi and 3000 psi, the sensitivity increases as the flow rate through the signal pick-offs increase up to a particular flow rate. At 200-psi supply pressure, the sensitivity increases from 0.18 psi/100°/sec in the blocked-output mode to 0.4 psi/100°/sec at 90 cc/min. Then the sensitivity decreases to zero for higher flow rates. At supply pressures of 1000 to 3000 psi, the same trend is exhibited; however, the maximum could not be obtained because the pressure output signal was uncontrollable. For example, very small changes in the flow through the valves or small changes in angular rate caused signal drift and surges which were much greater than the actual signal.

- The difference in flow between the signal pick-offs, ΔQ, corresponding to the measured sensitivity at 0.5-gpm supply flow rate is so small that it cannot be measured with any degree of confidence. This result could possibly lead to difficulties when implementation of the vortex rate sensor in the stability-augmeniation system is attempted.

- The noise levels detected between 200 cps and 20,000 cps are the same for the case of no flow through the signal pick-offs and the flow through the signal pick-offs indicating that the noise levels are due to the instrumentation. At 210 cps, a large increase in noise level was observed, and over the entire range of frequencies between 20 and 20,000 cps, large noise levels were observed at 30, 120, 210, and 430 cps.

- During the course of the investigations, it was found that vibration of or sudden impact against the flow control valves caused large signal pressure changes. To overcome this difficulty, loose lines and valves were secured. Vibration will affect the performance of the vortex rate sensor at very low signal pressure levels such as are encountered at 0.5-gpm supply flow rates.

- The results drawn from the experimental program indicate that a vortex rate sensor will operate at high (3000 psi) supply pressures and over a wide range of temperature conditions. The implementation of the vortex rate sensor with amplification stages remains a source of investigation to establish fluidic stability augmentation system and fluidic control system feasibility at very high pressures.

6. RECOMMENDATIONS

Experimental results obtained from the investigation of the feasibility of the high-pressure hydraulic vortex rate sensor indicate that further study should be initiated for the purpose of integrating the vortex rate sensor into a high-pressure hydraulic fluidic stabilization and control system. To further the effort, the following should be done:

- Redesign of the signal pick-offs in the variable-geometry vortex rate sensor and a continuation of the optimization program to increase signal levels for a flow rate of 0.5 gpm.

- Integration of the vortex rate sensor with one or more stages of amplification to determine the feasibility of obtaining usable power gain using hydraulic-fluidic components.

- Evaluation of noise characteristics associated with the combination of the vortex rate sensor and fluidic amplification stages at high (3000 psi) supply pressures.

- An analytical study to determine sizing, gains, flows, and pressures required in the fluidic-hydraulic stages which include the vortex rate sensor and signal amplification.

APPENDIX

HEAT CONDUCTION (FORCED CONVECTION) EQUATIONS FOR COOLING OF MIL-H-5606 OIL

The forced convection relationships needed to compute the length of the tubing in the heat exchanger coil necessary to reduce the temperature of the MIL-H-5606 oil to specified levels are given in the following pages. The symbols used in this appendix are defined as follows:

A	surface area, ft^2
a	cross-sectional area, ft^2
C_p	specific heat, Btu/lbm - ^oF
D	diameter, ft
h_c	convective heat transfer coefficient, Btu/hr-ft^2-^oF
h_∞	external convective coefficient, Btu/hr-ft^2-^oF
k	thermal conductivity of fluid, Btu/hr-ft -^oF
K	thermal conductivity of tube, Btu/hr-ft -^oF
L	tube length, ft
log	natural logarithm
$\dot{M}$	mass flow, lb/hr
Nu	Nusselt number
Pr	Prandtl number
q	heat flow, Btu/hr
Q	fluid volume flow, ft^3/sec
R_1	internal radius, ft
R_2	external radius, ft
T_{ext}	exit temperature of fluid, ^oF

T_{in}	entrance temperature of fluid, ^{o}F
T_{∞}	temperature of cooling environment, ^{o}F
Re	Reynolds number
U	overall heat transfer coefficient, $Btu/hr\text{-}ft^{2}\text{-}^{o}F$
V	fluid velocity, ft/sec
ν	kinematic viscosity, ft^{2}/sec
ρ	fluid density, lbm/ft^{3}

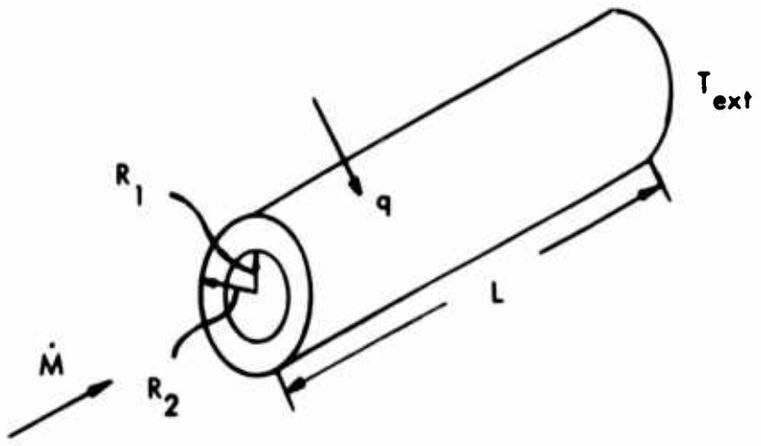

Total Heat Flow Required

$$q = \dot{M} C_p [T_{in} - T_{ext}] \tag{19}$$

Convective Heat Transfer Parameters

$$Re = VD/\nu \tag{20}$$

$$Pr = \nu/a \tag{21}$$

$$a = k/\rho C_p \tag{22}$$

Laminar Flow

$$Nu = 3.65 + \frac{.0668\,(D/L)\,Re\,Pr}{1.0 + .04(Re\,Pr\,D/L)^{2/3}} \tag{23}$$

$$h_c = N_u\, k/D \tag{24}$$

h_∞ is based on boiling of environment (cooling agent), or evaluate as free or forced convection over external tube surface

$$q = \frac{\Delta T}{\frac{1}{h_c A_1} + \frac{\log(R_2/R_1)}{2\pi LK} + \frac{1}{A_2 h_\infty}} = \frac{2\pi \Delta TL}{U} \qquad (25)$$

Therefore, $L_1 = \frac{qU}{2\pi \Delta T}$.

An iteration process must be performed using equations (23), (24), and (25) such that L_1 solves all three if the original L_1 does not agree with L computed in equation (23).

Unclassified
Security Classification

DOCUMENT CONTROL DATA - R & D

(Security classification of title, body of abstract and indexing annotation must be entered when the overall report is classified)

1 ORIGINATING ACTIVITY (Corporate author) Singer-General Precision, Inc. Kearfott Group Little Falls, New Jersey	2a. REPORT SECURITY CLASSIFICATION Unclassified 2b. GROUP

3 REPORT TITLE

INVESTIGATION OF HIGH-PRESSURE HYDRAULIC VORTEX RATE SENSOR

4 DESCRIPTIVE NOTES (Type of report and inclusive dates)

Final Report

5 AUTHOR(S) (First name, middle initial, last name)

Michael J. DeSantis
Edward L. Rakowsky

6 REPORT DATE	7a. TOTAL NO. OF PAGES	7b. NO. OF REFS
July 1970	94	

8a. CONTRACT OR GRANT NO.	9a. ORIGINATOR'S REPORT NUMBER(S)
DAAJ02-69-C-0008 b. PROJECT NO. Task 1F162203A14186 c. d.	USAAVLABS Technical Report 70-19 9b. OTHER REPORT NO(S) (Any other numbers that may be assigned this report)

10 DISTRIBUTION STATEMENT

This document is subject to special export controls, and each transmittal to foreign governments or foreign nationals may be made only with prior approval of U. S. Army Aviation Materiel Laboratories, Fort Eustis, Virginia 23604.

11. SUPPLEMENTARY NOTES	12. SPONSORING MILITARY ACTIVITY
	U.S. Army Aviation Materiel Laboratories Fort Eustis, Virginia

13. ABSTRACT

The study was undertaken to establish the feasibility of a high-pressure (3000 psi) hydraulic vortex rate sensor for application in a helicopter hydraulic stability-augmentation system. The feasibility of low-pressure fluid stabilization systems has been demonstrated. The primary component that requires development for implementation in a high pressure system is the vortex rate sensor. The high-pressure hydraulic vortex rate sensor has an on-board built-in supply of hydraulic fluid which is used in the primary hydro-mechanical flight control of the vehicle. A small amount of hydraulic fluid under high pressure can be diverted from the main system to the vortex rate sensor, used to perform a sensing function, and returned to the main hydraulic system. The fluid systems approach incorporating the high-pressure hydraulic vortex rate sensor offers improved reliability, maintainability, and reduced cost over conventional electromechanical systems. The present experimental program is to evaluate the performance of a hydraulic vortex rate sensor over a wide range of operating temperatures and pressures. A variable-geometry capability was incorporated in the design and fabrication of the experimental model to evaluate the effects of the vortex chamber diameter, passage gap heights, and signal pick-off location on the signal output of the device. A limited theoretical trade-off analysis was performed to determine the functional relationships between the output signal and geometric and flow parameters. Based upon this analysis, three chamber diameters were fabricated.

DD FORM 1 NOV 68 1473 REPLACES DD FORM 1473, 1 JAN 64, WHICH IS OBSOLETE FOR ARMY USE.

Unclassified
Security Classification

14 KEY WORDS	LINK A		LINK B		LINK C	
	ROLE	WT	ROLE	WT	ROLE	WT
High-pressure hydraulic vortex rate sensor						
Low-pressure fluid stabilization						
Hydraulic fluid						